

(NASA-CR-138122) SCALE MODEL TESTING OF  
DROGUES FOR FREE DRIFTING BUOYS Final  
Report, Sep. 1972 - Sep. 1973 (Draper  
(Charles Stark) Lab., Inc.) 443 P HC  
\$10.25 140

N74-21922

Unclas  
16687

CSSL 20D G3/12

R-769

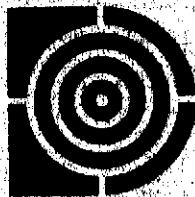
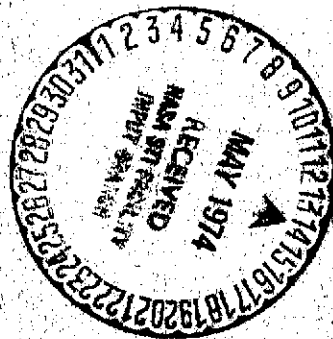
SCALE MODEL TESTING OF DROGUES  
FOR FREE DRIFTING BUOYS

by

William A. Vachon

September 1973

Technical Report



**The Charles Stark Draper Laboratory, Inc.**  
Cambridge, Massachusetts 02139

Approved for public release; distribution unlimited

REPORT DOCUMENTATION PAGE		READ INSTRUCTIONS BEFORE COMPLETING FORM
1. REPORT NUMBER R-769	2. GOVT ACCESSION NO.	3. RECIPIENT'S CATALOG NUMBER
4. TITLE (and Subtitle) Scale Model Testing of Drogues for Free Drifting Buoys		5. TYPE OF REPORT & PERIOD COVERED Final Report Sept. 1972 - Sept. 1973
		6. PERFORMING ORG. REPORT NUMBER
7. AUTHOR(s) William A. Vachon		8. CONTRACT OR GRANT NUMBER(s) NAS 8-28916
9. PERFORMING ORGANIZATION NAME AND ADDRESS Charles Stark Draper Laboratory, Inc. 68 Albany St. Cambridge, MA 02139		10. PROGRAM ELEMENT, PROJECT, TASK AREA & WORK UNIT NUMBERS
11. CONTROLLING OFFICE NAME AND ADDRESS National Data Buoy Office Mississippi Test Facility Bay St. Louis, MS 39520		12. REPORT DATE September 1973
14. MONITORING AGENCY NAME & ADDRESS (if different from Controlling Office)  Same		13. NUMBER OF PAGES 143
		15. SECURITY CLASS. (of this report)  Unclassified
15a. DECLASSIFICATION/DOWNGRADING SCHEDULE		
16. DISTRIBUTION STATEMENT (of this Report)  Approved for public release; distribution unlimited		
17. DISTRIBUTION STATEMENT (of the abstract entered in Block 20, if different from Report)		
18. SUPPLEMENTARY NOTES		
19. KEY WORDS (Continue on reverse side if necessary and identify by block number) Drifting Oceanographic Buoys Drogues Drogue Testing Lagrangian Oceanographic Buoys		
20. ABSTRACT (Continue on reverse side if necessary and identify by block number) Instrumented model drogue tests were conducted in a ship model towing tank. The purpose of the tests was to observe and measure deployment and drag characteristics of such shapes as parachutes, crossed vanes, and window shades which may be employed in conjunction with free drifting buoys. Both Froude and Reynolds scaling laws were applied while scaling to full scale relative velocities of from 0 to 0.2 knots. Data		

20. Abstract (Cont.)

indicate that a parachute and other shapes which depend on velocity for deployment can be poor choices. A weighted window shade drogue is recommended because of its performance, high drag coefficient, simplicity, and low cost. The proper drogue area and ballast weight must, however, be selected in order to insure proper drag performance and depth locking accuracy. Detailed theoretical performance curves are presented for parachutes, crossed vanes, and window shade drogues. Theoretical estimates of depth locking accuracy and buoy-induced dynamic loads pertinent to window shade drogues are presented as a design aid. An illustrative example of a window shade drogue design is presented.

R-769

SCALE MODEL TESTING OF DROGUES  
FOR FREE DRIFTING BUOYS

by  
William A. Vachon

THE CHARLES STARK DRAPER LABORATORY, INC.  
CAMBRIDGE, MASSACHUSETTS 02139

September 1973

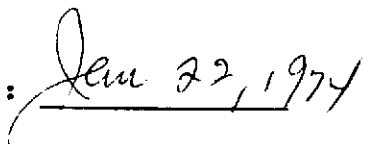
TECHNICAL REPORT

Approved:



Philip N. Bowditch  
Head, Scientific Technology Dept.

Date:



Approved for public release; distribution unlimited

;

## ACKNOWLEDGMENT

This report was prepared by The Charles Stark Draper Laboratory, Inc. under Contract NAS 8-28916 with the National Data Buoy Office and administered by the National Aeronautics and Space Administration.

The author wishes to thank all those who contributed to the work described. Special thanks are due to Mr. G. Petrie, Cmdr P. Morrill and Cmdr C. Niederman of the National Data Buoy Office for their support and encouragement. At the C.S. Draper Lab special thanks are also due to Mr. P. Bowditch and Mr. J. Dahlen for their constructive comments, to Mr. R. Martorana and Mr. C. Dafnoulelis for their steadfast and creative assistance during the arduous testing phase, and to Mrs. K. Hall and Mrs. G. Grover for their patience in typing the manuscript.

The publication of this report does not constitute approval by the National Data Buoy Office of the findings or conclusions contained herein. It is published only for the exchange and stimulation of ideas.

Scale Model Testing of Drogues for  
Free Drifting Buoys

TABLE OF CONTENTS

<u>Section</u>	<u>Description</u>	<u>Page</u>
1.0	Introduction	1
2.0	Free Drifting Buoy Description	2
2.1	History of LaGrangian Current Sensors	4
2.2	Mathematical Considerations	8
3.0	Test Shapes and Configurations	14
3.1	Parachutes	15
3.2	Bucket Sea Drogues	15
3.3	Conical Sea Anchors	17
3.4	Crossed Vanes	17
3.5	Buoyed Fishing Net	19
3.6	Cylinder	19
3.7	Sphere	21
3.8	Window Shade or Curtain Drogues	21
4.0	Test Description	21
4.1	Reynolds Scaling	27
4.2	Froude Scaling	28
4.3	Froude Scaling of Window Shade Drogues	30
5.0	Test Apparatus	34
6.0	Test Results	37
6.1	Parachute Tests	39
6.2	Bucket Droque Tests	46
6.3	Conical Sea Anchor Tests	47
6.4	Crossed Vanes Tests	48
6.5	Buoyed Fishing Net Tests	55
6.6	Cylinder Tests	56
6.7	Sphere Tests	57
6.8	Window Shade Droque Tests	58

TABLE OF CONTENTS (Cont.)

<u>Section</u>	<u>Description</u>	<u>Page</u>
7.0	Test of Plastic Sheets in the Ocean	76
8.0	Error Estimation	77
9.0	Conclusions and Recommendations	79
	References	81
Appendix A:	Model Drogue - Detailed Test Results	85
Appendix B:	Full Scale Drogue Theoretical Performance Curves	95
Appendix C:	Window Shade Drogue Depth Locking Accuracy	108
Appendix D:	Wave-Induced Drogue Dynamic Loads	112
Appendix E:	Example - Specification of a Window Shade Drogue	124

## List of Figures

<u>Figure</u>	<u>Description</u>	<u>Page (s)</u>
1.	Free Drifting Buoy, Standard Configuration	3
2.	Free Drifter Vector Diagrams	10
3.	Simplified Buoy Statics, Plan View	12
4.	Sea Drogues	16
5.	Two Axis Crossed Vane Model	18
6.	Test Model Drogues	20
7.	Tow Tank Test Summary	23,24
8.	Drag Coefficients of Simple Shapes	31
9.	Heave Input and Drag Measurement Apparatus	35
10.	Model Drogue Deployment Response	40
11.	Drag Characteristics of Sea Drogues	42
12.	Effect of Vertical Heave on Parachute Drag	44
13.	Drag Characteristics of 2-Axis Clamped Vanes	50
14.	Drag Characteristics of 3-Axis Clamped Vanes	51
15.	Photos of Froude and Reynolds Tests of Window Shade Drogues	60
16.	Window Shade Drogue Test Summary	62
17.	Window Shade Drogue Test Summary (Cont.)	63
18.	Window Shade Drogue Froude Scaling Results	66
19.	Window Shade Drogue Reynolds Scaling Results	67
20.	Hydrodynamic Forces on Window Shade Drogues	68
21.	Window Shade Drogue Lift-to-Drag Versus Tether Inclination Angle	70
A-1 through A-9	Summary - Model Drogue Test Results	86-94
B-1	Parachute Drogue Performance Curves	97
B-2	Two-Axis Vane Performance Curves	98
B-3	Three-Axis Vane Performance Curves	99
B-4	Window Shade Drogue Performance Curve (25-pound ballast)	100
B-5	Window Shade Drogue Performance Curve (50-pound ballast)	101

## List of Figures (Cont.)

<u>Figure</u>	<u>Description</u>	<u>Page(s)</u>
B-6	Window Shade Drogue Performance Curve (100-pound ballast)	102
B-7	Window Shade Drogue Performance Curve (150-pound ballast)	103
B-8	Window-Shade Drogue Performance Curve (200-pound ballast)	104
B-9	Window-Shade Drogue Performance Curve (300-pound ballast)	105
B-10	Locus of Window Shade Drogue Instability Points When $F_D = W$	106
B-11	Dimensionless Window Shade Drogue Performance Curves	107
C-1	Drogue Depth Accuracy	110
D-1	Pierson-Moskowitz Sea Spectra for Fully Developed Seas	115
D-2	Dynamic Forces From Near-Surface Window Shade Drogues on Non-Compliant Buoy	117
D-3	Drogue Dynamic Loads	121
D-4	Window Shade Drogue Dynamic Shock Load Conditions	122
E-1	Schematic of Pertinent Parameters in the Specification of a Drogue	125

## 1.0 Introduction

A surface-trackable free drifting buoy is an alternative to moored buoys as a means of deriving oceanographic data. Figure 1 depicts a standard configuration of a free drifter which might contain a parachute drogue and weight at the bottom, a tether line, and a surface buoy containing lights, radio, sensors, etc., on the surface.

At present a free drifting buoy can be built for a fraction of the cost of a moored buoy with attached current sensors. Quite often the free drifting buoy is also simpler and less time consuming to deploy and in some cases is considered expendable. In employing a free drifting buoy as a LaGrangian current sensor only an approximate value of the current velocity at the drogue depth is derived by monitoring the position of the surface buoy. Knowledge of surface wind and currents enhances the knowledge of the current velocity. A moored buoy could, however, supply an Eulerian or fixed position current velocity at as many depths as there are current meters, a feature lacking in the free drifter. It is conceivable that current meters could be attached at various points on a deep free drifting configuration and the measured relative vector velocity recorded on the current meters added to the buoy drift velocity in order to obtain the velocity field in the water column. Such an idea seems feasible but renders the free drifter no longer expendable and negates the free drifting buoy advantages of simplicity and low cost.

Information is available or can, in general, be calculated on the drag characteristics of both a buoy and the tether line. The drogue element is, however, more complex and in many cases its drag does not easily lend itself to calculations. During the past year model drogue tests have been conducted by

the Charles Stark Draper Laboratory for the National Data Buoy Office in an effort to empirically determine the performance characteristics of various drogue elements. Instrumented tests have been performed in a ship model towing tank wherein full scale ocean relative velocities of 0 to 0.2 knots have been scaled by a scale factor of approximately 16, employing both Froude and Reynolds scaling laws. Forty different drogue configurations have been evaluated in terms of such features as simplicity, cost, on-deck storage, deployability, and constancy of drag area ( $C_D A$ ). This report briefly outlines the history of free drifters, a mathematics which would describe their steady state behavior in the water, the purposes and types of towing tests, the test apparatus, results, theoretical performance curves, recommendations, and useful theoretical design information based on an interpretation of the test results.

## 2.0 Free Drifting Buoy Description

A free drifting buoy is an unmoored buoy which will drift in the direction of the net force caused by wind and water. Attempts are generally made to couple the buoy drag to a current at a specific water depth such that the buoy will follow that current to the exclusion of currents at other depths. The standard free drifting buoy shown in Figure 1 is called a Lagrangian sensor in that it measures parameters as it travels with the water of interest rather than measuring the same parameters as the water passes by, as in the case of moored sensors. The former method derives its name from the Lagrangian mathematical operator which describes various dynamical processes seen while moving at the velocity of the fluid. The use of moored buoys as a sensor base is referred to as an Eulerian method of measurement because of the mathematics employed to describe dynamic phenomenon seen from a fixed reference base.

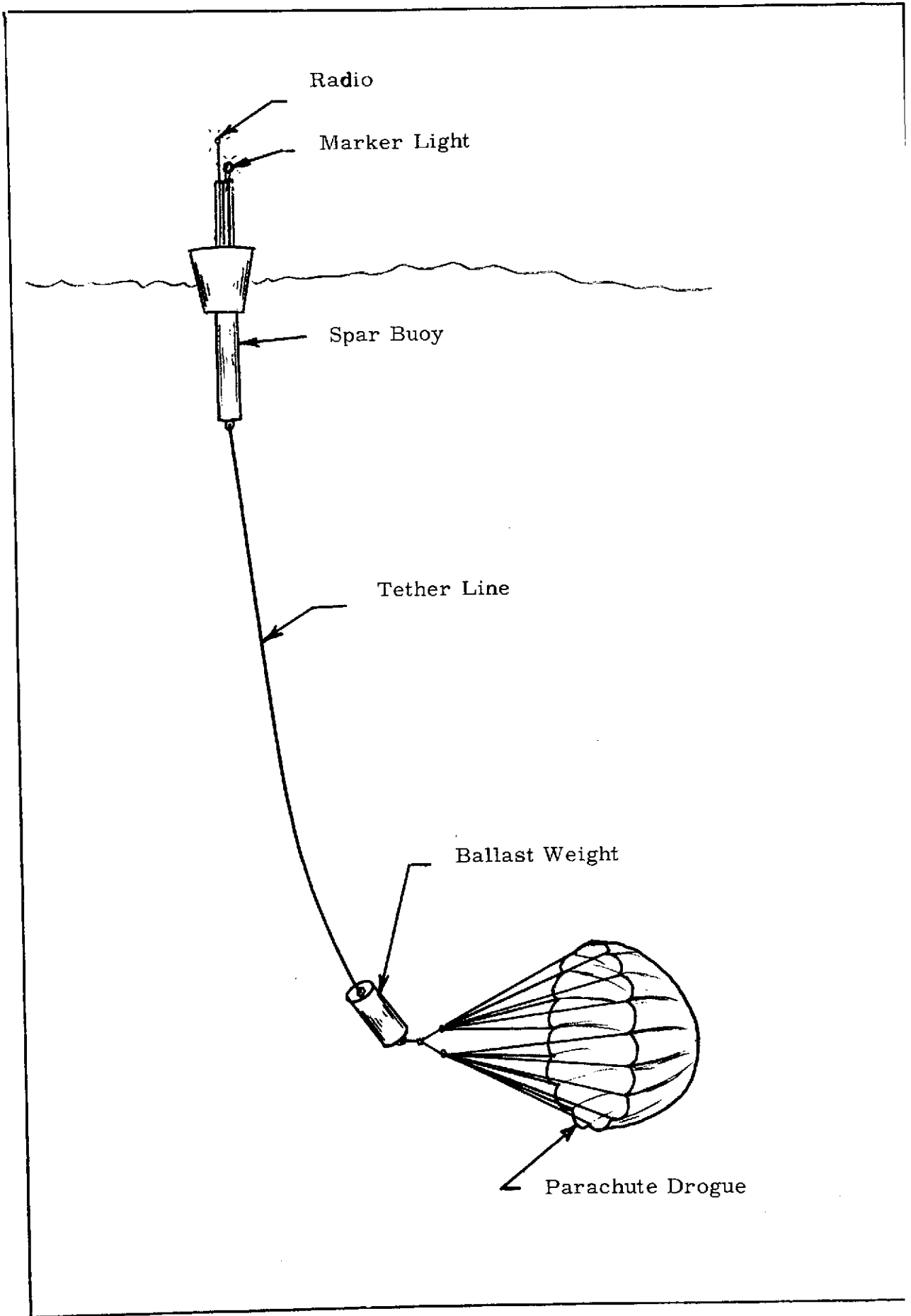


FIGURE 1  
Standard Drifting Buoy Configuration

A LaGrangian buoy requires that its position or velocity be known as a function of time in addition to knowing the value of the parameter being measured. The simplest case of the LaGrangian buoy contains no sensors at all. Its position as a function of time is indicative of the velocity of the water which it is designed to follow.

Free drifting buoys may be used for other reasons. A buoy alone may be placed on the ocean surface and allowed to freely drift with the currents in order to provide a series of near-surface and meteorological measurements from a moving base. Other buoys are well coupled to great depths in an attempt to couple them to a zero current level. In these cases the measurement of parameters other than current velocity (e.g., meteorological data) may be of importance.

## 2.1 History of LaGrangian Current Sensors

A detailed history of the use of drogues as LaGrangian current sensors is covered in a recent report by Monahan and Monahan (1973). It is seen that the first reported use of free drifting drogued buoys (weighted sails as drogues) is in the 16th century. They did not, however, find wide use until approximately the 1950's after which many investigators applied them. This writing will attempt to highlight their recent history and some of the major developments. Numerous applications will, of necessity, not be mentioned but, hopefully, most of the important aspects will be covered.

In 1857 an Englishman, Captain Spratt (1871) of the MEDINA, suspended weighted wooden current crosses to depths as great as 300 fathoms in the Sea of Marmora (adjacent to Turkey) for current measurement. The surface elements were simple metal floats. A weighted drogue with a surface buoy found application in the mid 1800's as a method of determining the discharge

of some of the canals of Europe. Investigators from the U.S. Coast Survey employed deep crosses to investigate the flow patterns and currents in and around New York city (Mitchell, 1859), the straits of Florida (Mitchell, 1867), and the Gulf Stream (Pillsbury, 1890). At the same time members of the Royal Navy were employing crosses of canvas or sailcloth to measure flows in the Strait of Gibraltar (Carpenter and Jeffreys, 1870; and Nares, 1872).

Current crosses or crossed vanes of up to 6 feet on a side were employed in current surveys until a 1-foot tow net with a "balloon buoy" was first used by a Scot (Buchanan, 1885 and 1895) in measurements from cable ships and a 4-foot canvas cone was employed by an Englishman (Thompson, 1895) in an Atlantic equatorial survey.

The application of drogues for the measurement of deep ocean currents seemed to have elapsed until the 1950's. In the meantime numerous investigators were apparently developing their own mechanical ocean current sensors for application with moored buoys. One interesting application for drogues did, however, arise after World War I. The Royal Navy, apparently desiring to minimize the drift of airships in winds, employed sea anchors for drag when the ships were on or near the sea surface. Numerous model drogue tests were conducted in a tow tank (Baker, 1918). The optimum drogue for their needs turned out to be a cloth sea bucket with rigid circular rings exhibiting a length-to-diameter ratio of approximately one (See Figure 4B).

The 1950's saw a marked resurgence of interest in the application of a LaGrangian current measurement. The study of the Pacific equatorial undercurrent, later called the Cromwell current, spawned the use of large fish nets and crossed vanes for the measurement of surface currents and conical sea anchors

for the measurement of deep currents in 1952 (Cromwell, Montgomery, and Stroup 1954; and Montgomery and Stroup, 1962).

In measurements up to this time the velocity of the deep drogue was determined by knowing its relative velocity with respect to a ship by either visual or radar buoy tracking. The ship's velocity was determined by sequential celestial position fixes. In 1953, however, Stommel (1954) employed a drifting telemetering buoy and a crossed vane drogue to measure currents to depths of 530 feet in the vicinity of Bermuda in the central north Atlantic. The buoy crudely measured the average relative current velocity between radio transmissions, the average wind speed, the instantaneous wind and buoy directions. The four parameters were transmitted to a tape-recording shore station. The buoy position was crudely monitored by a mobile radio direction finding station.

Numerous investigators of the mid 1950's began to use parachutes as drogues (Volkman, Knauss, and Vine, 1956; Cromwell, 1956; Knauss and King, 1958; and others) using known wind velocities and directions for drift corrections. At the same time another type of LaGrangian sensor was being developed by J. C. Swallow (1955). He developed a neutrally buoyant float (later known as a Swallow float) which had no surface element at all. By carefully designing the proper buoy compressibility and density the buoy (in this case a small cylinder) would descend to a depth at which it was neutrally buoyant and follow the currents at that level with no outside error influence. The float position was determined acoustically by a set of hydrophones lowered from a tracking ship.

Numerous other investigators have built neutrally buoyant floats since that time. Of note is the work of Pochapsky (1961 and 1963) which shed light on small scale motions (eddies) in the open ocean. More recently investigators have deployed neutrally buoyant floats in the Sargasso Sea within the deep

ocean sound channel whose center is at a depth of approximately 1200 meters (Rossby and Webb, 1970 and 1971). Position and in some cases water temperature data are transmitted acoustically via the SOFAR (Sound Fixing And Ranging) sound channel which permits transmission of very low frequency acoustic information to distances 1000 km. The signal is generally recorded at three or four shorebased listening stations which are synchronized in time. Signal arrival time lags between different stations permits the unique positioning of the float.

The surface-trackable free drifting buoy, on the other hand, was employed with increased frequency in the late '50's and through the 1960's (Kawamoto, 1958 and Oceanographic Section, 1956). Parachute drogues saw application in the measurement of the Atlantic equatorial undercurrent (Metcalf, Voorhis, and Stalcup, 1962; and Stalcup and Parker, 1965). For a surface buoy Stalcup and Parker employed a 3 meter long fiber-glass skiff containing a radio transponder, a light, and radar reflectors. Position and velocities were fixed by either satellite positioning of a tracking ship or by acoustic ship positioning relative to a subsurface reference buoy. Parker (1963) had also developed a foam-collared, radio-telemetering spar buoy which employed a parachute drogue. In this instance the position was monitored by aircraft at bi-weekly intervals for a period of 126 days.

Parachute drogues were recently employed by Leetma (1972 and 1973) to measure the flow reversal of the East African Somali current to the spring monsoons. 24-foot diameter parachutes were deployed at depths as great as 100 meters for periods of approximately a week over a period of two months. Many of the current measurements were used to increase the confidence of measurements being made by a GEK (geomagnetic electrokinetograph) from a tracking ship. The drogue system was designed and built at the C.S. Draper Laboratory.

A series of tow tank tests on full and reduced scale drogues was recently undertaken in 1971-1972 by personnel at the University of Michigan (Monahan, Kaye, and Michelena; 1973). Their studies were part of an overall Eulerian and Lagrangian current measurement of the circulation in Grand Traverse Bay, Lake Michigan. Four drogue types were tested; a 2-axis crossed vane (current cross), a "vee" drogue, a window shade drogue, and a pilot parachute. Drag data are reported on only the "vee" drogue and current cross. Data for the current cross generally agree with the data reported herein.

The advent of miniaturized and high precision electronics permitted the installation of radio transmitters aboard the buoys which could periodically transmit a signal for state of health, temperature, or position for extended periods. More recently polar-orbiting NIMBUS satellites have been used for radio-transmitted buoy position fixes in mid ocean (Ewing and Striffler, 1970) eliminating the need for a tracking ship. The satellite position accuracy has been on the order of 5 nm.

It appears that drifting buoys will continue to employ NASA-launched satellites. A present series of NIMBUS F satellites are being launched and many experimenters hope to employ the on-board RAMS (Random Access Measurement System) package for data transmittal and position fixing. At the same time scientists at the Woods Hole Oceanographic Institute are planning to employ navigation systems similar to the worldwide OMEGA system (Swanson and Tibbals, 1965) for surface buoy position fixing from shore-based radio stations.

## 2.2 Mathematical Considerations

The steady state mathematical analysis of a free drifting buoy, containing a surface buoy and a deep drogue, differs with that of a moored buoy. For the drifting buoy with both

ends free, the independent parameters are the weight and buoyancy distribution of the whole buoy, the drag areas ( $C_D A$ ) of each part of the buoy, mooring line elasticity, and the current velocity profile as a function of depth. The dependent parameters are drift velocity or drogue depth and the buoy draft.

For a moored buoy the independent parameters are the weight and buoyancy distribution of the whole mooring except the anchor, the water depth, plus all of the other independent parameters applicable to a drifting buoy. The dependent parameters are buoy draft and horizontal position relative to the anchor. Basically the water depth is important for a moored buoy while the total weight and depth of the "anchor" or bottom end is important to a drifting buoy.

A computer program directly applicable to the steady state analysis of free drifting buoys was developed at the Naval Ship Research and Development Center (NSRDC) in Bethesda, Maryland (Wang and Moran, 1971). The program takes all of the previously mentioned independent parameters as input data and solves for drift velocity and buoy draft.

The somewhat general case of a deep current acting in one direction on the subsurface drogue and a surface wind and current acting on the buoy as shown in Figure 2 is an aid in developing some mathematics pertinent to surface-trackable free drifting buoys. The coordinate system is also shown in Figure 2 with appropriate unit vectors  $\hat{i}$ ,  $\hat{j}$ , and  $\hat{k}$  in the x, y, and z directions respectively.

The vector summation of forces on the free drifting buoy can be represented as follows:

$$\sum \vec{F} = 0 = \vec{F}_D + \vec{F}_W + \vec{F}_{B/W} + \vec{W}_B + \vec{B} + \vec{W}_\ell + \vec{L} \quad (1)$$

where the first three terms on the right of the equation only have components in a horizontal direction and the last four

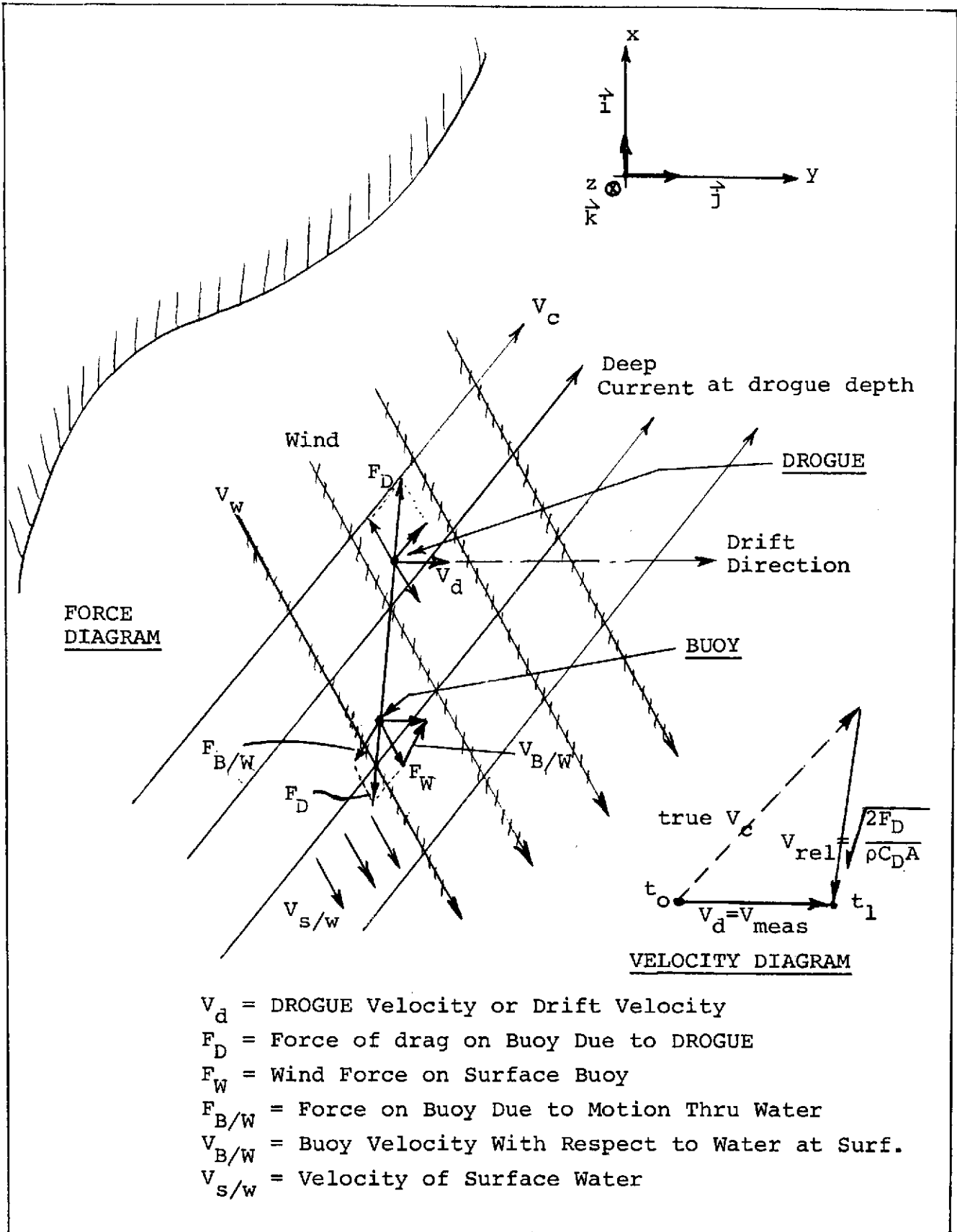


Fig. 2 Free Drifting Buoy Vector Diagrams

terms have components only in the vertical direction. The forces can be seen in Figures 2 and 3 and are defined as follows:

$$\begin{aligned}
 \vec{F}_D &= \text{drag force due to drogue (lines up with} \\
 &\quad \text{tether line)} \\
 \vec{F}_W &= \text{force due to wind and wind-induced surface} \\
 &\quad \text{current} \\
 \vec{F}_{B/W} &= \text{force on the buoy due to its motion through} \\
 &\quad \text{the water while being towed by the drogue} \\
 \vec{W}_B &= \text{net weight of ballast and drogue material} \\
 \vec{B} &= \text{net buoyancy of buoy} \\
 &= \text{total buoyancy - buoy weight} \\
 \vec{W}_\ell &= \text{net weight of mooring line} \\
 &= \int_0^S \rho_c \vec{g} ds \qquad (2) \\
 \vec{L} &= \text{drogue lift force (if present)} \\
 \rho_c &= \text{tether line wetted mass per unit length} \\
 \vec{g} &= \text{gravity force} \\
 ds &= \text{element of tether line length (scalar)} \\
 S &= \text{total length of tether line (scalar)}
 \end{aligned}$$

Other parameters of interest must also be defined in order to present a moment balance equation. These are the following (see Fig. 3.):

$$\begin{aligned}
 \vec{r} &= \int_0^R (\vec{i} dx + \vec{j} dy) \qquad (3) \\
 &= \text{distance from buoy to cable segment } ds \\
 &\quad \text{at distance } R \text{ (scalar } R < S) \text{ along cable.} \\
 R &= \text{tether line length to element } ds.
 \end{aligned}$$

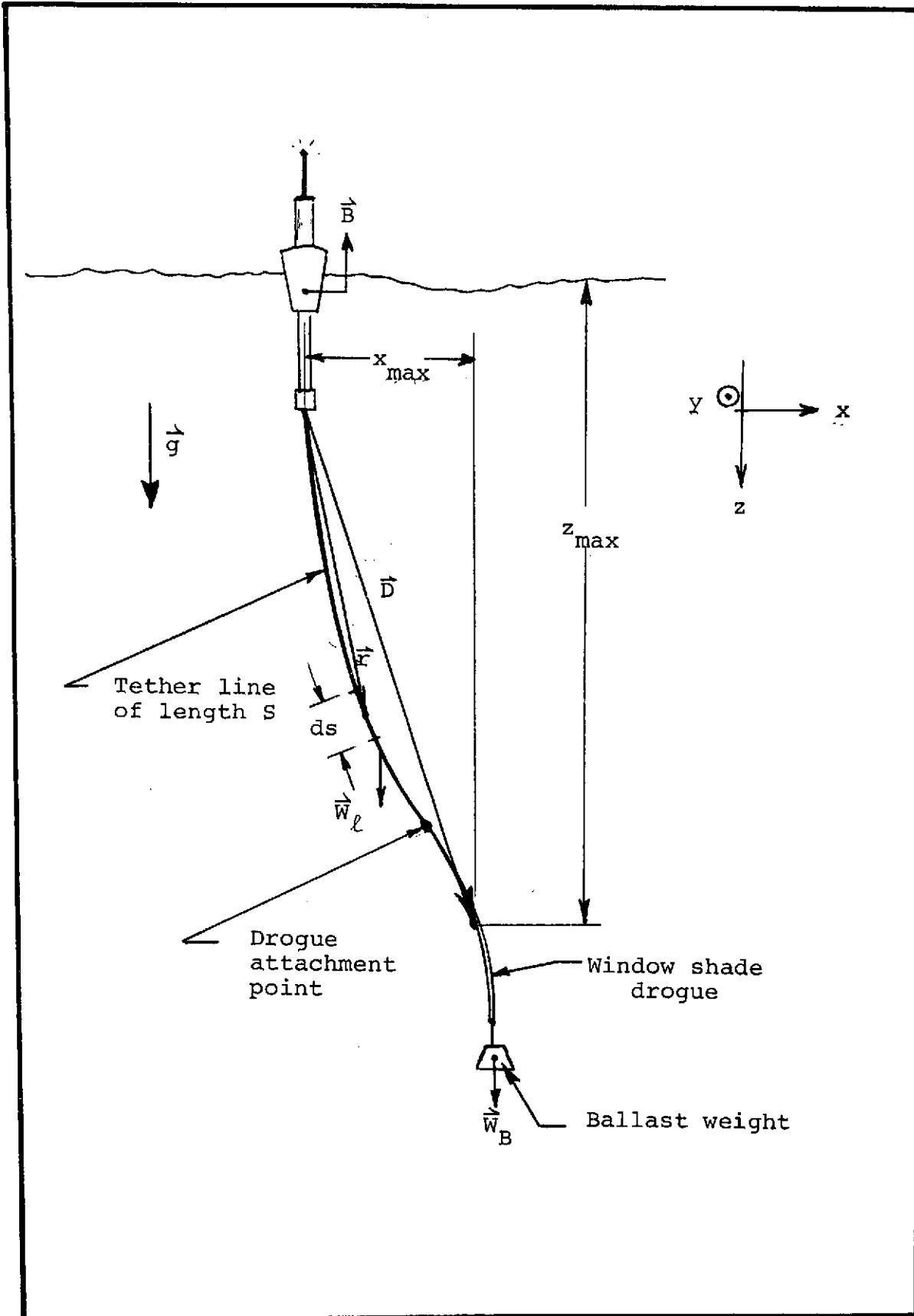


Fig. 3 Simplified Buoy Statics - Plan View

$$\begin{aligned}
\vec{D} &= \text{radius vector between buoy and center of} \\
&\quad \text{drag of drogue} \\
&= \vec{i} x_{\max} + \vec{j} y_{\max} + \vec{k} z_{\max} \quad (4) \\
d &= \text{tether line diameter} \\
C_D A &= \text{drag area of drogue} \\
C_{DC} &= \text{drag coefficient of tether line} \\
\vec{V}_{\text{rel}} &= \text{relative velocity of water mass seen by drogue} \\
\vec{V}'_{\text{rel}} &= \text{relative velocity of water mass seen by tether} \\
&\quad \text{line}
\end{aligned}$$

A summation of moments taken about the buoy leads to the following vector equation:

$$\begin{aligned}
\vec{M}_B = 0 = & -\vec{w}_B \times \vec{D} - \rho_c \int (\vec{g} \times \vec{r}) ds \\
& + \vec{L} \times \vec{D} + \frac{1}{2} \rho |V_{\text{rel}}| C_D A \vec{V}_{\text{rel}} \times \vec{D} \\
& + \frac{1}{2} \rho |V_{\text{rel}}| C_{DC} d \int_0^S (\vec{V}'_{\text{rel}} \times \vec{r}) ds \quad (5)
\end{aligned}$$

In equation (5) the relative velocity at the drogue is composed of two components as follows:

$$\vec{V}_{\text{rel}} = \vec{V}_d - \vec{V}_c \quad (6)$$

where  $\vec{V}_d$  is the drift velocity of the whole drogue/buoy combination (see Fig. 2) and  $\vec{V}_c$  is the water velocity at the depth of the current.

By reference to the force diagram in Figure 2 it is assumed that the tension in the drogue,  $F_D$ , lines up with the tether line (i.e., drogue develops no side lift) and not in the direction of drift. In the vector velocity diagram the true velocity measured by monitoring the buoy position at times

$t_0$  and  $t_1$  is the summation of the drift velocity in the direction of the current plus the relative velocity by the drogue which gives rise to drogue tension,  $F_D$ . Therefore if one knows the value of relative velocity,  $V_{rel}$ , it is possible to approximate the current velocity,  $V_C$ , by using the vector velocity triangle shown in Figure 2.

The determination of relative velocity at the drogue can be done in many ways. It might be possible to do it directly with a current meter if one could afford the cost and if surface-induced mooring dynamic motion did not degrade the measurement. The thrust of the work reported herein has, however, assumed that an easier determination would be the vector sum of all the forces above the drogue. This value would be either by a measurement or a calculation of wind and water drag on the buoy and tether line. Knowing the total drag on the drogue then permits one to apply the following equation to estimate relative velocity

$$V_{rel} = \sqrt{\frac{2F_D}{\rho C_D A}} \quad (7)$$

The application of equation (7) necessitates a knowledge of the  $C_D A$  product. The work reported herein documents the tests directed towards the measurement of the  $C_D A$  product of numerous drogues, while selecting an optimum shape configuration in terms of the outlined program goals.

### 3.0 Test Shapes and Configurations

Ten different shapes were tested in the M.I.T. Ship Model Towing Tank. Most shapes contained many variations such that a total of 40 different configurations were tested.

The following test shapes were chosen on the basis of historical precedence:

- (1) Parachute
- (2) Bucket sea drogue
- (3) Conical sea anchor
- (4) Two axis crossed vanes
- (5) Buoyed fishing net streaming parallel to the direction of flow

Other new shapes were conceived on the basis of program goals and ultimately tested in a scale model version. These included the following:

- (1) Three axis crossed vanes
- (2) Cylinder, vertically aligned
- (3) Sphere
- (4) Plastic sheet in the form of a window shade

This section describes the shapes and variations to each shape that were model tested in the towing tank.

### 3.1 Parachutes

Three different model parachute configurations similar to that shown in Figure 4A were tested; a 16.5" diameter (deployed diameter) slightly negatively buoyant toy parachute approximating a hemispherical shape when deployed, a 26" diameter neutrally buoyant nylon chute formed from a flat circular section; and a 30" diameter nylon chute with a heavy 15-gram ring at its apex making it very negatively buoyant. All three chutes contained 8 shroud lines of equal length (when untwisted), of length equal to approximately 90% of the deployed chute diameter.

### 3.2 Bucket Sea Drogue

A single bucket sea drogue was fabricated of unbleached muslin material in the same proportions as a bucket drogue

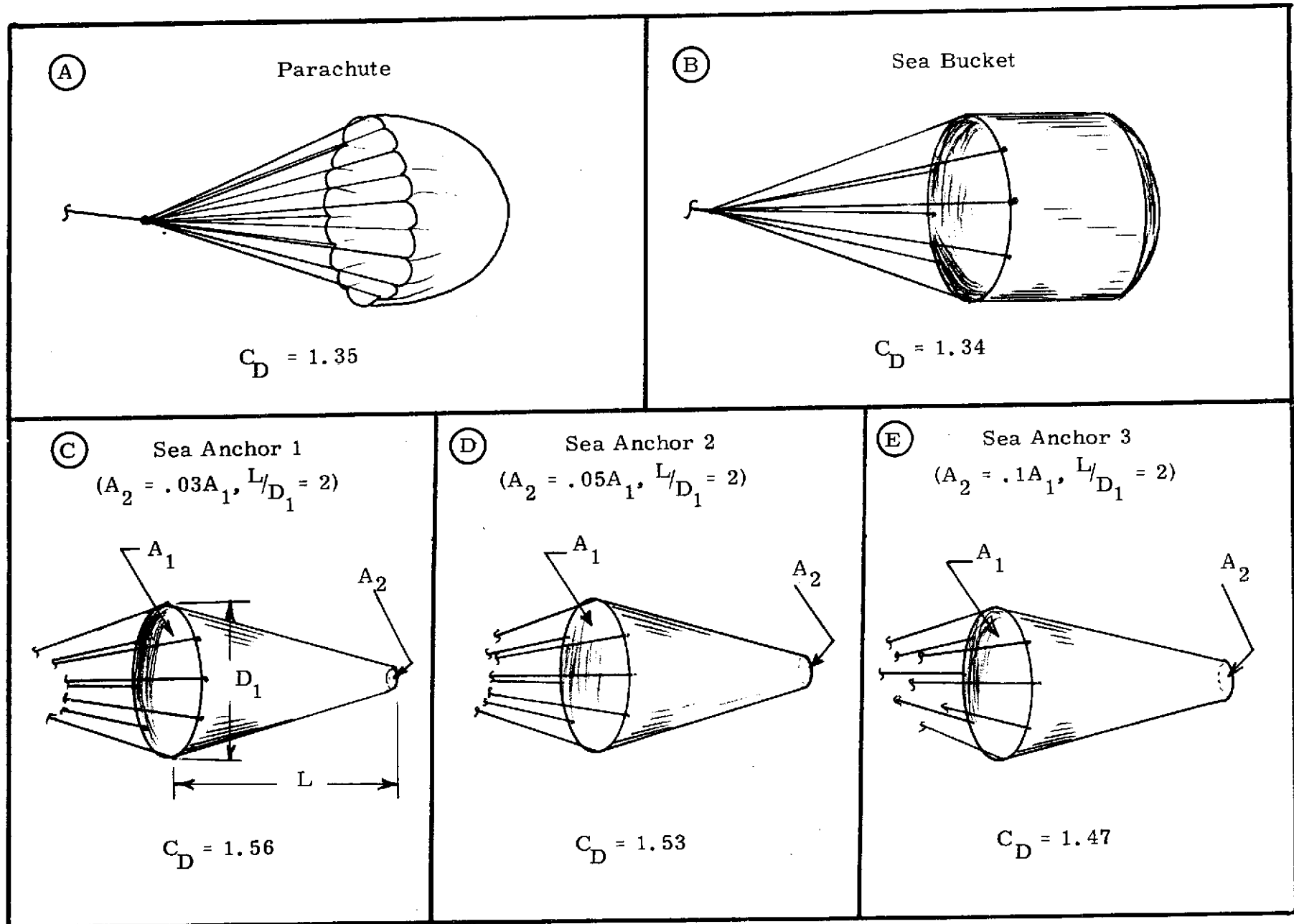


Figure 4  
Model Sea Drogues

favorably reported by Baker (1918) (see Figure 4B.). It had a 15" diameter and a bucket depth of approximately 11 1/4". The bucket bottom was rounded with a maximum belly depth of 4 inches. There were 8 shroud lines 30-inches long. The diameters of the top and bottom of the bucket were rigidized by only a sewn seam instead of a rigid ring or rope.

### 3.3 Conical Sea Anchors

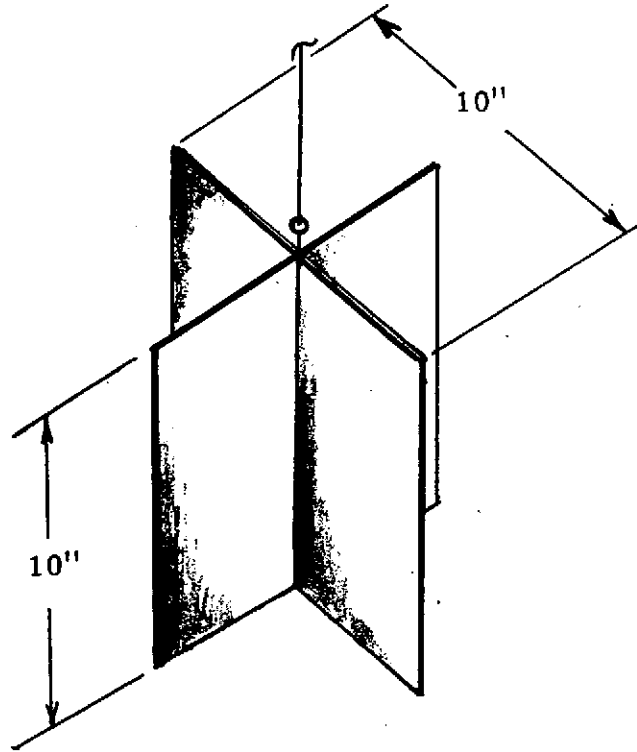
Three conical sea drogues were fabricated of unbleached muslin as shown in Figures 4C, D, and E. Drogues such as this had been successfully employed by Montgomery and Stroup (1962). The inlet diameter of each drogue was held constant at 15 inches while the down-stream spill hole had areas of 3, 5, and 10 percent of that of the inlet hole. The literature had indicated that a 5% downstream spill hole had exhibited the best stability to lateral oscillations. No large oscillatory differences were observed in the shapes described. All three sea anchors had a length to major diameter ratio of 2 because tests described by Montgomery and Stroup (1962) also indicated this ratio as an optimum for oscillation stability.

### 3.4 Crossed Vanes or Current Crosses

The following six versions of crossed vane drogues were tested and their average drag coefficient reported:

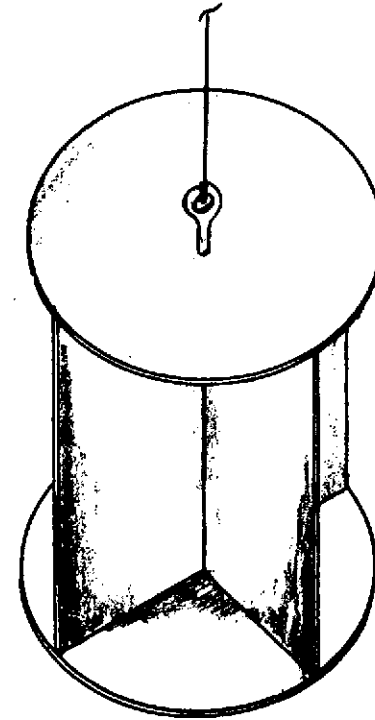
- (1) 2-axis, aluminum (.062" wall thickness)  
10"×10" plates, no end plates (see Figure 5).
- (2) same as (1) with 10" diameter end plates (.062" wall) (see Figure 5).
- (3) 3-axis, aluminum (.062" wall thickness),  
10"×10" plates, no end plates.
- (4) same as (3) with 10" diameter end plates  
(.062" wall).

No End Plates



$$C_{D,A} = 0.83 \text{ ft}^2$$

With End Plates



$$C_{D,A} = 0.9 \text{ ft}^2$$

Figure 5

Two Axis Crossed Vanes Models

- (5) 2-axis, polyethylene walls (.006" thick), 10"×10", no end walls.
- (6) 3-axis, polyethylene walls (.006" thick) 10"×10", no end walls.
- (7) 3-axis, aluminum (.062" wall) 10" w.× 20" h. plates, with end plates

Figure 5 is a sketch of a typical 2-axis crossed vane drag device. The design is generally implemented by interleaving 2 plates about a central axis as a common boundary such that the plates are mounted at 90 degrees from each other. Figure 5 also shows the presence of end plates. End plates were hoped to approximate an infinitely long crossed vane wherein drag reduction due to end spillage is negligible compared to the overall plate drag.

### 3.5 Buoyed Fishing Net

Montgomery and Stroup (1962) had employed large purse seine nets as drag services for locking to surface currents. A fishing net is an appealing surface drogue in that many large, old nets are readily available and can be easily stored on the deck of a ship. Figure 6A shows the manner in which models were constructed of fine mesh fishing nets for tow tank tests. Two different mesh sizes were tested in the manner described.

### 3.6 Cylinder

A weighted plastic cylinder with solid discs for end plates was tested. (See Figure 6B.) It was anticipated that a full scale model of such a shape could be easily collapsed by compressing the shape along its longitudinal axis, causing the plastic to deform. In its fully collapsed condition the two discs would be adjacent to each other, separated by only the collapsed plastic. In this state the device could be

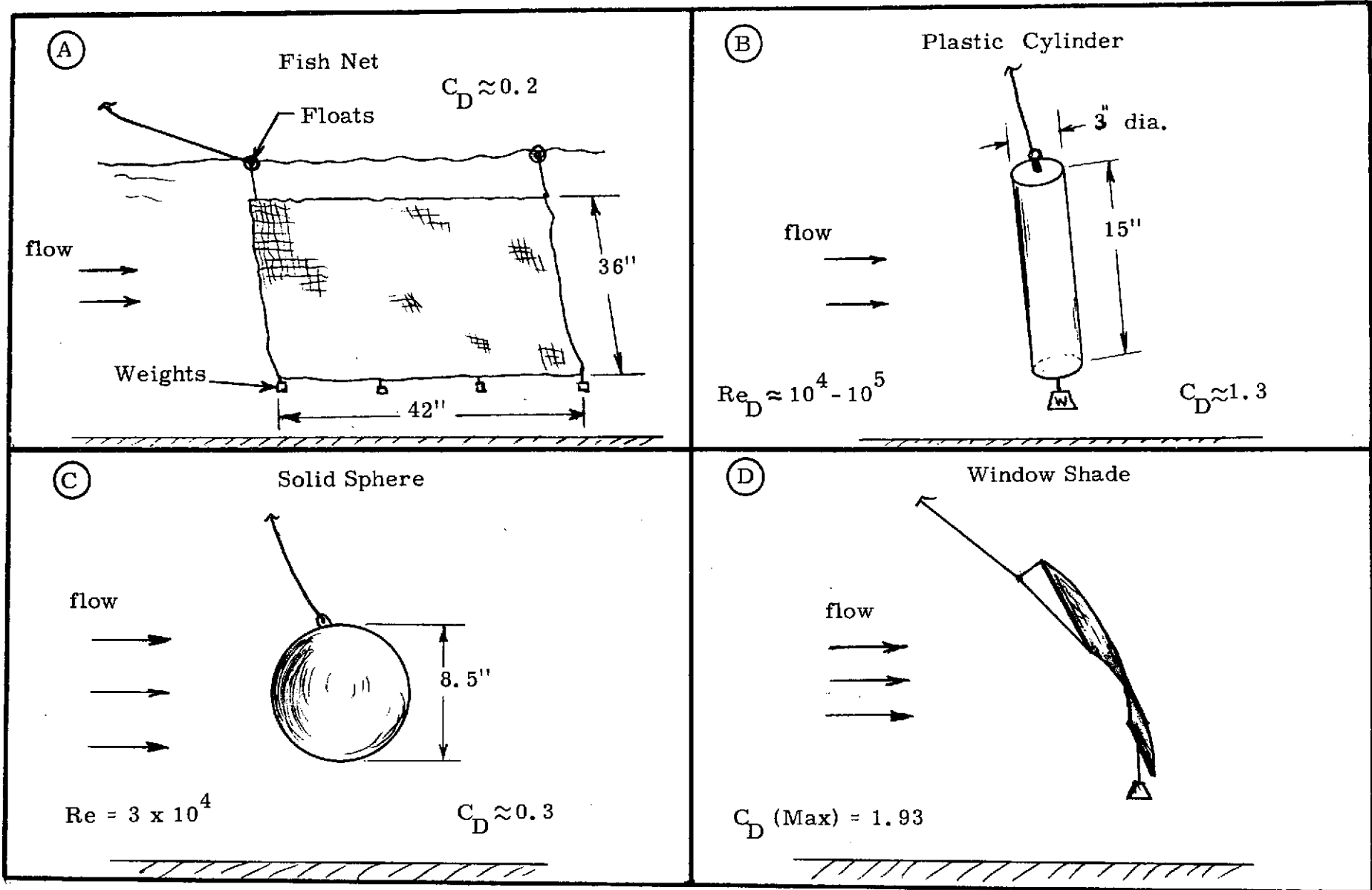


Figure 6  
Test Model Drogues

easily stored aboard the deck of the ship. When being deployed, the ballast weight at the bottom would bring about the full extension of the cylinder walls.

### 3.7 Sphere

A solid sphere, as shown in Figure 6C, was tested preliminary to building and testing an equivalent floppy, water-filled plastic sphere. A full scale, thin-walled plastic sphere which is inflated with ambient water can be made extremely large and yet occupy a modest volume for deck storage. In spite of the small drag coefficient of a sphere, the lack of real size limits on the sphere permits the drag area,  $C_D A$ , to be as large as desired. For example, a 30-foot diameter sphere with a .006-inch thick wall contains a material volume of only 1.41 cubic feet of material. For most plastics such as Herculite\* this device would weigh only 94 pounds, a weight which can be managed on a ship's deck.

### 3.8 Window Shade or Curtain Drogues

A sheet of thin-walled plastic in any shape (rectangle, triangle, or diamond) which is supported by one (triangles and diamonds) or two (rectangles) poles horizontally oriented is referred to as a window shade drogue. An example of a rectangular version is shown in Figure 6D. Numerous shapes were tested, all of which were pendulously suspended by a single string and ballasted on their bottom edge.

### 4.0 Test Description

The basic goals of the scale model drogue test program were manifold. In general the tow tank tests to be described sought answers to the following questions:

---

\* Herculite is the trade name for a polyvinyl chloride (PVC) plastic material reinforced by nylon yarn, manufactured by the Herculite Protective Fabrics Corp., N.Y., N.Y. It is especially resistive to degradation from ultraviolet rays.

(1) What are the deployment characteristics of a shape like a parachute or sea bucket which depend on a relative velocity to achieve a rated drag area?

(2) What are the full scale drag coefficients and drag areas of candidate shapes and configurations as a function of relative velocity?

(3) How does buoy-induced dynamic heave motion influence the performance of a drogue?

Figures 7A and 7B outline the test approach that could theoretically be followed in order to answer many questions relating to drogues. The basic tests involved measuring the drogue drag force and applying the following equation to get drag area:

$$C_D A = \frac{F_D}{\frac{1}{2} \rho V_{rel}^2} \quad (8)$$

To get the drag coefficient,  $C_D$ , the drag area was in all cases divided by the full frontal area of the drogue if it were hanging vertically and fully perpendicular to the flow.

Figures 7A and 7B are self explanatory. The last test is aimed at measuring by how much a drag element's drag coefficient or drag area is altered by the introduction of a dynamic heave which might normally arise from a buoy. The amount of heave a drogue will receive is a function of many parameters including the sea state, buoy response characteristics, mooring line elasticity, and drogue depth. In the model tests the drogues were pendulously suspended from a 2.5-foot length of .050-inch diameter cotton string. Peak-to-peak heave amplitudes of 1.5, 2.56, and 3.6 inches were imparted at different times, all at a frequency of 1.6 Hz. This is a Froude scaled response frequency equal to a full scale response of 0.4 Hz. This value is the heave natural frequency of the Lockheed Low Capability

Test Type	Test Shape(s) and Reason for Test	Method of Holding Drag Element	Scaling Method	Input
1	Solid body (e. g. crossed vanes) Establish $C_D$ for basic geometry irrespective of Froude effects.	Clamped	Reynolds	Steady Pull
2	Solid body. Establish $C_D$ for geometry including Froude effects.	Suspend from string. Use scaled ballast weight.	Reynolds	Steady Pull
3	Plastic version of shapes tested in 1 and 2. Look for effects of plastic versus solid wall.	Suspend from string. Use scaled ballast weight.	Reynolds	Steady Pull
4	Parachutes, sea anchors, etc. Establish $C_D$ of device as function of velocity at Reynolds speeds.	Suspend from string. Use scaled ballast weight.	Reynolds	Steady Pull
5	Solid body (e. g. crossed vanes). Establish baseline $C_D$ in Froude scaling tests.	Suspend from string. Use scaled ballast weight.	Froude	Steady Pull

Figure 7A.

## TOW TANK TEST SUMMARY

Test Type	Test Shape(s) and Reason for Test	Method of Holding Drag Element	Scaling Method	Input
6	Plastic version of shapes tested in 5. Look for effects of solid vs. plastic walls at Froude speeds. Establish $C_D$ of device as function of velocity at Froude speeds.	Suspend from string. Use scaled ballast weight.	Froude	Steady Pull
7	Parachutes, sea anchors, etc. Establish $C_D$ of device as function of velocity at Froude speeds.	Suspend from string. Use scaled ballast weight.	Froude	Steady Pull
8	Same shapes as in 5, 6, and 7. Compare drag data looking for effects due to heave only.	Suspend from string. Use scaled ballast weight.	Froude on both speed and heave frequency	Steady Pull and Heave
9	Parachutes, sea anchors, etc. Look for minimum velocity required for full deployment. Derive $C_{DA}$ as function of velocity.	Suspend from string. Use scaled ballast weight.	Froude	Steady Pull

Figure 7B.

## TOW TANK TEST SUMMARY

Buoy (LCB) and midway between the heave natural frequencies of the Magnavox and G.E. LCB's. The intent of the first eight types of tests is to establish the dominant effect governing the performance of a drogue (gravity or viscosity) in addition to momentum forces. Froude scaling takes into account gravity effects in a scaled manner, while Reynolds scaling properly scales viscosity effects. It is not practical to properly scale for both effects simultaneously as will be shown.

Simply stated, the total drag force on a drag element can be written as being proportional to the three effects of pressure, viscosity, and gravity as follows:

$$F_D = K_1 \rho V^2 A + K_2 \mu \frac{\partial V}{\partial r} A + K_3 \rho \mathcal{V} g \quad (9)$$

where:  $K_1, K_2, K_3$  are proportionality constants

$\rho$  = fluid density

$V$  = fluid relative velocity

$A$  = body projected area or surface area

$\mu$  = fluid viscosity coefficient

$r$  = radial distance from body

$\mathcal{V}$  = volume of body material

$g$  = gravitational constant

If  $L, L^2,$  and  $L^3$  are substituted for radius ( $r$ ), area ( $A$ ), and volume ( $\mathcal{V}$ ) respectively, the partial derivative becomes merely  $V/L$  and equation (9) becomes more simply:

$$F_D = K_1 \rho V^2 L^2 + K_2 \mu V L + K_3 \rho L^3 g \quad (10)$$

In order to insure proper scaling and apply the above equations all dimensions should be reduced by a constant scale factor ( $\lambda$ ) between the full scale and the model according to the relation:

$$L_s = \lambda L_m \quad (11)$$

where s and m refer to the full scale and model respectively. Therefore a model of the same material density as the full scale should be lighter by a factor of  $\lambda^3$ .

Drag forces on bluff bodies in a flow field are always dependent on pressure forces (i.e.,  $\rho V^2$  forces).

Many shapes exhibit a drag force that is always independent of gravity forces. A clamped plate in a flow field is an example. On the other hand a pendulously supported flat plate in a flow field exhibits a drag force very dependent on its weight or in other words on gravity forces. The drag force on the pendulous plate is, however, still dependent on the fluid viscosity as well. This is the case of the pendulous free drifting drogue.

In order to accurately predict the forces that a full scale model will encounter by model tests it is necessary to keep the ratio between the pressure forces and the second dominant effect constant. If the second dominant effect were viscous forces one should keep the ratio of the first and second force terms in equation (10) constant. That is

$$R = \frac{\rho V^2 L^2}{\mu V L} = \frac{\rho V L}{\mu} \quad (12)$$

This is the Reynolds number.

If gravity forces were a more dominant effect than viscous forces one would keep the following ratio constant between model and full scale tests:

$$Fr^2 = \frac{\rho V^2 L^2}{\rho L^3 g} = \frac{V^2}{Lg} \quad (13)$$

This ratio is the square of the Froude number (Fr).

It can be seen that it is not practical to keep both the Froude and Reynolds number constant simultaneously. If it is assumed that both equations (12) and (13) are constants equal to R and Fr respectively, from (13)  $V = Fr\sqrt{Lg}$  is substituted in (12) to give:

$$\frac{R}{Fr} = \left( \frac{g^{1/2} L^{3/2}}{\nu} \right)_m = \left( \frac{g^{1/2} L^{3/2}}{\nu} \right)_s \quad (14)$$

where:

$$\nu = \frac{\mu}{\rho} = \text{fluid kinematic viscosity.}$$

Rearranging this equation gives:

$$\nu_m = \left( \frac{g_m}{g_s} \right)^{1/2} \left( \frac{L_m}{L_s} \right)^{3/2} \nu_s = \left( \frac{g_m}{g_s} \right)^{1/2} \frac{\nu_s}{\lambda^{3/2}} \quad (15)$$

This equation says that in order to keep full scale and model Reynolds and Froude numbers constant simultaneously the kinematic viscosity of the model test fluid should be decreased by the dimensional scale factor to the 1.5 power. This is very hard to do for scale factors greater than 2 when the full scale working fluid is water. The following three sections will describe the test approaches employing both Reynolds and Froude scaling and methods of minimizing the problems arising from the above inability to simultaneously scale by both methods.

#### 4.1 Reynolds Scaling

The basic intent of Reynolds scale model testing is to preserve similitude on boundary layer and flow separation effects. Both effects depend on viscosity and have a strong influence on the drag coefficient at low Reynolds numbers ( $R \approx 100$ ) and at high values ( $R \approx 10^4$  to  $10^5$ ) where flow becomes fully turbulent. In

the latter case the drag coefficient will be generally reduced as the flow becomes turbulent depending on the shape and roughness.

It can be seen in Figure 7A that Reynolds scaling would be employed in four different types of tests. The first type is a straight-forward measurement of the drag of a completely submerged solid body in a clamped configuration. In this case there are no permissible Froude effects on the body itself because it is clamped. If it is submerged sufficiently it should not generate waves which are also gravity dependent.

The second type of test is run with the same shapes as in test 1. In this case the drag device is pendulously suspended by a string. Differences in the test data between test 1 and 2 are attributable to the new effect permitted, gravity or Froude effects.

The third type of test is conducted in exactly the same manner as test 2 except the walls of the test device are fabricated of plastic. If the device is weighted in the same manner differences in the data between test 2 and 3 are due to the fact the device is made of plastic.

The fourth type of test is very much like the third, except that the shapes depend on a minimum relative velocity in order to fully deploy. It was found that the velocity at which the shape (e.g., parachute) is fully deployed is a function of its weight in water. Therefore, test 4 is really only useful after the shape is fully deployed.

#### 4.2 Froude Scaling

For the case of non-neutrally buoyant drag devices, which greatly dominated the tests described herein, gravitational forces are an important part of the performance. Of the shapes and configurations described in section 3 only the shapes which

depend on a minimum velocity for deployment (e.g., parachutes) will maintain approximately a constant area in high flow conditions. This fact is due to the multiplicity of symmetric tether lines, which secure the drag device to a common tether point, attempting to constantly balance moments in high flow conditions. In low flows, however, it is shown that the deployment characteristics of such shapes are gravity sensitive.

Shapes such as crossed vanes, cylinders, or window shade drogues which are suspended by basically a single point above the device will pivot in a pendulous manner as flow changes. In the process, the drag area ( $C_D A$ ) of the device will change and is a function of the drogue weight distribution and the amount of ballast weight attached beneath. Therefore, Froude scaling is necessary to account for the effects of the weight of both the drogue and the ballast.

Froude scaling tests of pendulous drogues to a first approximation produce a scaled drogue shape and streaming angle with respect to vertical as a function of velocity. In this case the gravity forces are balancing the pressure or drag forces imparted by the flow in order to achieve moment balance about the attachment point [see equation (5)]. The drag force on the device may not be exactly scaled because the viscous (i.e., Reynolds) effects somewhat influence the drag coefficient through boundary layer and flow separation effects. For a first approximation these differences in drag coefficient can be neglected and the drogue shape and streaming angle recorded as the basic result of the Froude tests. Subsequently higher speed Reynolds scale model tests can be run in which the same shape and angle are reproduced by an appropriate choice of ballast weights. In this manner Froude scaling tests are conducted in order to specify a geometry for subsequent Reynolds tests. The drag data from the Reynolds tests so conducted

accounts for both gravity and viscous effects. This test approach does, however, have its practical limitations which will be described in the test results section.

As described the method is not exact. It can be made very accurate, though, if the proper scale factor and speed ranges are chosen. As shown in Figure 8 the drag coefficient of a sphere, an infinite cylinder, and a disc as a function of Reynolds number varies markedly. For Reynolds numbers between approximately 400 and  $5 \times 10^5$  the value of  $C_D$  varies by less than 25% (Batchelor, p. 341). Therefore by operating over an equivalent range of Reynolds numbers for all pendulous shapes, the drag coefficient associated with the low velocity Froude tests will not greatly differ from the full scale value. Because the  $C_D$  value appropriate to a given Froude test dictates only the physical shape that a Reynolds test will employ, differences in  $C_D$  at Froude speeds are less important on the overall result.

For those tests in which a vertical dynamic motion of the attachment point is used to simulate buoy motion, Froude scaling applies. Such is true because the drogue response is dictated by the weight (mass) of the drogue which depends on gravity. For these tests the Froude number is modified by substituting  $V = \omega L$  in equation (13). This results in a frequency dependent Froude number:

$$Fr = \omega \sqrt{\frac{L}{g}} \quad (16)$$

Therefore it can be seen that in order to hold Fr constant the frequency of a model test is increased by the square root of the scale factor ( $\lambda = 16$  for these tests).

#### 4.3 Froude Scaling of Window Shade Drogues

Window shade scale model drogue testing provides an opportunity to employ a modified Froude Scaling. If it can be

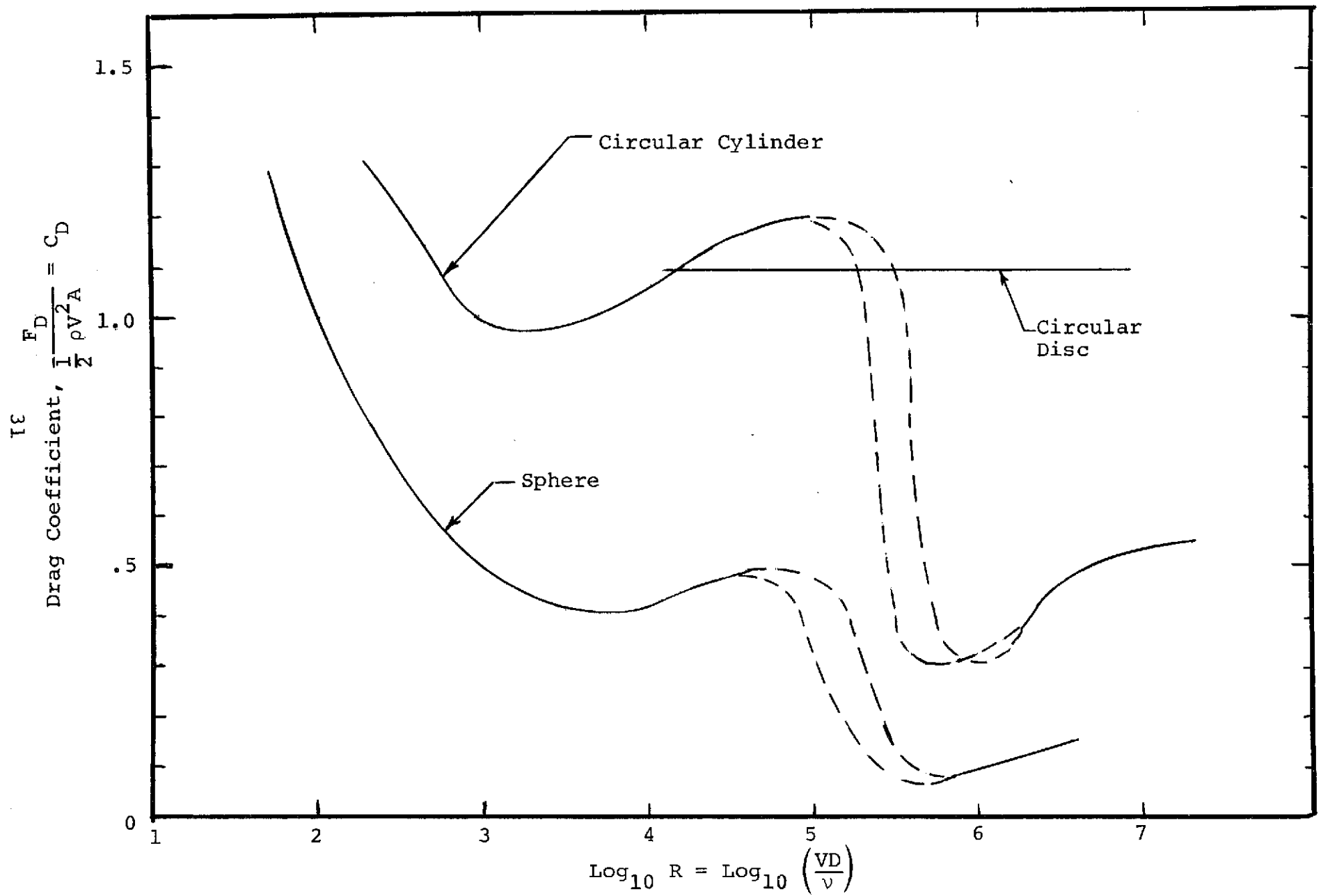


Fig. 8 Drag Coefficients of Simple Shapes (from Batchelor, 1967)

assumed that the models are towed at sufficient depths, such that surface waves are not produced, the following scaling technique would hold true in the case of fabric models, the thickness of which is the same as the full scale version. For Froude scaling in general the following applies:

$$\left(\frac{\text{pressure forces}}{\text{gravity forces}}\right)_m = \left(\frac{\text{pressure forces}}{\text{gravity forces}}\right)_s \quad (17)$$

where the subscripts m and s apply to the model and the full scale version respectively. These force ratios can be written in the following manner:

$$\left(\frac{\rho_w V^2 LW}{\rho_d LWtg}\right)_m = \left(\frac{\rho_w V^2 LW}{\rho_d LWtg}\right)_s \quad (18)$$

where:

- $\rho_w$  = water density
- L = drogue length
- W = drogue width
- t = drogue thickness
- $\rho_d$  = drogue density (lbs/ft<sup>3</sup>)

The length and width can be cancelled on each side of the equation within the parenthesis. In addition the gravity and water density terms can be cancelled on either side of the equation. By the fact that the window shade drogue material (herculite in most cases) is assumed to be the same material that would be used in the ocean,  $\rho_d$  and t are constant between model and full scale; allowing the cancellation of these terms on both sides of the equation. All of these cancellations leave the equality:

$$V_m = V_s \quad (19)$$

Thus, a modified Froude scaling is developed for window shade drogue models which assumes that the model is reduced in size in only two of the three dimensions, owing to the fact that the material thickness cannot be readily scaled. It does, however, mean that the ballast weight of the drogue should be reduced by  $\left(\frac{1}{\lambda^2}\right)$  from the full scale weight ( $\lambda =$  scale factor) and not by  $\left(\frac{1}{\lambda^3}\right)$ .

By keeping the model velocity equal to the full scale ocean velocity, rather than reduced by  $\frac{1}{\sqrt{\lambda}}$  as normal Froude scaling dictates, the drag forces on the drogues are higher and easier to measure because the signal-to-noise ratio is increased.

During the modified Froude scaling tests the window shade drogue shape is recorded by underwater Polaroid photos of the drogue projected against a uniform grid pattern. As already described efforts are later made to duplicate this same shape at the higher speeds found in Reynolds scaling by increasing the ballast weight by an appropriate amount. By duplicating the shape derived in Froude tests during a Reynolds test, Froude or gravity effects are for the most part eliminated. In this manner the drag coefficient,  $C_D$ , is derived as a function of Reynolds number only. An error would again arise if surface waves are generated during the Reynolds tests. This problem is present irrespective of the Froude scaling approach.

## 5.0 Test Apparatus

All scale model experiments were conducted in the M.I.T. Ship Model Towing Tank, operated by the Ocean Engineering Department of M.I.T. The tank itself measures 52.5 feet long by 9 feet wide. It can be filled to a maximum water depth of 50 inches.

The test devices are supported from and towed by a carriage which is supported on rollers at a height of approximately 15 inches above the highest water level. Drag forces are measured on the tow carriage by a force block device which employs horizontal beam bending as a spring. The position of the beam is electrically monitored by an LVDT (Linear Variable Differential Transformer).

The maximum towing force which the carriage can withstand is uncertain (approx. 150 pounds) but the capability of the force blocks varies with the beam dimensions. A total beam deflection of .056 inches caused transducer bottoming in order to protect the force blocks from yielding.

Numerous modifications to the existing carriage drive mechanism and force blocks were required in order to conduct the scaled tests at very low (Froude) speeds. At the low speeds the drag devices produced very low drag forces. In addition, a device shown in Figure 9 was designed to be mounted on the carriage in order to simulate the buoy-induced heave at the upper end of a mooring line. This device consisted of a scotch yoke linear, vertical displacement drive powered by a motor driving an infinitely variable belted speed reducer. As shown in Figure 9 the drag force measuring device (LVDT not shown) moves with the heave input. The portion of the heave device which travels vertically is constrained by linear bearings to slide on vertical guide rods.

When testing clamped devices such as crossed vanes or drogues such as parachutes which depend on a relative velocity for deployment, a low drag ( $C_D \approx .2$ ) faired strut was attached to

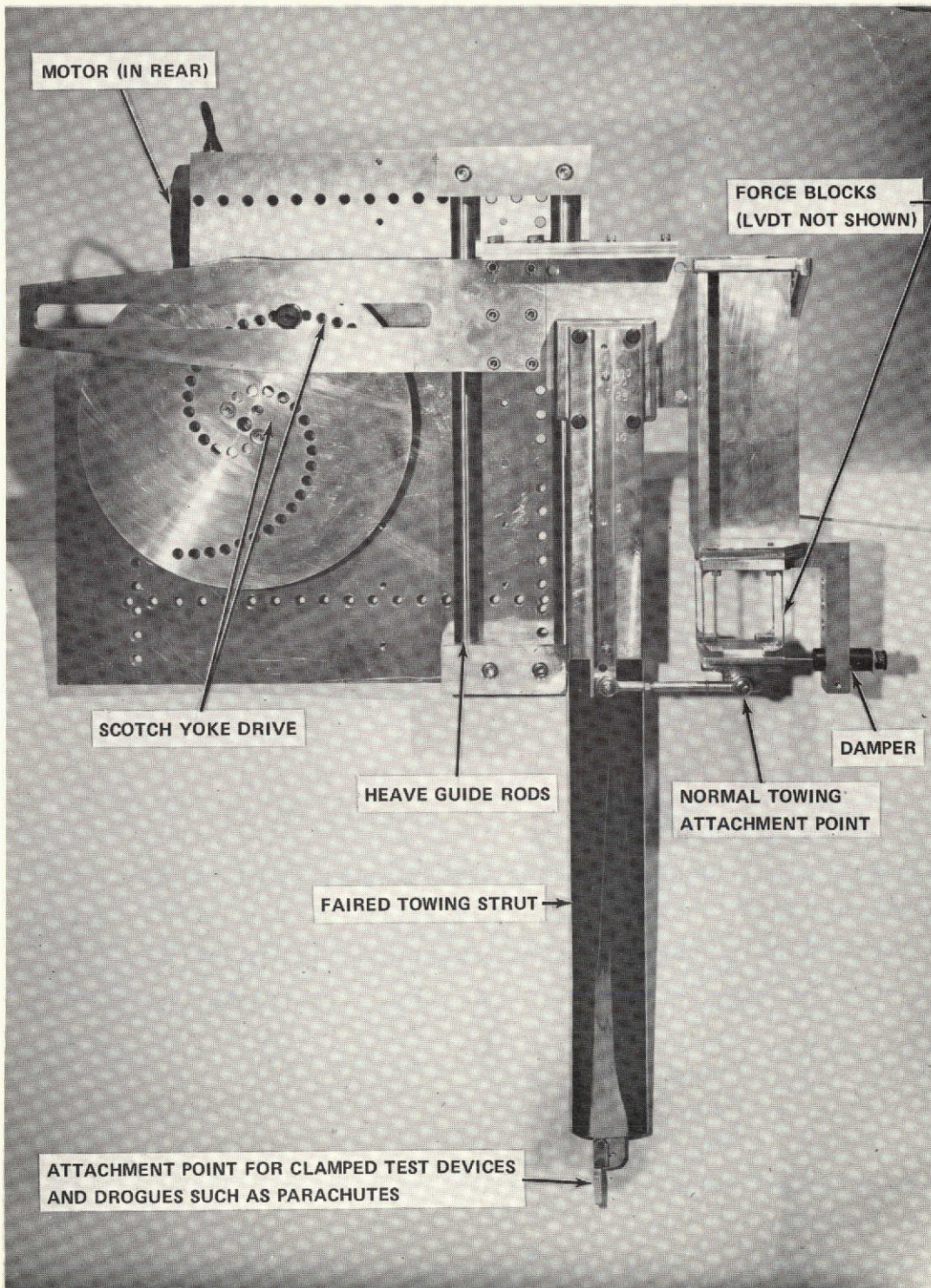


Fig.9 Heave input and drag measurement apparatus.

the heave mechanism as shown in Figure 9 and allowed to pivot on a bearing at its upper end. The test shapes were then attached at the bottom of the strut. The drag force was imparted to the force blocks via a variable ratio moment arm advantage which kept the LVDT and force blocks out of the water.

The following is a list of tow carriage capabilities as they originally existed and after modifications:

Electrical:

10 cables, 5 shielded wires/cable

115 VAC power (1 amp max.)

After Modification: 115 VAC power (15 amp. max.) carriage:

<u>Before Modifications</u>	<u>After Modifications</u>
Speed Range: .2 to 6.57 knots (in 80 steps)	.013 to 6.57 knots (infinitely variable to .39 knots)
Heave Amplitude: None	1.5" p/p to 12" p/p
Heave Frequency: None	.3 Hz to 1.8 Hz
Tension Range:.1 to 50 lbs.	.003 to 60 lbs

At the very low tension ranges mechanical damping was introduced in order to minimize vibrations of the flimsy force blocks. Numerous tests were also conducted in order to ascertain the effects of heave on a low force measurement.

## 6.0 Test Results

The results indicate that a window shade drogue, when properly sized, can be the best overall drogue in terms of the program goals. Tests were conducted on all the shapes described in section 3 and covered 9 working days during three test phases. A total of 539 test runs were made including calibrations. The first test phase (4 days) included pure drag tests of most of the shapes at both Reynolds and Froude scaling speeds. During the second test phase (3 days) Froude scaling tests were continued and vertical heave was introduced. The third test phase (2 days) concentrated on steady drag tests of only window shade drogues in many different shapes. Super 8 mm movies and 35 mm still photos were taken of many of the test runs. Figures A-1 through A-9 in Appendix A present a tabular summary of all the model test results. This section describes the results for all the drag devices.

### 6.1 Parachute Tests

As described earlier, numerous investigators began employing parachutes as current locking devices during the 1950's and have been used extensively up to the present. The parachute is an attractive drogue device from many viewpoints:

- (1) ease of storage and assumed simplicity of deployment
- (2) low cost and availability (many chutes for oceanographic purposes can be obtained on a government surplus basis).
- (3) high drag coefficient

As pointed out by Volkmann et al (1956), one of the first users of large parachutes, the normally-reported drag coefficient of a chute in air varies with material porosity between the values of 1.3 and 1.7. It is further pointed out

that the parachute is inherently unstable in that it will stream at angles of between  $22^\circ$  and  $45^\circ$  to the flow direction depending on material porosity. It has more recently been shown by Heinrich and Haak (1971) that different parachute designs are more susceptible to the instability problem at low effective porosity. The circular flat chute is the most unstable design, streaming at an angle of approximately  $45^\circ$  to the flow at zero porosity, while the personnel guide surface is the most stable. All chute designs become more stable as the porosity is increased; however, the drag coefficient decreases.

The problem of the streaming angle of the chute as an error source on current direction has been neglected in general by oceanographers in that limited observations by SCUBA divers seem to indicate that a downward angle is preferred. The tow tank tests reported herein find that such is true only if the chute is negatively buoyant. Furthermore, it was found that if the model chute was negatively buoyant after opening, it streamed at downward angle at low speeds ( $V \approx 0.2$  Knots) and gradually rose up and then sideways (angles of  $30^\circ$  to  $40^\circ$ ) as the speed increased ( $V \approx 0.5$  Knots). It was eventually observed that the chute oscillated from side-to-side and down to the extreme angles in a somewhat pendulous manner. The period of oscillation of the chutes varied with the towing speed as vortex shedding theory describes but oscillatory periods were not measured precisely.

For a model chute which for all practical purposes was neutrally buoyant the chute would stream directly parallel to the flow at low velocities. As the speed increased it would go to the extreme angles of  $30^\circ$  to  $45^\circ$  and slowly move in a coning manner with respect to flow along the central axis of the cone. It did not seem to display the same oscillatory response as a function of speed that was observed by more negatively buoyant models.

Two types of tests were conducted on model parachutes:

- (1) Deployment tests - through Froude scaling measure the minimum velocity required to cause the chute to "inflate" and give a full rated drag coefficient.
- (2) Steady pull tests - measure the drag coefficient as a function of Reynolds number.

Figure 10 shows the results of deployment tests on 3 model parachutes. In these tests Froude scaling was applied because gravity forces are assumed to be a dominant effect on deployment characteristics. The chutes were placed in the water and towed in stages at higher and higher speeds until they deployed and gave their full drag coefficient. Figure 10 plots the measured drag area as a function of relative velocity.

It can be seen that there is a knee in each curve when the chute fully deploys. The chute which is most neutrally buoyant (number 1) deployed at between .02 and .03 knots. By Froude scaling with a scale factor of 16 this speed is equivalent to a full scale speed of approximately .08 to .12 knots.

Chute number 2 attained its full drag coefficient at a speed of approximately .05 knots, equivalent to approximately 0.2 knots in a full scale version. At very low speeds the measured drag area increased. It is believed that at these speeds viscous shear forces began to be a primary drag and not dynamic pressure forces.

Chute number 3 dramatically demonstrates the role of gravity or weight on the chute deployment. A 15-gram ring, used for retrieving the chute by spilling the flow, was mounted at the center of the canopy (shown in Figure 10.). This weight severely inhibited the initial deployment by keeping the chute weighted down. It also caused the chute to assume a downward

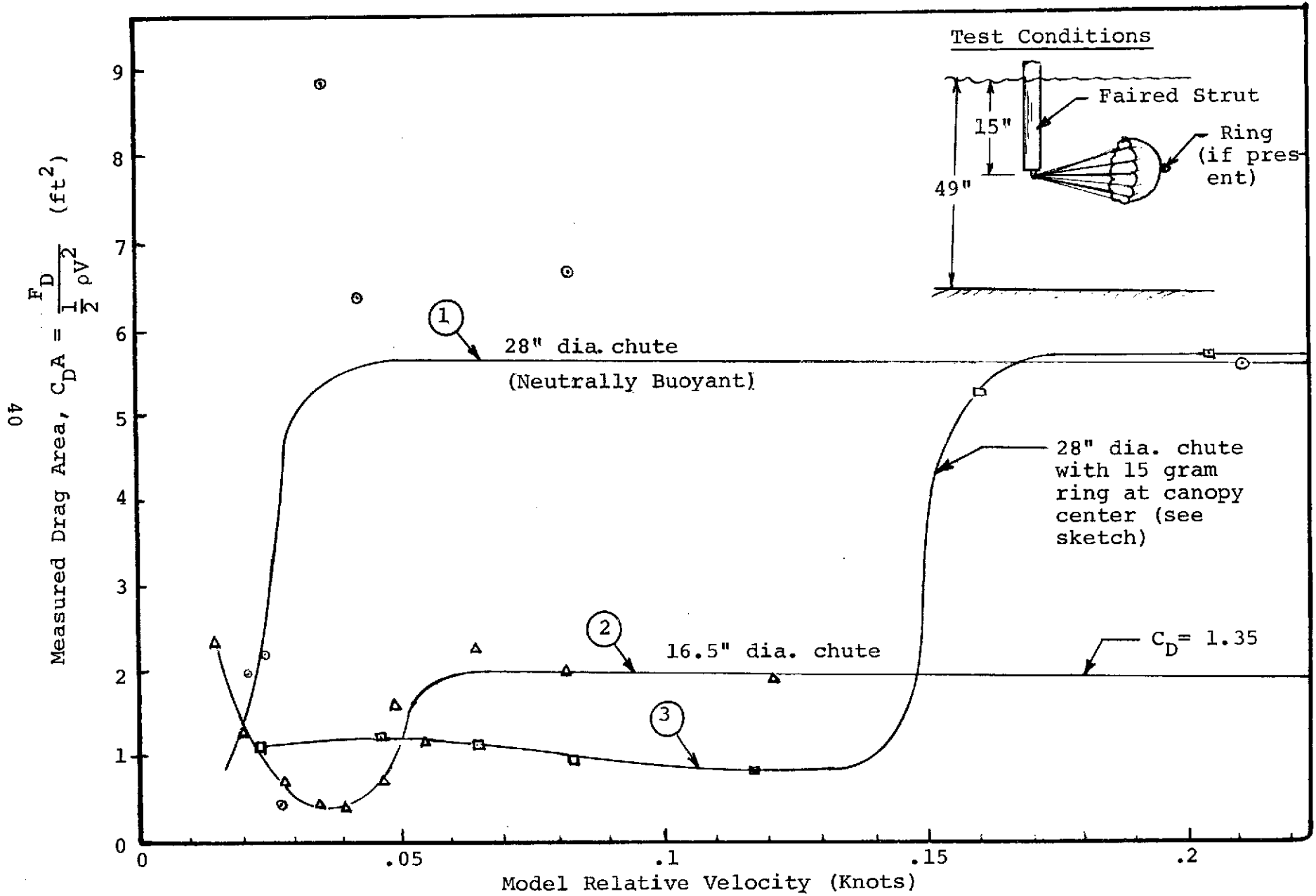


Fig. 10 Model Parachute Deployment Response

angle with respect to its tether point at all times after opening. The angle was a function of the relative velocity and drag coefficient as follows:

$$\theta = \tan^{-1} \left( \frac{W}{\frac{1}{2} \rho V^2 C_D A} \right) \quad (20)$$

where  $W$  is the weight of the chute in water and  $A$  is the resolved component of area normal to the flow.

Chute 3 exhibits deployment characteristics which are a strong function of gravity effects. In this case Froude scaling is a proper mechanism for scale model testing. This test says that by employing a convenient scale factor of  $\lambda = 16$ , the full scale deployment velocity would be approximately 0.6 knots. The equivalent chute would be approximately 37 feet in diameter and have a 7.4-pound weight at its center. The conclusion is that parachutes and in fact all such shapes which require a finite relative velocity for deployment should be as neutrally buoyant as possible. Figure 11 is a plot of the drag coefficient of velocity - dependent shapes as a function of Reynolds number. One of the five curves is that of the 16.5-inch diameter parachute model. It can be seen that at the lower velocities and Reynolds numbers ( $Re < 10^4$ ) the drag coefficient decreases in the same manner as shown in Figure 10. Over the Reynolds number range of  $2 \times 10^4$  to  $2 \times 10^5$  the measured drag coefficient varied between 1.35 and 1.40. This value agrees well with values reported in Hoerner (1965, p. 13-24) for a streaming, non-porous parachute in air.

A limited number of tests were conducted in order to ascertain the effect of vertical heave on the average drag coefficient of a sea drogue. A 1.5-inch (peak-to-peak) heave at a frequency of 1.6 Hz caused the measured drag coefficient to increase by 13 and 16 percent in two different tests.

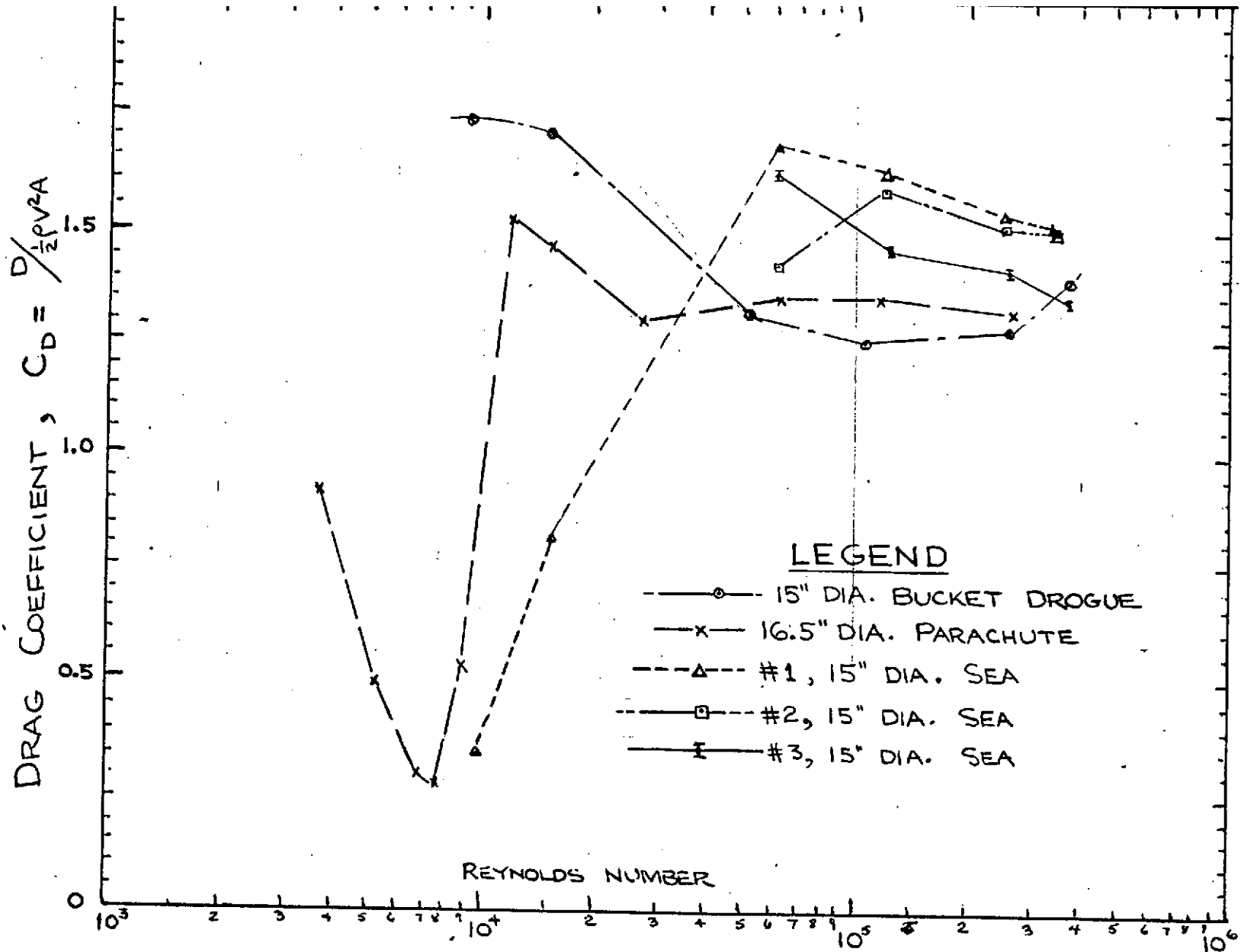


FIGURE 11

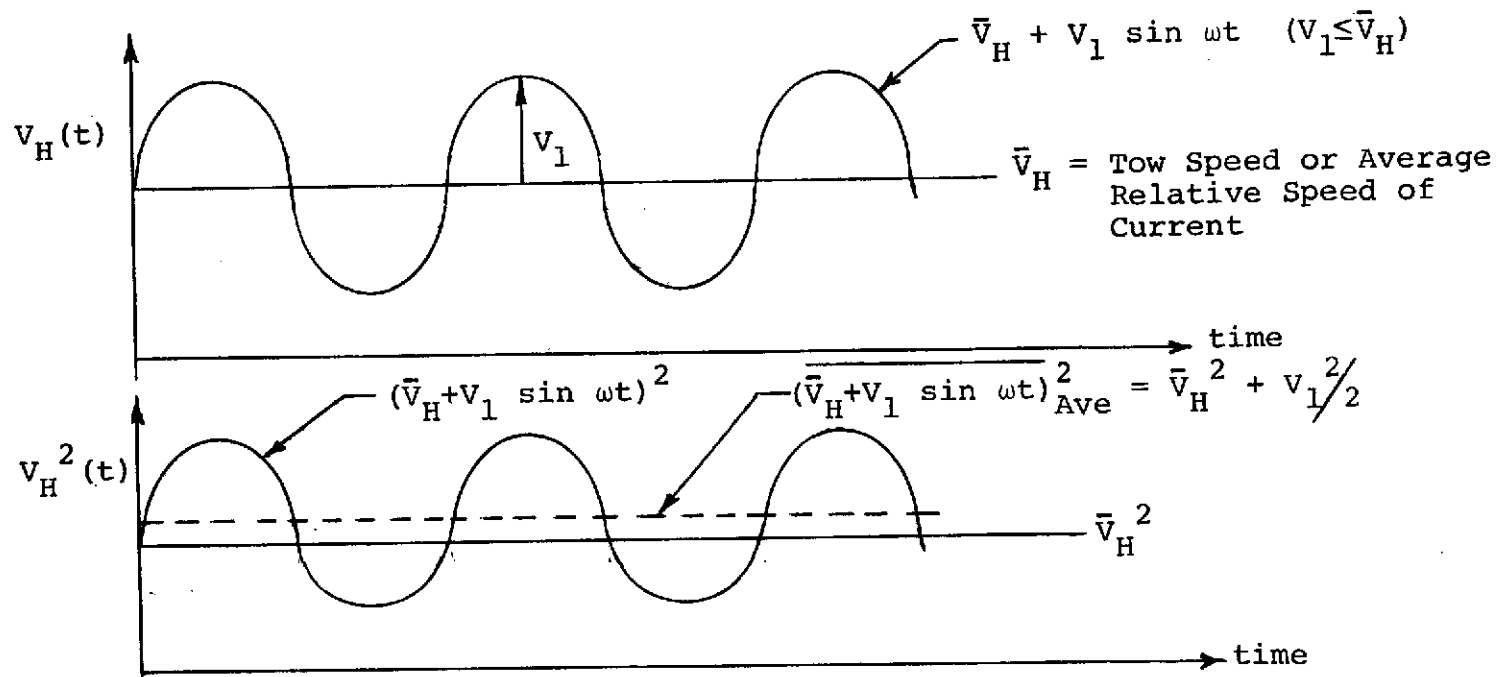
DRAG CHARACTERISTICS OF SEA DROGUES

Instrumentation problems and lack of time prohibited a complete exploration of the sensitivity of the drag coefficient of pendulous drogues to vertical heave.

An underwater viewing window permitted one to observe the performance of the drogues while they were being towed and receiving vertical heave. In general a parachute would pivot about its tether point and move in the direction of the tether line in response to an upward heave. It would have a component of velocity in both the horizontal and vertical directions. As the tether point heaved downward, the drogue would slow down well below its average velocity in order to maintain an average horizontal velocity equal to the towing velocity.

Figure 12 displays 5 parameters as a function of time which help to theoretically describe how heave can apparently augment a measured drag coefficient. The component of horizontal velocity ( $\bar{V}_H$ ) for the case of steady pull with no heave and the case of steady pull plus vertical heave ( $V_H + V_1 \sin \omega t$ ) are shown in the upper plot. The lower plot contains the square of each parameter in the upper plot plus the average value of their square. In this situation  $V_1$  is the amplitude of the horizontal component of velocity due to buoy heave which is superimposed on the steady relative velocity of  $\bar{V}_H$ . It is assumed that the tether line cannot support compressive loads. Therefore flow is assumed to always impinge on the drogue from one direction.

The average value of the square of the tow speed is merely the tow speed squared. The average value of the square of the tow speed plus the square of a superimposed sinusoidal velocity is greater than the square of the tow speed by one-half the maximum sinusoidal velocity squared. It is this additional factor of  $\frac{1}{2} V_1^2$  that contributes to the apparent increased drag coefficient in the presence of heave as shown in the lower part of Figure 12. For example if  $V_1 = 0.5\bar{V}_H$  (i.e.,



$$(C_D)_{\text{Steady}} < (C_D)_{\text{Heave}}$$

$$\frac{(F_D)_{\text{St}}}{\frac{1}{2} \rho \bar{V}_H^2 A_{\perp}} = \frac{\frac{1}{2} \rho \bar{V}_H^2 (C_D)_{\text{St}} A_{\perp}}{\frac{1}{2} \rho \bar{V}_H^2 A_{\perp}} < \frac{(F_D)_{\text{Hv}}}{\frac{1}{2} \rho \bar{V}_H^2 A_{\perp}} = \frac{\frac{1}{2} \rho (C_D)_{\text{St}} A_{\perp} \overline{(\bar{V}_H + V_1 \sin \omega t)^2}}{\frac{1}{2} \rho \bar{V}_H^2 A_{\perp}}$$

$$(C_D)_{\text{St}} < (C_D)_{\text{St}} \left[ \frac{\bar{V}_H^2 + V_1^2/2}{\bar{V}_H^2} \right] = (C_D)_{\text{Hv}}$$

NOTE: Subscript St denotes steady and Hv denotes heave.

Figure 12 Effect of Vertical Heave on Parachute Drag

one-half the tow speed) the measured drag coefficient in the presence of heave would be increased by 12.5% as given by the equation:

$$(C_D)_{\text{heave}} = (C_D)_{\text{steady}} \left( \frac{\bar{v}_H^2 + \frac{1}{2} V_1^2}{\bar{v}_H^2} \right) \quad (21)$$

Another interesting effect was observed during the heave tests. It was seen that the length of the shroud lines between the drogue ballast weight and chute itself influences the tilt of the chute in the presence of heave. The vertical component of heave imparted from the tether line at the attachment point to the chute will produce a tilt of the chute. If the shroud lines are long this effect and its associated errors will be reduced.

A device which is fully submerged in a uniform fluid (i.e., no density gradients), away from surface and wall effects, and is perfectly neutrally buoyant should not really employ Froude scaling for model testing because gravity forces are completely balanced by buoyancy forces. In such a case the bending stiffness of the material itself is a restraint to drogue deployment. In this case a more meaningful scaling approach might hold the ratio of pressure forces to bending stiffness forces constant in what might be called a dimensionless drogue number ( $Dr$ ) as follows:

$$Dr = \frac{\rho V^2 L^2}{\frac{Et^3}{D}} = \frac{\rho V^2 L^3}{Et^3} \quad (22)$$

where:

- E = Young's modulus of the material
- t = thickness of material
- D = drogue diameter  $\approx L$

This number is mentioned purely in an expository manner and was never applied during the tests described herein.

Parachutes are not a recommended drogue device for the reasons described. In addition it was observed during the tests that the model chutes were very prone to fouling and twisting of shroud lines. During initial deployment this problem could occur. Also if a drogue being towed through the water was stopped the momentum of the trailing fluid would in many cases carry the drogue into its shroud lines bringing about either a fouling or a twisting of shroud lines. The reestablishment of flow would eventually unfoul a chute but shroud lines might still be twisted. The velocity required for full deployment was quite often higher after such a fouling. It is felt that this phenomenon could occur in the ocean if the current should go to zero or reverse. Another problematic case might be if surface effects from the buoy should cause the drogue to reverse its direction of motion. Many investigations have employed spreaders on chutes to enhance deployment and minimize fouling. It is not clear that they help the overall performance. A heavy spreader, whose weight is not compensated by additional buoyancy, could be detrimental to chute performance. A chute which is always open but negatively buoyant might hang down and not present its full area to a current flow. Therefore, it would be very difficult to reliably employ a known  $C_D A$  product for drift error corrects (equation 7). A point in favor of the parachute, bucket, and sea anchor drogues is their better immunity to dynamic loads in the presence of buoy heave.

## 6.2 Bucket Drogue Tests

One bucket sea drogue was constructed as shown in Figure 4B. It was tested in the same manner as model parachutes for both deployment response and overall drag coefficient. The deployment response tests are not as extensive as for parachutes but the same general comments apply. A bucket drogue is

essentially a modified parachute that should be neutrally buoyant for best deployment response.

The unbleached muslin bucket model was slightly negatively buoyant and deployed at a speed of less than .05 knots. Because of its weight, though, it hung down; not presenting its full open area to the flow. As shown in Figure 11 it maintained an even higher drag coefficient at the very low velocities than when it became fully "inflated" streaming normal to the flow. It is felt that in these cases viscous forces on the sides of the bucket augmented the drag. When fully deployed the average measured drag coefficient over a range of Reynolds numbers from  $2 \times 10^4$  to  $4 \times 10^5$  was 1.34. It oscillated less than a chute but it essentially behaved the same.

For the same reasons as parachutes, bucket drogues are not a recommended drag element. Although no good data were derived on the effects of heave on the drag coefficient it is felt that the same phenomenon observed for parachutes exists for buckets. That is, heave would increase the apparent drag coefficient proportional to the square of the sinusoidal component of horizontal velocity at the drogue.

### 6.3 Conical Sea Anchor Tests

The three sea anchor models described in Figures 4C, D, and E exhibited the steady pull drag coefficient data plotted in Figure 11. As expected, the average drag coefficient (approx. 1.5) over a Reynolds number range of  $5 \times 10^4$  to  $4 \times 10^5$  decreased as the spill hole size was enlarged. Figure 4 and Appendix A display the drag data.

One set of drogue deployment response tests was conducted on sea anchor number 1 ( $A_2 = .03A_1$ ). The hollow

aluminum rings employed in order to stabilize the inlet and outlet holes caused the drogue to be buoyant. As a result an appreciable velocity was required in order to offset the buoyancy forces and obtain the full drag coefficient. The data associated with this test are plotted in Figure 11 at the low Reynolds numbers.

Due to instrumentation difficulties no meaningful data were obtained to show the effects of heave on the drag coefficient. It was observed that even with a 2.5-foot string and a 2.56-inch (peak-to-peak heave, the drogue moved very little in response to the heave. The shroud lines, whose length was twice the drogue diameter, merely pivoted about the drogue and absorbed the heave motion. It is felt that for this test and those to be described, the variation of the drag coefficient with heave was so small that differences were within the test measurement accuracy. In the remaining tests, only qualitative observations of the effects of heave will be discussed. In general a sea anchor appears to have many of the drawbacks of a parachute. It can foul itself on its shroud lines in much the same manner although possibly not as readily. It requires a minimum relative velocity in order to achieve its rated drag coefficient. An additional chief drawback is that if it is built with rigid rings it becomes cumbersome to store a large version on a ship. It has, however, a degree of merit lacking in parachutes and buckets. The downstream spill hole tends to make the drogue stream in the direction of flow with a minimum of oscillations.

#### 6.4 Crossed Vanes Tests

As described in section 3.4, seven different configurations of crossed vanes were tested. Five of the configurations involved tests with solid aluminum 2- and 3-axis models. The other two configurations were identically sized polyethylene plastic versions of the 2- and 3-axis models.

Numerous clamped tests were conducted on the aluminum models while clamped to the bottom of the strut shown in Figure 9. The 2- and 3-axis crossed vanes were tested with their common axis in a vertical direction but, were tested at different azimuth angles in order to observe the effect on the drag coefficient. In addition each setup was tested with and without endplates. Tests were not conducted with the vane axis inclined to the vertical direction in that a certain amount of lift force would be developed in addition to drag. The method of mounting and measurement that was employed in the clamped tests did not permit one to separate out the two effects. Non-clamped tests, wherein the device is pendulously suspended, permit the measurement of only drag forces when the device is free to incline with respect to vertical. In these cases the crossed vanes would spin rapidly at various times. At other times they would spin in the opposite direction, more slowly, or not at all. It appeared to be a random occurrence based possibly on conditions which may have existed at the beginning of the particular tow. The measured average drag coefficient of a spinning crossed vane was slightly higher than the average value for the clamped version at different azimuth angles.

Figures 13 and 14 display the drag coefficients for 2- and 3-axis aluminum clamped crossed vanes respectively as a function of Reynolds number. Appendix A contains a more complete version of the same data. The area employed in calculating the drag coefficient for clamped tests is always the area normal to the flow. For example, the data in Figure A-2 (Appendix A), devices 6 and 7, can be compared. The full area of the 10"x10" plate (i.e.,  $A_1 = 100 \text{ in}^2 = .694 \text{ ft}^2$ ) is employed with device number 6. For device number 7, however, an area of  $A_1 \cos 30^\circ = .601 \text{ ft}^2$  is employed because the vanes are rotated by  $30^\circ$ , reducing the area normal to the flow. When the vanes are pendulously suspended, with no preferred azimuth angle to the flow,

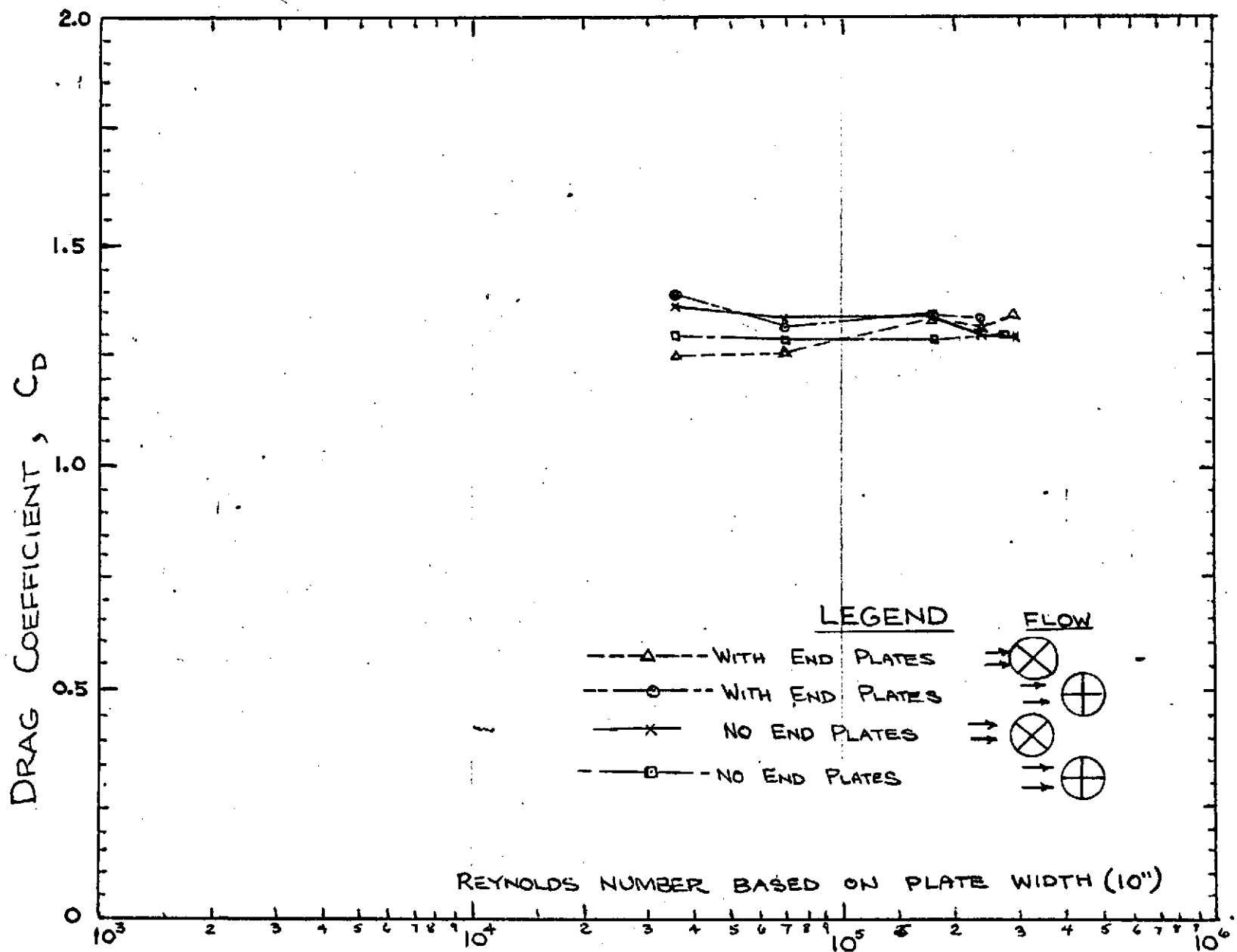


FIGURE 13  
 DRAG CHARACTERISTICS OF 2-AXIS VANES (CLAMPED)

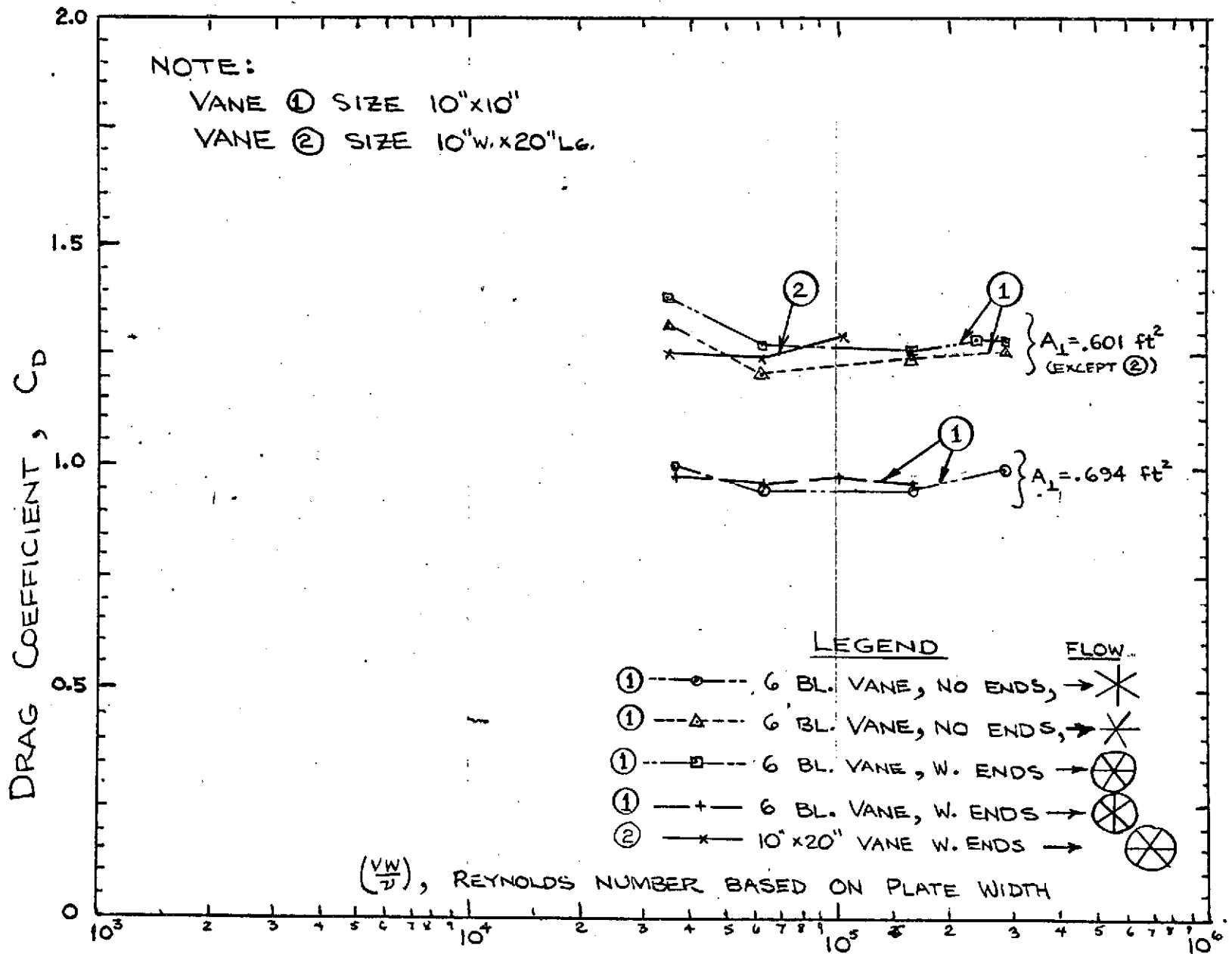


FIGURE 14  
 DRAG COEFFICIENTS OF 3-AXIS VANES (CLAMPED)

the area on which the drag coefficient is calculated is described in Appendix A.

It can be seen in Figure 13 that the drag coefficient of a 2-axis crossed vane is relatively insensitive to the presence of end plates, azimuth angle, and Reynolds number for Reynolds numbers between  $3 \times 10^4$  and  $3 \times 10^5$ . Appendix A, Figures A-2 and A-3, however, show that the drag area ( $C_D A$ ) of a 2-axis crossed vane is markedly greater for the case of a flow streaming normal to one surface and parallel to the other surface than at 45 degrees to both surfaces.

Figure 14 shows data for two different 3-axis vanes, one 10-inches long and the other 20-inches long. By examining the data it can be seen that end plates essentially do not alter the drag coefficient. Secondly, the drag coefficient does vary with the azimuth direction of the flow with respect to the plates. Appendix A, Figure A-2, however, shows that the drag area (i.e.,  $C_D A$  product) is nearly independent of azimuth angle. This is a big plus for a 3-axis vane design. A third observation is that lengthening the device and testing it with end plates still does not alter the drag data. This fact agrees in principal with reported drag data for a flat plate. (Hoerner, 1965, p. 3-16, Fig. 28). These data say that the flat plate length-to-width ratio must be at least 5 before one starts to see a diminution of end effects and an increase of drag coefficient from the square plate value of 1.18. To get the full drag coefficient of a 2 dimensional flat plate with negligible end effects (i.e.,  $C_D = 1.98$ ), the plate would be over 40 times longer than its width. Therefore, the drag coefficient of a crossed vane gains little by increasing its length-to-width ratio over realistic limits. Purely from the point of view of maintaining a constancy of high drag area with azimuth angle, a 3-axis crossed vane appears superior to a 2-axis version.

When the same aluminum shapes were suspended in a pendulous manner by a string they were now free to rotate in azimuth as well. In general the measured drag area of vanes with no end plates was approximately 10% higher than those with end plates, with higher values occurring at higher speeds. This is counter to intuition and cannot be readily explained. One would expect that when allowed to comply with the flow in a pendulous manner it would achieve an inclined aspect wherein the flow would impinge on the plates at an acute angle, reducing the drag coefficient and, more importantly, area normal to the flow.

In general the drag coefficients of pendulous, solid vanes with end plates also increased by approximately 3% over the clamped version. This is understandable in that the end plates contribute to the drag as the vane inclines itself in a flow. In addition the actual geometric area perpendicular to the flow increases with inclination angles up to 45°. It is felt that end plates on a crossed vane drogue are helpful if the drogue is deep in the ocean. If, however, the drogue is to be used in near-surface applications (e.g., less than 100 meter depth) the end plates present a drag to vertical motion induced by buoy dynamics which may pull a buoy beneath the waves or cause materials fatigue and mooring failure. It is felt that, in general, the horizontal drag gained by the end plates would not justify the potential dangers in such applications. The dangers would vary with the buoy design and should be weighed accordingly.

Plastic versions of both 2- and 3-axis crossed vane drogues with no end walls were tested in a pendulous manner. Their drag results are listed only in Figures A-3 and A-4 (device numbers 19, 20, 21). Device number 15 and 19 should be compared in that they were both run at Reynolds scaling speeds. A comparison of all pertinent results in Appendix A

indicates that the pendulous drag coefficient of plastic crossed vanes with no end walls is greater than that of the aluminum version by between 10 and 20%. Based on the full wall area of .694 ft<sup>2</sup> an average value of  $C_D = 1.4$  was derived for the 3-axis plastic version and an average value of  $C_D = 1.1$  was derived for the aluminum model at Reynolds speeds.

Similar proportional increases in  $C_D$  should be realized by going to plastic in a 2-axis version but good comparative data at Reynolds speeds was not derived for the plastic version. The average Reynolds-scaled drag coefficient for the pendulous aluminum, 2-axis model with no end plates was found to be 1.2. With end plates the value increased to approximately 1.3.

It is felt that the presence of plastic walls in a crossed vane design causes the walls to comply with the flow; creating a concaved shape. Such a shape possibly creates a further trapping effect for the flow over that of a flat plate in a manner similar to a parachute. In this manner the drag coefficient might increase.

Plastic crossed vanes are an appealing current locking device because they exhibit a high drag area; are potentially lightweight and relatively inexpensive to build, and hopefully can be collapsed and stored on a deck. A 3-axis version is particularly appealing because the drag area product is nearly constant with azimuthal rotation of the drogue. The choice of employing end walls or not should be weighed in terms of the dynamics of a particular application. A further consideration is that a crossed vane containing end walls will impart appreciably higher tether line tensions during a retrieval operation. Alternatively, the operation can be slowed down in order to maintain the tension values encountered on a drogue with no end walls. This fact may be inconsequential if the drogue is being retrieved by a powered winch.

A suggested practical means of implementing a 3-axis crossed vane design is to employ 3 rigid poles, pivoted about their center, on each end of the drogue as a means of supporting the walls. The poles could be pivoted together in parallel for storage. The plastic walls would then permit the unit to roll up like a window shade for deck storage. A strong plastic which could support a ballast weight is desirable for the walls. Ultimately the ballast weight could be used as the driving force for full automatic deployment once implanted in the water. The weight could cause the rolled walls to pay down and out and when completely unfurled, the tension assumed by the three parallel walls could trigger a preloaded spring release to fully deploy the walls at 60 degrees to each other.

Heaving tests were conducted on crossed vane drogues. The data are inconclusive, however, because of the difficult instrumentation problem of measuring minute changes in a small drag force in the presence of considerable noise caused by the dynamic input from the heave mechanism. It is, however, felt that heave would increase the drag coefficient slightly for the same reason described in the parachute section. This effect would tend to be greater for a crossed vane with end plates because the vane would be inclined somewhat towards the tether line and into the flow in the presence of a relative velocity. As the tether line responds to an upward motion of the attachment point it pulls the vanes both horizontally and vertically. Because of the inclined angle of the vanes the plates assume a portion of the drag force. It is for this reason that vanes with end walls may not be a good choice for near-surface drogues.

#### 6.5 Buoyed Fishing Net Tests

Two different 36"x42" net samples were tested in a buoyed configuration as shown in Figure 6A. Test results

indicate that on the average a drag coefficient of approximately 0.2 can be used based on the full area of the net. Devices 24 and 25 of Figure A-5 (Appendix A) show more details associated with the test results. It appears that if materials are available, including a net of sufficient size, a buoyed net may be a very viable means of coupling to surface currents.

## 6.6 Cylinder Tests

Two versions of a cylindrical drogue were tested with limited success. Identically-sized solid aluminum and polyethylene cylinders (3" dia. × 15" long) were towed at Reynolds scaling speeds (0.3 to 1.54 knots). The Reynolds numbers based on the cylinder diameter were between  $10^4$  and  $10^5$ . In addition the plastic cylinder was towed at Froude scaling speeds of 0.02 to 0.1 knot.

Different drag coefficients were measured on the aluminum cylinder compared to the plastic cylinder at Reynolds speeds. The plastic cylinder, supported by a string in a pendulous manner, as would be found on a buoy, exhibited drag coefficients of between 0.99 and 1.45 with an average value of 1.31 (see Figure A-5, Appendix A). These values agree in general with the drag coefficients of cylinders reported in the literature, (see Fig. 8) although the average for plastic is higher. It was observed that the front surface of the cylinder bows in due to impinging flow, possibly augmenting the drag coefficient by the cup-shaped area thus formed.

The aluminum cylinder was towed at Reynolds speeds in a clamped configuration. The data are not shown in Appendix A but, the drag coefficients lie between 0.79 and 1.34 with an average value of 1.03. This value is in line with the value reported in the literature (1.0 to 1.2) but is slightly on the low side. Cylinder oscillations were observed possibly as a result of Karman vortex shedding.

A collapsible, plastic cylinder with its longitudinal axis aligned vertically is an appealing drag element from a few points of view. First, it develops a decent drag coefficient irrespective of flow direction (1.0 to 1.2). Secondly, the geometry appears simple to fabricate. Thirdly, a drogue can be made with rigid end plates and collapsible plastic walls that could permit compact deck storage; limited only by the diameter of the end plates. The cylinder could be made quite long in order to increase the total drag area.

In spite of its advantages the cylinder is still more bulky to store and complicated to assemble than a window shade drogue. At the same time it will develop a component of lift at higher relative velocities which further tends to reduce the drag area in a manner analogous to a window shade drogue. These points will be covered in more detail when window shade drogues are discussed.

#### 6.7 Sphere Tests

An 8.5" diameter hollow aluminum sphere was tested in a clamped configuration at Reynolds speeds of from 0.31 to 2.0 knots. The results are shown in Figure A-6 (Device No. 28). The measured drag coefficients (ave.  $C_D = .16$ ) are seen to be low compared to the values reported in the literature ( $C_D$  0.4 to 0.5, see Figure 8). The measured drag coefficient decreased with increasing speed. It was observed that the cylinder vibrated in its clamped mount perhaps due to vortex shedding.

A sphere is an appealing drag device in that its shape could be replicated in the form of an inflatable plastic ball in the ocean. This ball could be made extremely large and, in spite of the relatively low value of  $C_D$ , the  $C_D A$  product, which is important, could be made very large. Furthermore, a sphere would present the same drag area to flow from any direction, such that when one is correcting for errors in

relative velocity by the application of equation (7), the  $C_D A$  is invariant. A sphere, however, is not a recommended drag device for the following reasons. The drag area,  $C_D A$ , per unit of plastic material (weight and cost) for a sphere does not approach the efficiency of a window shade drogue. A scheme or device would have to be developed which would permit the inflation of the sphere with ambient water, once implanted. This device could be simple and inexpensive, yet it would be potentially a point of failure or unreliable performance for a spherical drogue. Lastly, because its drag area is invariant with respect to angle, dynamic motion induced by buoy motion would generate very large vertical drag forces on the buoy which might drag certain buoys under the waves or as a minimum generate large dynamic loads which could lead to fatiguing and failure of mooring line components.

#### 6.8 Window Shade Drogue Tests

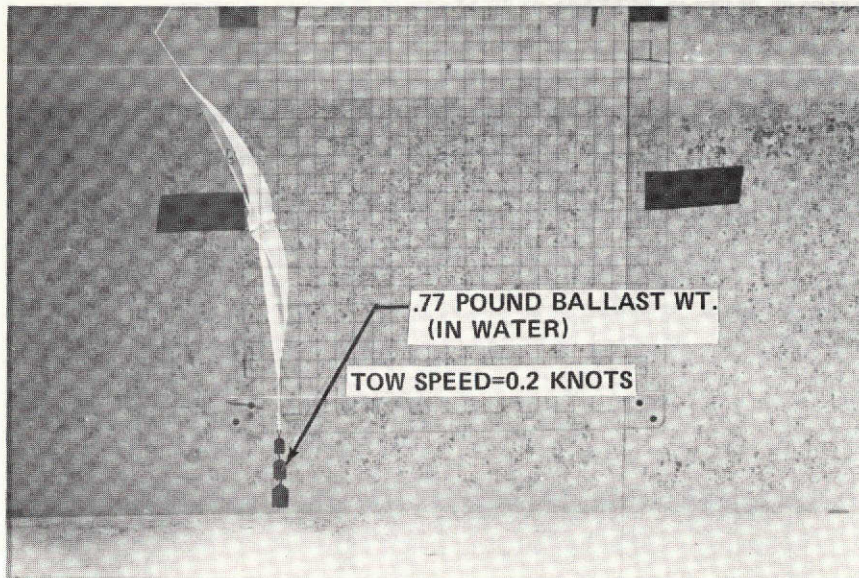
The window shade drogue tests were configured in search of answers to the following questions:

- (1) Which shape displays the most constant  $C_D A$  product in the presence of relative velocities?
- (2) How does this  $C_D A$  at a given relative velocity vary with the ballast weight?
- (3) Which shape or shapes respond best to changing current directions?
- (4) How much lift force does each shape generate as a function of relative velocity and ballast weight?
- (5) What  $C_D A$  as a function of relative velocity and ballast weight should be used on a full scale model.
- (6) Which shape seems to be the easiest to build, store, assemble, and deploy on the deck of a ship?

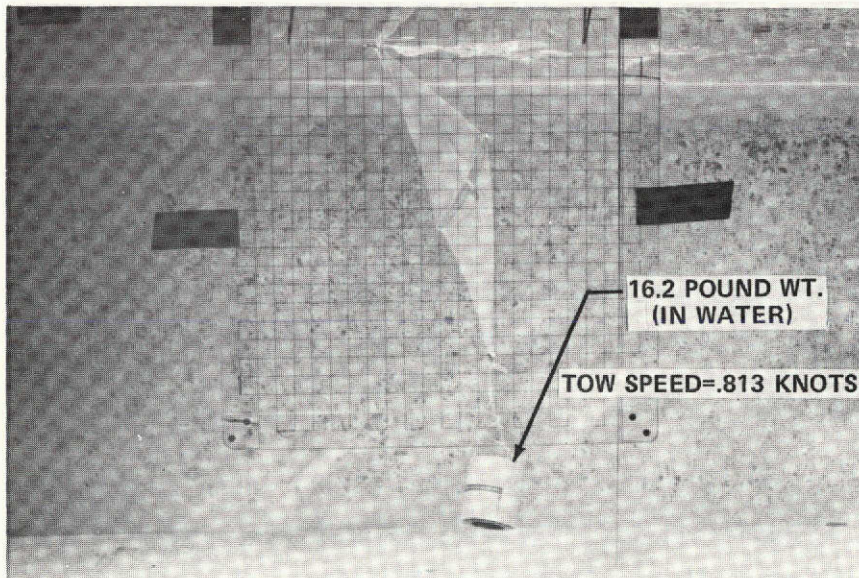
Both Froude and Reynolds scaling were employed in an

attempt to answer these questions. Froude scaling was used to establish the shape of a drogue as a function of velocity and ballast weight. A Polaroid photo was made of each shape through an underwater window as shown in Figures 15A and 15B. This photo viewed the tether line through a transparent grid of lines as a measure of the drogue shape. Simultaneously the angle of the tether line with respect to vertical was measured visually against a protractor in the background. Once the drogue shape was known from the Froude scaling tests, Reynolds scaling tests were run at higher speeds. The shapes generated at Froude speeds were reproduced at the Reynolds speeds by increasing the ballast weights. The drag coefficient measured at the Reynolds speeds should then be an easily scaled value which takes into account Froude or gravity effects, which dictate shape, as well as viscous effects derived by employing Reynolds scaling.

It may not be immediately evident but a window shade drogue will tend to stream in a flow such that its open face is perpendicular to the flow. This is only true if the drogue tether point is attached in line with the center of the drogue. It does not even have to be attached directly to the drogue itself but through a triangular yoke, formed of tether line, the apex of which is in line with the drogue vertical centerline. As the attachment point is moved further from the centerline the drogue will tend to stream at more acute angles to the flow. The extreme case of attaching the tether point in line with the end of the drogue will cause the drogue to stream parallel to the flow. When pulled from a point in line with the centerline, the drogue streams normal to the flow because such a condition is completely symmetric; the torques caused by end condition drag about the centerpoint are balanced. In simple terms, the condition is stable because as the drogue rotates away from the condition normal to the flow the drag coefficient of the upstream



**FROUDE SCALING TEST**  
**(SHAPE 8, FIG. 17)**



**REYNOLDS SCALING TEST**  
**(SHAPE 8, FIG. 17)**

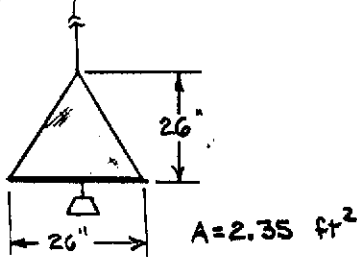
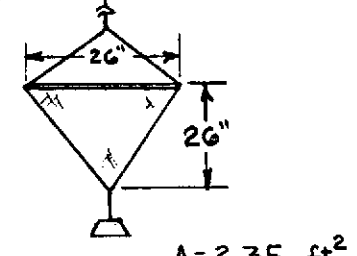
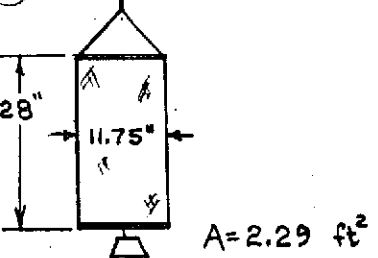
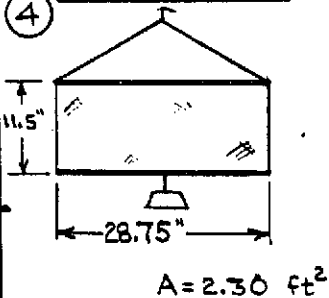
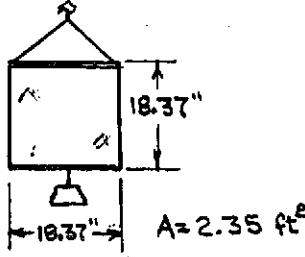
Fig. 15 Photos of Froude and Reynolds tests of window shade drogues.

end of the drogue will be greater than that of the downstream end, creating a stable restoring torque.

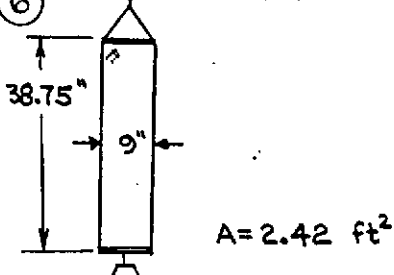
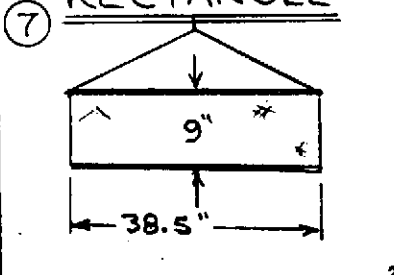
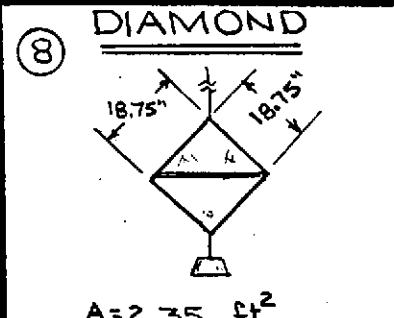
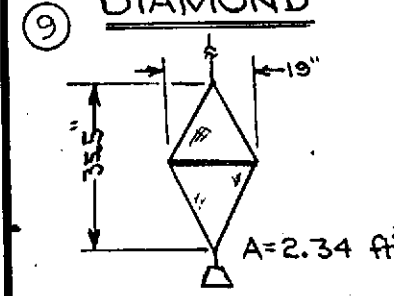
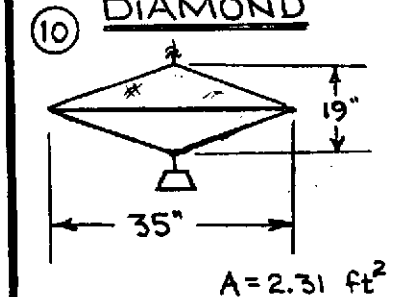
Figures 16 and 17 show a description of the window shade drogue shapes, test speeds, and measured drag coefficients for 10 drogues. These data are also summarized in Appendix A. Appendix A also contains results on an additional window shade drogue (device No. 39) which is identical to No. 5 in Figure 16, but slightly larger. The results are the same within the measurement accuracy.

Figures 16 and 17 contain much information derived from Froude scaling tests in which the model velocity,  $V_m$ , is equal to the full scale velocity as described in section 4.3. Difficulty was, however, encountered in trying to conduct Reynolds tests in which the shapes derived in Froude scaling tests were duplicated. The problems were threefold, all centering around the large ballast weights required in order to duplicate the shapes:

- (1) The heavy weights (16-pounds, maximum) placed such severe strains on the plastic drogue materials that they unrealistically distorted the shape with stress lines and in most cases required material reinforcement in order to prevent a failure due to tearing.
- (2) The ballast weight attached to the bottom of the drogue in a pendulous manner oscillated sideways at large amplitudes perpendicular to the relative velocity. The oscillations, possibly receiving energy from drogue vortex shedding, reached amplitudes of up to  $\pm 20$  degrees at speeds of 0.8 knots.
- (3) The heavy ballast weight placed an uncalibrated load on the force measurement blocks in a direction normal

SHAPE DESCRIPTION	FROUDE SCALING RESULTS		REYNOLDS SCALING RESULTS	
	SPEED	C <sub>D</sub>	SPEED	C <sub>D</sub>
<b>① TRIANGLE</b> 	0.039 KN.	1.53	0.31 KN.	1.63
	0.099 KN.	1.22	0.61 KN.	1.36
	0.2 KN.	1.73	0.813 KN.	1.37
<b>② TRIANGLE</b> 	0.039 KN	1.95	—	—
	0.099 KN.	1.72	0.31 KN	1.46
	0.2 KN.	1.53	.407 KN.	1.45
<b>③ RECTANGLE</b> 	0.039 KN.	1.54	0.31 KN	1.81
	0.099 KN.	2.13	0.61 KN.	2.03
	0.2 KN.	1.77	0.813 KN.	1.85
<b>④ RECTANGLE</b> 	0.039 KN.	2.29	0.31 KN.	1.0
	0.099 KN.	1.77	0.61 KN.	1.92
	0.2 KN. -	1.56	0.813 KN.	1.89
<b>⑤ SQUARE</b> 	0.039 KN	1.97	.61 KN	1.85
	0.099 KN	1.83	.813	1.89
	0.2 KN	1.63	1.0 KN	1.75

WINDOW SHADE DROGUE TEST SUMMARY  
 FIGURE 16

SHAPE DESCRIPTION	FROUDE SCALING RESULTS		REYNOLDS SCALING RESULTS	
	SPEED	C <sub>D</sub>	SPEED	C <sub>D</sub>
<b>⑥</b> <u>RECTANGLE</u> 	.039 KN	1.92	-	-
	.099 KN	1.88	-	-
	.2 KN.	1.53	-	-
<b>⑦</b> <u>RECTANGLE</u> 	.039 KN	2.03	-	-
	.099 KN	2.16	-	-
	0.2 KN	1.44	-	-
<b>⑧</b> <u>DIAMOND</u> 	0.02 KN	1.72	0.31 KN.	1.83
	0.099 KN	1.58	0.61 KN	1.87
	0.2 KN.	1.53	0.813 KN.	1.92
<b>⑨</b> <u>DIAMOND</u> 	.039 KN	1.40	-	-
	.099 KN	2.30	-	-
	0.2 KN	1.76	-	-
<b>⑩</b> <u>DIAMOND</u> 	.039 KN	1.92	-	-
	.099 KN	1.84	-	-
	0.2 KN.	1.68	-	-

WINDOW SHADE DROGUE TEST SUMMARY  
 FIGURE 17

to their sensitive axis. A simple analysis shows that this load can alter the measurement spring constant in a small but non-linear manner. Earlier tests had indicated that such a problem was in general negligible. It is, however, mentioned here for completeness of thought.

The problems described lead to a somewhat more erratic behavior in the Reynolds data than in the Froude data. The problems also limited the amount of ballast weight that could be used on the small model sizes. Sixteen pounds (in air) was the maximum weight used. As a result, in order to duplicate the shapes measured at Froude speeds, the Reynolds speeds had to be reduced; changing the dimensional scale factor of the tests from 16 to a maximum of 8.

As mentioned earlier, the tether line angle ( $\theta$ ) with respect to vertical at the drogue attachment point was measured. In addition, the total weight ( $W$ ) of the drogue and ballast weight (in water) was measured. These parameters were combined with the drag force measurement ( $F_D$ ) in the following relation to enable the calculation of drogue lift force ( $L$ ):

$$\tan \theta = \frac{F_D}{W-L} \quad (23)$$

The ability to accurately measure the lift force or lift-to-drag ratio is very sensitive to the accuracy of the  $\theta$  measurement. This fact can be seen by writing equation (23) in the following form:

$$\frac{L}{F_D} = \frac{W}{F_D} - \frac{1}{\tan \theta}. \quad (24)$$

By taking the derivative of  $L/F_D$  with respect to  $\theta$ , a sensitivity of the lift-to-drag ratio to the angle measurement is derived as follows:

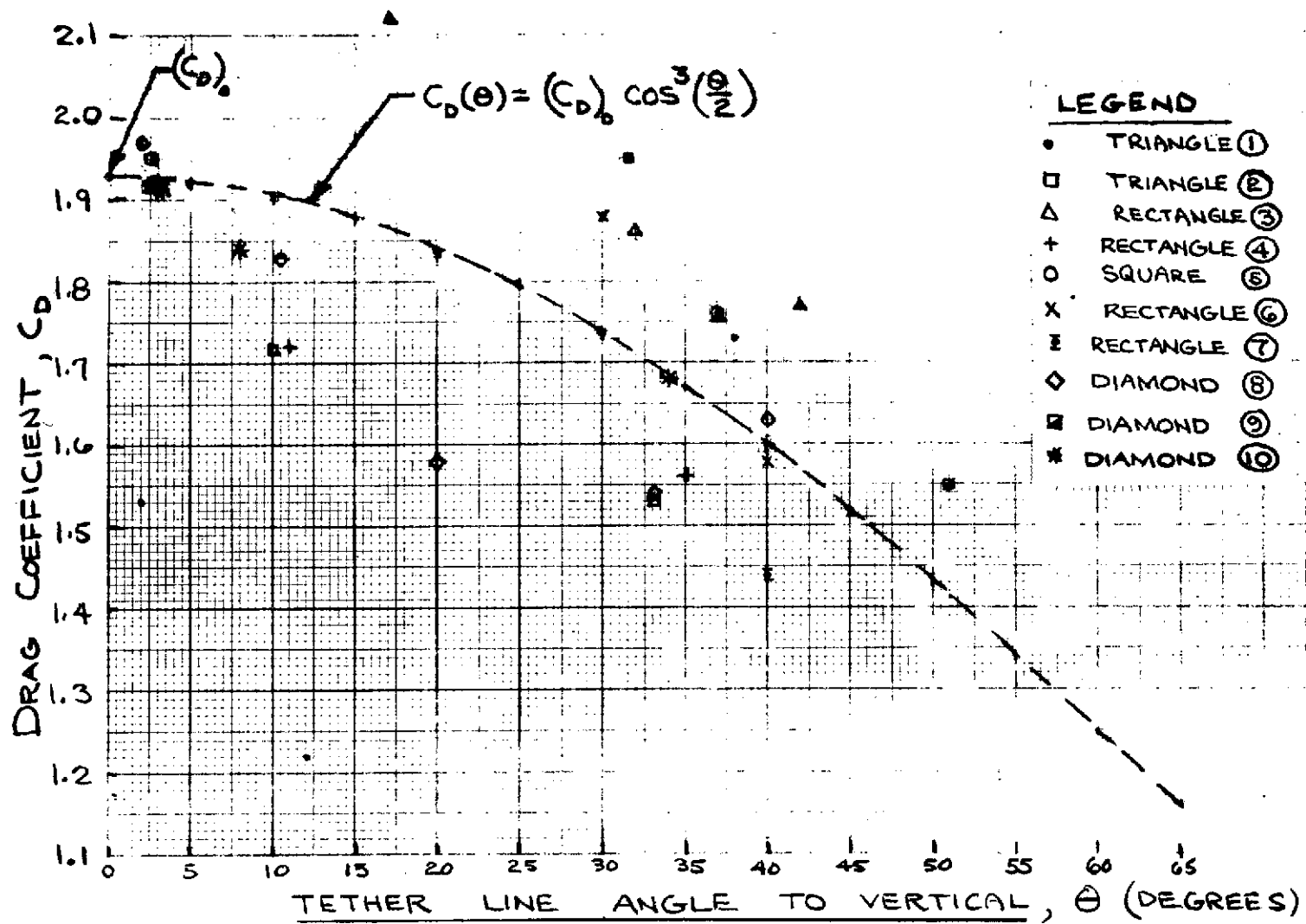
$$\frac{\partial (L/F_D)}{\partial \theta} = \frac{1}{\sin^2 \theta} \quad (25)$$

Equation (25) says that the ratio is extremely sensitive to errors in the angle for small angles because the sine of a small angle is very small. As an example, at an angle of 15 degrees the value of  $\frac{1}{\sin^2 \theta}$  is  $0.26 \text{ (degree)}^{-1}$ . In other words an error of one degree in measuring  $\theta$  will give rise to a 0.26 error in the lift-to-drag ratio. When one considers that for an angle of  $15^\circ$  the  $\frac{L}{D}$  ratio should be on the order of 0.26, it can be seen that the technique described has definite limitations for smaller angles. At an angle of  $\theta = 35^\circ$  the value of  $\frac{1}{\sin^2 \theta}$  is 0.053, showing a much better ability to measure lift at higher angles. The problem is not all that bad, as will be seen below, because one really only worries about drogue lift at higher angles.

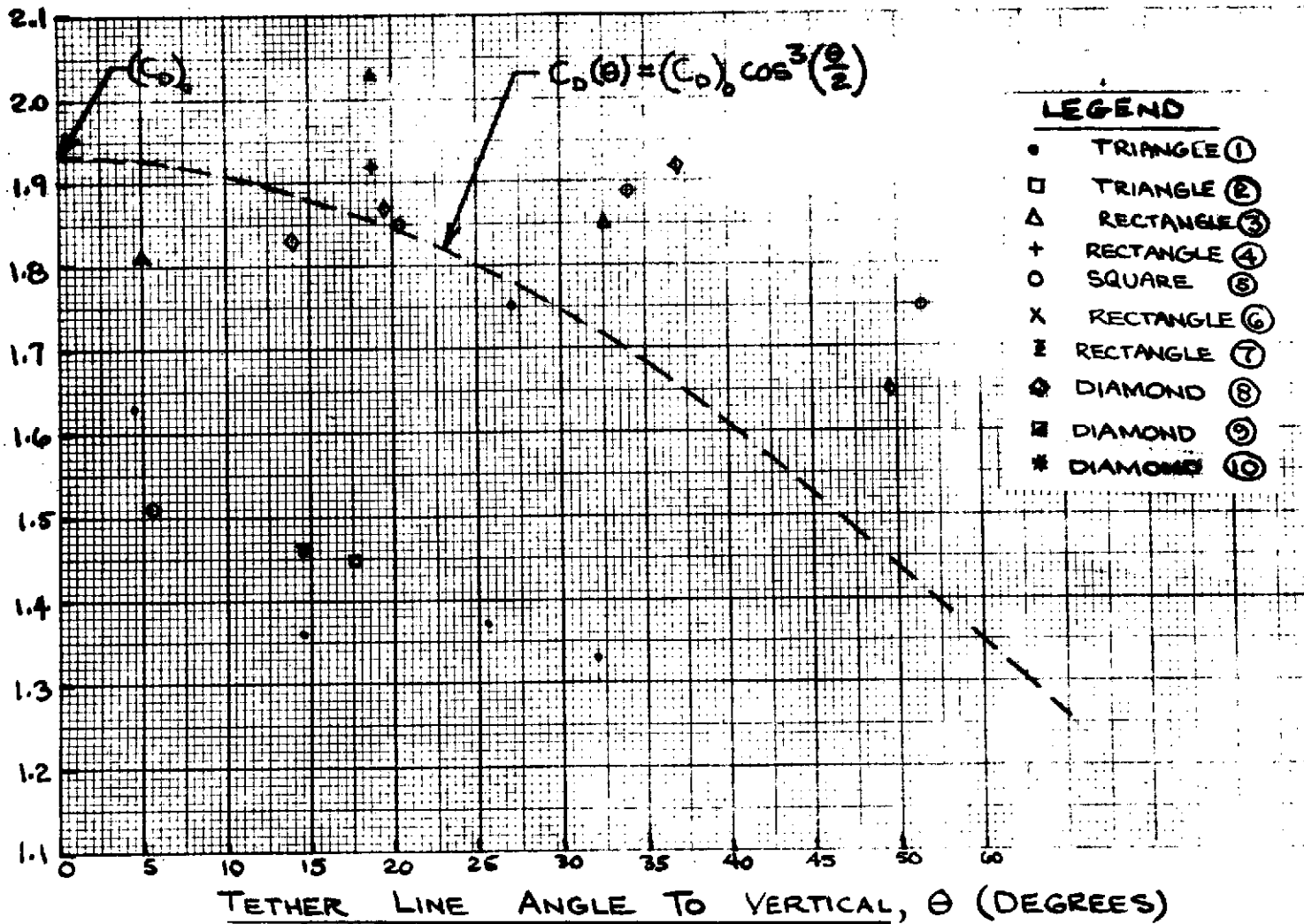
Figures 18 and 19 plot the measured drag coefficients of window shade drogues as a function of  $\theta$  for Froude and Reynolds scaling respectively. The data contain considerable scatter but, the value of  $C_D$  generally decreases with increasing  $\theta$ , as would be expected. That is, as the drag loads on a drogue increase, the bottom of the drogue rises higher, relative to the tether point, reducing the frontal area to flow and reducing the apparent drag coefficient based on the full frontal area.

In Figures 18 and 19 is also plotted a theoretical curve which attempts to analytically describe the  $C_D$  as a function of  $\theta$ . In the given relation,

$$C_D(\theta) = (C_D)_0 \cos^3 \left( \frac{\theta}{2} \right) \quad (26)$$



FROUDE SCALING TEST RESULTS  
FIGURE 18



REYNOLDS SCALING TEST RESULTS  
FIGURE 19

$(C_D)_0$  represents the maximum obtainable drag coefficient when the drogue is vertical (ie.  $\theta=0$ ). The derivation of this relation can be best seen by the use of Figure 20.

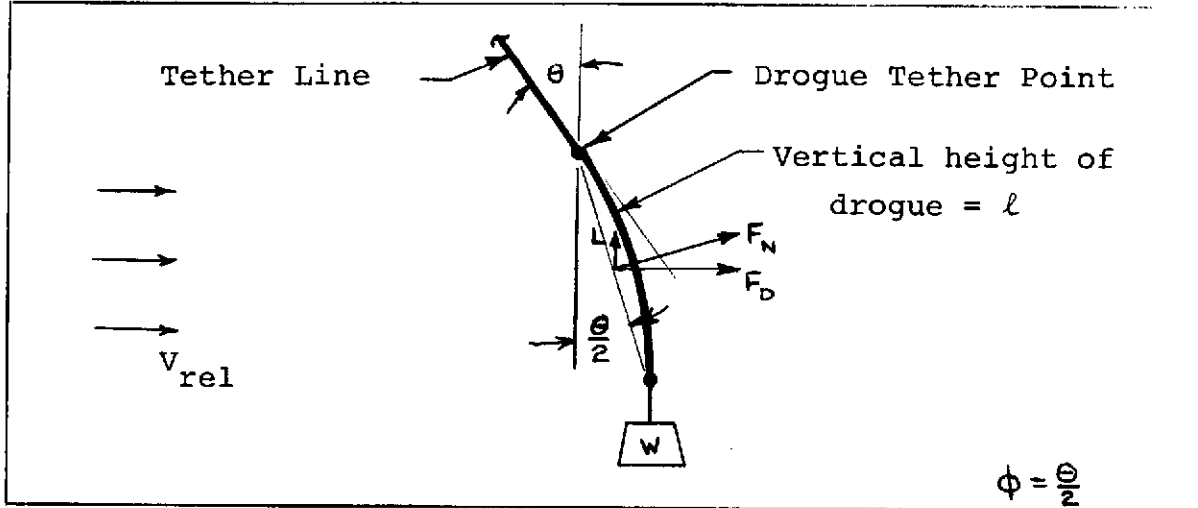


Figure 20

#### Hydrodynamic Forces on Window Shade Drogues

Figure 20 depicts a drogue from above the attachment point to below the ballast weight. If it can be assumed that the drag force on the ballast weight is negligible a line tangent to the bottom of the drogue is in the vertical direction. If it can be further assumed that a profile of the drogue forms part of an arc of a circle, a geometric theorem indicates that the average angle of the drogue between tether and weight attachment points is  $\frac{\theta}{2}$ . The drag force normal to the drogue ( $F_N$ ) at its average inclination angle is given by the relation:

$$F_N = \frac{1}{2} \rho (V_{rel} \cos \frac{\theta}{2})^2 (C_D)_0 A_{\perp}. \quad (27)$$

If the component of drag due to fluid shear parallel to the surface is neglected for small values of  $\theta$  the horizontal drag force can be given as:

$$F_D = F_N \cos \left( \frac{\theta}{2} \right) = \frac{1}{2} \rho (C_D)_0 A_{\perp} V_{rel}^2 \cos^3 \left( \frac{\theta}{2} \right) \quad (28)$$

This equation, when compared with equation (7), leaves the result given by equation (26).

The value of  $(C_D)_0$  in numerous Froude and Reynolds tests was measured to be between 1.92 and 1.97. An average value of  $(C_D)_0 = 1.93$  is assumed. This value at first seems inordinately yet appealingly high when compared to those for crossed vanes and parachutes. It has, however, been found in the literature (Hoerner, 1965, p.3-13 Fig. 23 and p.3-16, Fig. 28) that for square, rigid plates with sharp corners or plates with a large length-to-width ratios, a drag coefficient of up to 1.98 has been reported. The assumed value of  $(C_D)_0 = 1.93$  for window shade drogues may be less because the plastic walls might somewhat comply with the flow around the edges.

The lift-to-drag ratio of numerous test drogues has been plotted in Figure 21 as a function of tether line inclination angle. As described, the ability to measure this ratio is difficult at low angles. This fact is evident in Figure 21. At higher angles, however, it is further evident that the data group together well, indicating an increased measurement accuracy.

Figure 21 also shows an analytically derived lift-to-drag ratio derived directly from the forces shown in Figure 20.

That is:

$$\frac{L}{F_D} = \frac{F_N \sin \left(\frac{\theta}{2}\right)}{F_N \cos \left(\frac{\theta}{2}\right)} = \tan \left(\frac{\theta}{2}\right). \quad (29)$$

It can be seen that this analytical curve passes directly through the data points ( $\theta \approx 50^\circ$ ) where the ratios for different shapes begin to converge due to the better measurement ability at higher angles. As a result a great deal of confidence is placed in the analytical derivations as representations of the measured data.

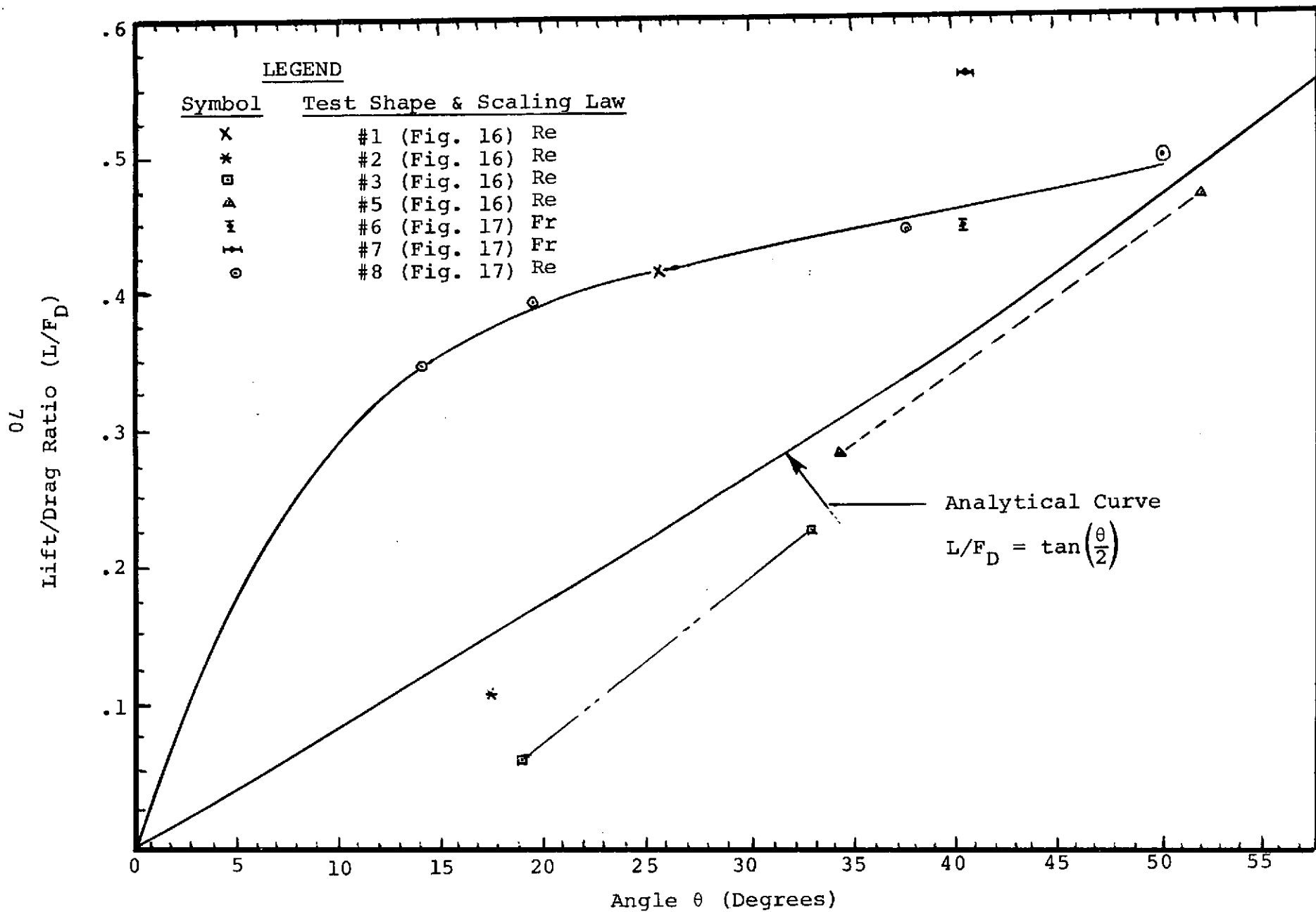


Fig. 21 Window Shade Drogue Lift-to-Drag Ratio Vs. Angle From Vertical

A useful method of applying the model window shade drogue test data in an easily understood manner is to derive nomographs which predict the drogue drift velocity as a function of drag force ( $F_D$ ) in the tether line, drogue area (A), and ballast weight (W). That is:

$$V_{rel} = f(F_D, A, W) \quad (30)$$

In order to achieve a useful mathematical relationship for a rectangular drogue, a moment balance is taken about the tether point in Figure 20 as follows:

$$\Sigma M_O = 0 = W\ell \sin\left(\frac{\theta}{2}\right) - \frac{1}{2} \rho (C_D)_O A_{\perp} V_{rel}^2 \left[ \cos^2\left(\frac{\theta}{2}\right) \right] \frac{\ell}{2} \quad (31)$$

This equation can be reduced to the form:

$$K_1 W = V_{rel}^2 \frac{\cos^2 \phi}{\sin \phi} \quad (32)$$

where:

$$\phi = \frac{\theta}{2} \quad (33)$$

and

$$K_1 = \frac{4}{\rho A_{\perp} (C_D)_O} \quad (34)$$

In order to eliminate  $\phi$  from equation (32) in favor of drag force,  $F_D$ , equation (28) is employed in order to substitute the following identities:

$$\cos^2 \phi = \left[ \frac{F_D}{\frac{1}{2} \rho (C_D)_O A_{\perp} V_{rel}^2} \right]^{2/3} \quad (35)$$

$$\sin \phi = \left[ 1 - \cos^2 \phi \right]^{1/2} = \left[ 1 - \left( \frac{F_D}{\frac{1}{2} \rho (C_D)_O A_{\perp} V_{rel}^2} \right)^{2/3} \right]^{1/2} \quad (36)$$

After appropriate substitutions of  $K_1$ , equation (32) is solved for  $F_D$  in the following working form:

$$(F_D)^{2/3} = -81.34 \frac{K_1^{1/3} W^2}{V_{rel}^{8/3}} + \frac{1}{2} \left[ \frac{2.645 \times 10^4 K_1^{8/3} W^4}{V^{16/3}} + \frac{102 K_1^{2/3} W^2}{V^{4/3}} \right]^{1/2} \quad (37)$$

where the constants are appropriate to the following system of units:

$$\begin{aligned} [K_1] &= \text{ft} / \text{lb-mass} \\ [W] &= \text{lb-force} \\ [V] &= \text{ft} / \text{sec} \end{aligned}$$

Equation (36) was put on a digital computer and curve families derived. Appendix B contains six nomographs (Figures B-4 through B-9) for ballast weights from 25 to 300 pounds and drogue areas from 25 square feet to 800 square feet. By reference to figures B-4 through B-5 it can be seen that a window shade drogue cannot develop a greater drag force than the weight of the ballast placed at the bottom of the drogue. As the tether line forces approach the ballast weight force, the drogue begins to stream at higher average chord angles ( $\theta/2$ ) with respect to the tether point. Ultimately, as the drag force exceeds the ballast weight force, the relative velocity will increase dramatically and the drogue drag force will drop off sharply going into an unstable part of the operating curve. It is unstable in that higher relative velocities cause the drogue to generate lower forces. It can be seen by lines of equal angle in the figures that under these conditions the values of  $\theta$  are relatively large and the drogues are streaming close to horizontal and functioning very ineffectively. In order to restore the drogues to an area of effective drag performance, below the knee in the curves, the velocity of the drogue through the water must be reduced below the value occurring at the knee

in the curve. Figure B-10 is a plot of the loci of instability drift velocity points at which the drag force ( $F_D$ ) equals the ballast weight ( $W$ ) for given drogue areas.

The curves presented in Figures B-4 through B-9 neglect tangential shearing forces on the drogue, in order to reduce the complexity of the mathematics. If such forces were taken into account, the maximum drag force at the peak of the curves might be increased by approximately 3% (see Appendix D for measured shear drag coefficient).

A useful theoretical dimensionless window shade drogue performance relation is derived from equations (28) and (31). By cancelling the length,  $l$ , in equation (31) and multiplying both sides by  $\cos \frac{\theta}{2}$  the following relation is derived:

$$W \left[ 2 \sin\left(\frac{\theta}{2}\right) \cos\left(\frac{\theta}{2}\right) \right] = \frac{1}{2} \rho (C_D)_0 A_{\perp} V_{rel}^2 \cos^3\left(\frac{\theta}{2}\right) = F_D \quad (38)$$

When the term within brackets is reduced by a trigonometric identity, the following is derived:

$$W \sin \theta = F_D \quad (39)$$

This relationship is employed in order to derive the dimensionless window shade drogue performance curve shown in Figure B-11. This curve is applicable to a rectangular window shade drogue of any area and ballast weight. Other shapes such as triangles would require a recomputation if the center of pressure were greatly displaced from the vertical center i.e.,  $\frac{l}{2}$ .

Tests were conducted in order to ascertain the effects of drogue heave on the drag performance. The complexity of the measurements and lack of time prohibited the acquisition of much reliable data. It was observed that for drogues aligned very near vertical (i.e.,  $\phi < 5$  to  $10^\circ$ ), vertical motion of the

upper end of the tether line produced negligible horizontal drogue motion which could alter drag performance due to the high added mass coefficient of the drogue in the presence of horizontal acceleration. At higher values of the ratio  $F_D/W$ , resulting in higher values of  $\phi$ , a greater error could be induced. It is still felt that a maximum error of less than 10% would result even at high values of  $\phi$  and large vertical inputs from the buoy. This number would be increasingly reduced for deeper drogues and for buoys with more elasticity in the mooring line.

A window shade drogue is the recommended drogue from the described series of tests. By close examination of the data in Figures 16 and 17 it appears that the drag coefficients of triangles is somewhat less than rectangles and diamonds. The merit of a single rigid member in a triangle and diamond is dramatically offset by the fact that for a given pole length and drogue height, only half the area of a rectangle can be achieved. The practical limits of keeping a pole length short enough to fit easily aboard a ship favors the use of two poles and a rectangular shape as being most efficient.

Tests indicated that the drag coefficients of the rectangular shapes tested (shown in Appendix A also) were all nearly the same. Furthermore, equations (31) and (32) indicate that the vertical drogue height is not a factor in minimizing drogue lift and as a result minimizing  $\phi$ . It can be seen that  $l$ , the drogue height, cancels in equation (31). Therefore, a short wide drogue to a first order approximation is as good in minimizing  $\phi$  as a long, narrow drogue.

A recommended window shade drogue design is a rectangle with a pole length that can be handled aboard ship (10 to 15-foot maximum length). The height of the drogue should be chosen such that the desired current locking accuracy is achieved with a given ballast weight and maximum anticipated drag force

arising from wind and current forces on the buoy. The recommended method of attaching the drogue to the tether line is by means of a triangular tether line yoke as shown in Figures 16 and 17. The apex of the yoke should be in line with the centerline of the drogue. In order to achieve a maximum drogue area, it is recommended that the triangular area within the attachment yoke be covered with drogue material also.

It is recommended that the drogue ballast weight be incorporated into a rigid bottom pole on a rectangular drogue. In this manner, the stress due to the static and dynamic loads induced by the weight are spread uniformly over the largest possible drogue cross-section, minimizing the chances of a fatigue failure. If the stresses on a given material, such as a thin-walled plastic sheet, were found to be unduly large, a load-carrying wire could be installed between the upper and lower poles. This added feature appears to be a necessity in a triangular or diamond-shaped drogue, wherein the drogue and weight are supported through narrow drogue cross-sectional areas.

In various model tests, concentrated ballast weight loads on the bottom pole caused the pole to deflect and, as a result, create adverse cross-sections in the presence of flow. For example, a load concentrated in the center of a lower, non-rigid pole caused only the central portion of the drogue to be rigidized, while the edges bent back with the flow. This effect created a "fee-fin" profile pointing into the flow which reduced the overall drag coefficient. Alternatively, concentrating the weights beneath the edges of the drogue with non-rigid poles, rigidizes the edges, allowing the central portion to belly inward in a flow condition. This condition is more advantageous than the first example. Taken to its logical extreme, however, this shape begins to look like a rectangular parachute which displays a markedly lower drag coefficient of 1.35. Therefore, it is recommended that the poles be rigid and the weight be as uniformly distributed as possible across the bottom of the drogue.

## 7.0 Test of Plastic Sheets in the Ocean

Ease of deck storage and deployment dictate the use of thin walled sheets of material for flexible, collapsible drogues. In the past parachutes have employed nylon material extensively but, however, as originally designed they were required to perform only in the benign air environment. When installed in the ocean for extended periods of time new questions arise regarding fishbite and material bleaching, erosion, and biodeterioration.

A total of 9 one square-foot samples of 3 different materials were implanted in the Northwest Atlantic for approximately 100 days in an attempt to gain insight into the problems. A sample of each material was placed on a Mid Ocean Dynamics Experiment (MODE) mooring at depths of 500, 1000, and 1500 meters. The geographic location was approximately 70° W. Long., 28° N. Lat. or 300 miles southwest of the island of Bermuda. The materials were installed and retrieved by personnel of the Woods Hole Oceanographic Institute (WHOI). The samples were fastened to the mooring line by nylon rope passing through grommets installed in the plastic samples. The sample materials were the following:

- #1 Herculite Marine DR (.0145" thick)
- #2 Herculite No. 6 (.0085" thick)
- #3 Plastic coated nylon ripstop (.005" thick) .

The samples were all returned and found to be essentially in perfect condition. During the retrieval of the samples installed at a 500 m. depth the samples became entangled in heavily loaded mooring chain. Holes were later observed in the Herculite samples and were tentatively attributed to chafing on the chains. In addition there was no observable material bleaching, erosion, or biological growth on any of the samples.

## 8.0 Error Estimation

The tests outlined in sections 4 and 5 were conducted in the most expeditious manner which would minimize costs and errors. The tow tank carriage speed was carefully calibrated at a fixed motor speed setting by the use of a tape measure and stop watch. Speed variations were achieved through changing known gear ratios. Considerable time was spent in modifying and updating the drag force measuring device in order to minimize errors observed in the earliest test phase. Errors still, however, remained.

Because the drag force measurement depends on the deflection of a mass on the end of a spring beam (see Figure 9) in the direction of carriage travel, the spring deflects in the presence of spurious carriage accelerations or vibrations. For example, the carriage rollers would occasionally stick and subsequently break free producing axial accelerations. At these times the spring-mass system would begin to oscillate. Because drag force values were averaged over a ten second period, an integer number of such oscillations would produce a cancelling effect. Not wanting to rely on this, two steps were taken to avoid errors:

- (1) An accelerometer was mounted on the tow carriage with its sensitive axis in the direction of travel. The output was recorded on a strip-chart recorder. When large carriage accelerations were observed the drag force data point was discarded.
- (2) An air dashpot damper was also mounted to the flexible member of the force measurement device in order to rapidly attenuate oscillations of the force blocks. Tests were run in the laboratory and the optimum damping constant selected.

The force measurement device was calibrated by appropriately supporting accurately-known weights by a string. Calibrations were taken both before and after the test and a maximum scale factor difference of less than 1% was observed.

Due to electrical noise, random zero shifts, and creep of the force blocks and their mounts a constant force measurement error of approximately  $\pm 0.4$  grams ( $\pm 0.001$  pounds) persisted. At the low drag forces the error as a percentage of the total measurement was higher. Constant checks on the zero stability aided in pinpointing these random occurrences and as a result the data were discarded. The overall accuracy of the resulting drag coefficient measurements at low speeds is felt to be within approximately 10%.

At higher speeds, other problems arose which degraded the accuracy of the drag coefficient measurements. Vortex shedding from numerous shapes induced oscillations which altered the drag characteristics of pendulously supported shapes. This error was small for most shapes such as sea drogues shown in Figure 4. In the case of the heavily-ballasted window shade drogues, however, during Reynolds scaling tests these oscillations reinforced a pendulum mode of oscillation. A calculation of the undamped natural period of a pendulum in the form of a window shade drogue was found to lie very close to the period of vortex-induced oscillation at higher towing speeds. This problem would not exist in the ocean because the relative velocity by a drogue should be very small. It is felt that the above problem lead to an overall non-systematic error of less than 15% in an individual measurement of drag coefficient. By averaging many test data points this value was considerably reduced, permitting the specification of the drag coefficient as a function of streaming angle as shown in Figures 18 and 19. A maximum error of 5% is felt to be a realistic estimate for the values ultimately used in generating the curves shown in Appendix B.

## 9.0 Conclusions and Recommendations

In light of the scale model drogue test results and subsequent analyses, a number of conclusions can be drawn. The weight of evidence on drag performance plus simplicity, cost, and aesthetic appeal point towards the use of a window shade or sail drogue. Unlike the parachute or water-entrapment type drogues, the drag force developed is not strictly a function of the relative or slip velocity by the drogue. If the drogue is not properly sized and weight ballasted, it may perform very poorly as a water mass locking device. A user should refer to data presented in the Appendix B nomographs and ballast the bottom of a window shade drogue with a weight greater than the largest anticipated drag load on the drogue. This value of ballast weight should also be selected in terms of desired depth locking accuracy. Appendix C presents a simple calculation scheme and a nomograph depicting depth locking ability. In general it is felt that a ballast weight should be at least twice as large as the largest anticipated drag load. The inertia loads for such a ballast weight in the presence of heave is shown in Appendix D to be a small part of the total buoy dynamic load.

Parachute drogues have definite advantages of low cost (government surplus), easy storage, an adequate drag coefficient, and relatively low dynamic forces induced by a heaving buoy. The latter advantage would seem to hold true only if the chute was deployed horizontally in a flow (i.e., neutrally buoyant as in Fig. 1). They are, however, subject to other problems. Upon initial deployment, a minimum current is required in order to open them and obtain the full rated drag area,  $C_D A$ . A non-zero relative velocity is also required to keep the parachute open. The value of these required velocities is a function of how much the chute itself differs from the neutrally buoyant condition. Once deployed in a low relative velocity situation, the chute will hang up (positively buoyant) or down (negatively buoyant) at an acute angle to the flow depending on the degree of non-neutral buoyancy.

In general, a buoy-induced dynamic motion of a drogue will alter their effective drag coefficient very little. Heave tends to augment the apparent drag coefficient. The amount of augmentation should increase with an increase of the tether line angle with respect to vertical. Drogues nearer the surface should experience greater changes. It is recommended that these and other performance parameters be checked in full scale experiments.

A rectangle is recommended as a generalized shape for a window shade drogue. It should have two poles; one at both the top and bottom. Both ends of the upper pole should contain tether lines which meet at a common point to which a single tether line is attached and leads to the buoy. It is recommended that the triangular area formed between the pole and the tether lines contain drogue material in order to increase the drag area. The poles, of nearly equal length, should be sized to achieve adequate drogue area yet permitting the drogue to store readily aboard a ship.

The ballast weight should be attached directly to or an integral part of the bottom pole. Weight should be distributed as much as possible in order to reduce stresses.

Nylon or Herculite materials are tentatively recommended for the drogue fabric. Further tests will help to qualify this during the coming year. The least expensive and/or lightest weight material, exhibiting nearly zero porosity, that can survive the environment is desirable. At present there appears to be no benefit to any specific color.

This writing presents much information, both in the body of the report and in the Appendices, that can be immediately incorporated into designing a window shade drogue. If the data presented in the Appendices are inadequate, equations are presented by which an investigator can generate additional data for individual needs, thus allowing a drift correction scheme for all combinations of drogues and ballast weights.

## REFERENCES

1. Baker, G.S., "Model Drogue Experiments," Rep. Memor. Adv. Comm. Aero., London, 425, 12 p. and 8 figs., 1918.
2. Batchelor, G.K., An Introduction to Fluid Mechanics, Cambridge Univ. Press, 1967.
3. Bowden, K.F., "The Direct Measurement of Subsurface Currents in the Ocean," Deep Sea Research, Vol. 2, pp 33-47, 1954.
4. Buchanan, J.Y., 1885, "On Oceanic Shoals Discovered in the S.S. DACIA in October 1883," Proc. Roy. Soc., Edinburgh, 13 pp 428-443 and Plate XII.
5. Buchanan, J.Y., 1895, "A Retrospect of Oceanography in the Last Twenty Years," Rep. Int. Geogr. Congr., 6th, London, 11, pp 403-435.
6. Carpenter, W.B., and J.G. Jeffreys, 1870, "Report on Deep Sea Researches Carried on During the Months of July, August, and September 1870 in H.M. Surveying-Ship PORCUPINE," Proc. Roy. Soc. London, 19, pp 146-221 and 2 charts.
7. Cromwell, Townsend, 1956, "Eastropic Expedition," Pacific Fisherman, July, pp 25-29.
8. Cromwell, T., R.B. Montgomery, and E.D. Stroup, "Equatorial Undercurrent in the Pacific Ocean Revealed by New Methods," Science, Vol. 119, pp 648-649, 1954.
9. Epple, H.K., "The Effect of the Porosity on Performance and Properties of Parachutes," Sept. 1969, DDC Acc. No. N71-12245.
10. Ewing, G.C., and F.L. Striffler, "Experience with a Drifting IRLS Buoy," W.H.O.I. Ref. No. 70-53, 1970 (Unpublished Manuscript).
11. Gaul, R.D. and J.E. Seward, Jr., "Nearshore Ocean Currents off San Diego, Calif.," J. Geophys. Research, 65, pp 1543-56, 1960.
12. Gerard, R. and M. Salkind, 1965, "A Note on the Depth Stability of Deep Parachute Drogues", Deep Sea Research, Vol. 12, pp 377-379.
13. Heinrich, H.G., and Haak, E.L., 1971, "Stability and Drag of Parachutes with Varying Effective Porosity," Air Force Flight Dynamics Lab Report No. AFFDL-TR-71-58, Defense Doc. Center (DDC) Acc. No. AD 729 858.

REFERENCES (Cont.)

14. Hoerner, S.F., "Fluid Dynamic Drag, Practical Information on Dynamic Drag and Hydrodynamic Information," published by the Author, Midland Park, N.J., 1965.
15. Johns, T.F., Auterson, E.I., "The Effects of Various Factors on Parachute Characteristics", Jan. 1944, DDC Acc. No. ATI 24671.
16. Kawamoto, Takeo, 1958, "The Construction of a Parachute Drogue", Oceanogr. Mag., Vol. 10, pp 9-12.
17. Knacke, T., Hegele, A., "Model Parachutes, Comparison Tests of Various Types", Jan. 1949, DDC Acc. No. ATI 67374.
18. Knauss, J.A., and J.E. King, 1958, "Observations of the Pacific Equatorial Undercurrent", Nature, London, Vol. 182, pp 601-602.
19. Leetma, A., 1972, "The Response of the Somali Current to the Southwest Monsoon of 1970", Deep Sea Research, Vol. 19, pp 319-325.
20. Leetma, A., 1973, "The Response of the Somali Current at 2° S. to the Southwest Monsoon of 1971", Deep Sea Research, Vol. 20, pp 397-400.
21. Marks, Wilbur, 1956, "Wind and Sea Scale for Fully-Arisen Sea", Table Compiled at David Taylor Model Basin.
22. Melzig, H., 1969, "The Influence of Porosity on Performance and Properties of Parachutes", DDC Acc. No. N71-12245.
23. Metcalf, W.G., A.D. Voorhis, and M.C. Stalcup, 1962, "The Atlantic Equatorial Undercurrent", J. Geophys. Res., Vol. 67, pp 2499-2508.
24. Metcalf, W.G., 1969, "Current Meter and Hydrographic Data from Crawford Cruise #165 in the Tropical Atlantic Ocean, Feb.-April 1968", W.H.O.I. Ref. No. 69-72 (Unpublished Manuscript).
25. Mitchell, Henry, 1859, "Report ... on the Physical Surveys of New York Harbor and the Coast of Long Island, with Descriptions of Apparatus for Observing Currents, etc.," Rep. Supt. Coast Surv. (Appendix No. 26), pp 311-17 and Plate 40.
26. Mitchell, Henry, 1967, "Report ... on Soundings Made to Develop the Character of the Strait of Florida Between Key West and Havana", Rep. Supt. U.S. Coast Survey (Appendix No. 15), pp 176-179.

REFERENCES (Cont.)

27. Monahan, E.C., G.T. Kaye, and E.D. Michelena, 1973, "Drogue Measurements of the Circulation in Grand Traverse Bay, Lake Michigan", Univ. of Michigan Sea Grant Tech. Report No. 35.
28. Monahan, E.C. and E.A. Monahan, 1973, "Drogues, Drags, and Sea Anchors", Univ. of Michigan Sea Grant Technical Report (In Publication).
29. Montgomery, R. B., and E.D. Stroup, 1962, "Equatorial Waters and Currents at 150° in July-August 1952," Johns Hopkins Oceanographic Studies, No. 1.
30. Moskowitz, L, 1964, "Estimates of the Power Spectrums for Fully Developed Seas for Wind Speeds of 20 to 40 Knots", Jour. Geophys. Res., Vol. 69, No. 24, pp 5161-5179.
31. Nares, G.S., 1872, "Investigations of the Currents in the Strait of Gibraltar, Made in August 1871, by Captain G.S. Nares, R.N., of H.M.S. SHEARWATER, Under Instructions from Admiral Richards, F.R.S., Hydrographer of the Admiralty", Proc. Roy. Soc. London, 20, pp 97-106.
32. Oceanographic Section, 1956, "Current Measurements in the Kuroshio with the Parachute Current Drogue (in Japanese)," Oceanogr. Rep. Japan Meteor. Agency, 5, 157-169.
33. Parker, C.E. 1963, "The Radio Drogue System", W.H.O.I. Ref. No. 63-12, (Unpublished Manuscript).
34. Parker, C.E. 1963, "Current Measurements Employing the Radio Drogue System", W.H.O.I. Ref. No. 63-13, (Unpublished Manuscript).
35. Pillsbury, J.E., 1890, "The Gulf Stream - A Description of the Methods Employed in the Investigation, and the Results of the Research", Rep. Supt. U.S. Coast Survey (Appendix 10), pp 459-620.
36. Pierson, W.J. Jr., 1964, "The Interpretation of Wave Spectrums in Terms of the Wind Profile Instead of the Wind Measured at a Constant Height", Jour. Geophys. Res. Vol. 69, No. 24, pp 5191-5203.
37. Pierson, W.J., Jr. and L. Moskowitz, 1964, "A Proposed Spectral Form for Fully Developed Wind Seas Based on the Similarity Theory of S.A. Kitaigorodski", Jour. Geophys. Res., Vol. 69, no. 24, pp 5181-5190.
38. Pochapsky, T.E., 1961, "Some Measurements with Instrumented Neutral Floats", Deep Sea Res., Vol. 8, pp 269-275.

REFERENCES (Cont.)

39. Pochapsky, T.E., 1963, "Measurement of Small-Scale Oceanic Motions with Neutrally-Buoyant Floats", Tellus XV, Vol. 4, pp 352-362.
40. Rossby, T.E., and D. Webb, 1970, "Observing Abyssal Motions by Tracking Swallow Floats in the SOFAR Channel", Deep Sea Res., Vol. 17, pp 359-365.
41. Rossby, T., and D. Webb, 1971, "The Four Month Drift of a Swallow Float", Deep Sea Res., Vol. 18, pp 1035-1039.
42. Spratt, T.A.B., 1871, "On the Undercurrent Theory of the Ocean, As Propounded by Recent Explorers", Proc. Roy. Soc., London, 19, pp 528-566.
43. Stalcup, M.C., and C.E. Parker, 1965, "Drogue Measurements of Shallow Currents on the Equator in the Western Atlantic Ocean", Deep Sea Res., Vol. 5, pp 535-536.
44. Stommel, H., 1954, "Serial Observations of Drift Currents in the Central North Atlantic Ocean", Tellus, Vol. 6, pp 203-214.
45. Swallow, J.C., 1965, "A Neutral Buoyant Float for Measuring Deep Currents", Deep Sea Res., Vol. 3, pp 74-81.
46. Swallow, J.C. and L.V. Worthington, 1957, "Measurements of Deep Currents in the Western North Atlantic", Nature, London, 179, pp 1183-1184.
47. Swanson, E.R., and M.L. Tibbals, 1965, "The OMEGA Navigation System", Navigation, Vol. 12, (1) pp 24-35.
48. Thompson, A.S., 1895, "Remarks on Ocean Currents and Practical Hints on the Method of Their Observation", Rep. Int. Geogr. Congr., 6th, London, pp 443-459, and folded table.
49. U.S.A.F. Parachute Handbook, ATI 35532, pp 78, 1951.
50. Volkman, G., J. Knaus, and A. Vine, 1956, "The use of Parachute Drogues in the Measurement of Subsurface Ocean Currents", Trans. Amer. Geophysical Union, Vol. 37, No. 5.
51. Wang, H.T., and T.L. Moran, 1971, "Analysis of the Two-Dimensional Steady-State Behavior of Extensible Free-Floating Cable Systems", Naval Ship Res. & Dev. Ctr. Report 3721.

## APPENDIX A

### Model Drogue - Detailed Test Results

For those scientists and experimenters who are seeking a more detailed knowledge of how various model drogue devices performed, a comprehensive set of results is presented. These results present the ranges of scaling parameters (Reynolds and/or Froude numbers), measured drag coefficients, and the average drag areas ( $C_D A$ ). Other important observations relating to the test are also mentioned.

Figures A-1 to A-9 tabulate the pertinent experimental data. Data in figures A-1 to A-3 are derived at Reynolds scaling speeds only; employing a dimensional scale factor of 16. The model towing speeds ranged from .31 to 2.53 knots which are equivalent to full scale model speeds of .02 knots (1 cm/sec) and .158 knots (8 cm/sec). Figure A-4 reports only Froude scaling results for crossed vanes. Figure A-5 through A-9 report both Reynolds and Froude scaling results. The model Froude scaling speeds in general ranged from .013 to .08 knots (i.e., .67 cm/sec to 4 cm/sec) which are equivalent to 2.7 cm/sec and 16 cm/sec. It was very difficult to derive meaningful data at speeds of .013 knots and less due to problems outlined in Section 8.0.

Device No.	Drag Device Size and Shape	Reynolds Number Range	Range of Drag Coefficients, $C_D$	Average Drag Coefficient, $C_D$	Comments and Observations
1	16.5" Dia. Parachute	$6.4 \times 10^4$ to $2.9 \times 10^5$	1.23 to 1.39	1.35	Coning action within $\pm 45^\circ$ ( $T \approx 5$ sec.). Severe (up to 50%) osc. in drag force. $A = 1.47 \text{ ft}^2$
2	15" Dia. Bucket Drogue	$5.8 \times 10^4$ to $5.6 \times 10^5$	1.25 to 1.43	1.34	Lateral oscillations $\pm 10^\circ$ at low speeds. Tows steady at $5^\circ$ off-set angle at higher speeds. $A = 1.22 \text{ ft}^2$
3	15" Dia. Sea Drogue ( $L/D = 2.0, A_2 = .03A_1$ )	$5.8 \times 10^4$ to $5.6 \times 10^5$	1.51 to 1.68	1.56	At lower speeds tows approx. $10^\circ$ off to side. $A = 1.22 \text{ ft}^2$
4	15" Dia. Sea Drogue ( $L/D=2.0, A_2 = .05A_1$ )	$5.8 \times 10^4$ to $5.6 \times 10^5$	1.45 to 1.60	1.53	Tows approx. $10^\circ$ off to side at lower speeds and less at higher speeds. $A = 1.22 \text{ ft}^2$
5	15" Dia. sea Drogue ( $L/D=2.0, A_2 = .1A_1$ )	$5.8 \times 10^4$ to $5.6 \times 10^5$	1.36 to 1.63	1.47	Tows approx. $5^\circ$ off to side at lower speeds and less at higher speeds. $A = 1.22 \text{ ft}^2$

FIGURE A-1 DRAG COEFFICIENTS OF DROGUE MODELS

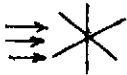
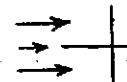
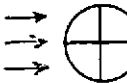
Device No.	Drag Device Size and Shape	Reynolds Number Range	Range of Drag Coefficients, $C_D$	Average Drag Coefficient, $C_D$	Comments and Observations
6	3-axis Crossed Vanes (10" x 10"), no ends flow 	$3.5 \times 10^4$ to $2.9 \times 10^5$	.97 to 1.06	1.02	$A = .694 \text{ ft}^2$ Ave. $C_D A = .706 \text{ ft}^2$ Geometry held rigidly
7	3-axis crossed Vanes (10" x 10"), no ends flow 	$3.5 \times 10^4$ to $2.9 \times 10^5$	1.24 to 1.37	1.29	Ave. $C_D A = .775 \text{ ft}^2$ $A = .601 \text{ ft}^2$ Geometry held rigidly.
8	3-axis Crossed Vanes with end plates flow 	$3.5 \times 10^4$ to $2.9 \times 10^5$	1.29 to 1.42	1.33	Ave. $C_D A = .812 \text{ ft}^2$ Geometry held rigidly. $A = .601 \text{ ft}^2$
9	3-axis Crossed Vanes with end plates flow 	$3.5 \times 10^4$ to $2.9 \times 10^5$	0.96 to .995	0.97	Ave. $C_D A = .673 \text{ ft}^2$ $A = .694 \text{ ft}^2$ Geometry held rigidly.
10	2-axis Crossed Vanes (10" x 10"), no ends flow 	$3.5 \times 10^4$ to $2.9 \times 10^5$	1.31 to 1.33	1.32	Ave. $C_D A = .912 \text{ ft}^2$ Geometry held rigidly $A = .604 \text{ ft}^2$
11	2-axis Crossed Vanes (10" x 10") no ends flow 	$3.5 \times 10^4$ to $2.9 \times 10^5$	1.32 to 1.39	1.35	Ave. $C_D A = .664 \text{ ft}^2$ Geometry held rigidly $A = .694 \text{ ft}^2$
12	2-axis Crossed Vanes (10" x 10") with end plates flow 	$3.5 \times 10^4$ to $2.3 \times 10^5$	1.36 to 1.41	1.38	$A = .694 \text{ ft}^2$ Ave. $C_D A = .956 \text{ ft}^2$ Geometry held rigidly.

FIGURE A-2 REYNOLDS SCALED DRAG COEFFICIENTS OF CLAMPED ALUMINUM CROSSED VANES

Device No.	Drag Device Size and Shape	Reynolds Number Range	Range of Drag Coefficients, $C_D$	Average Drag Coefficient, $C_D$	Comments and Observations
13	2-Axis Vanes (10" x 10"), with end plates → flow → 	$3.5 \times 10^4$ to $2.9 \times 10^5$	1.29 to 1.37	1.33	Ave. $C_D A = .654 \text{ ft}^2$ Geometry held rigidly $A = .49 \text{ ft}^2$
14	3-Axis Alum Vanes (10" x 20"), with end plates → 	$3.5 \times 10^4$ to $1.1 \times 10^5$	1.25 to 1.32	1.27	Ave $C_D A = 1.53 \text{ ft}^2$ Re based on width = 10" Geometry Held Rigidly $A = .601 \text{ ft}^2$
15	3-Axis Alum Vanes, No end plates, Pendulous on 2 ½ foot string	$3.5 \times 10^4$ to $1.1 \times 10^5$	1.1 to 1.21 Based on $A = .694 \text{ ft}^2$	1.18 based on $A = .694 \text{ ft}^2$ 1.36 based on $A = .601 \text{ ft}^2$	Ave. $C_D A = .819 \text{ ft}^2$ Solid Aluminum Vanes
16	3-Axis Alum Vanes, with end plates. Pendulous on 2 ½ foot string	$3.5 \times 10^4$ to $1.7 \times 10^5$	.85 to 1.37 Based on $A = .694 \text{ ft}^2$	1.1 based on $A = .694 \text{ ft}^2$ 1.28 based on $A = .601 \text{ ft}^2$	Ave. $C_D A = .767 \text{ ft}^2$ Solid Aluminum Vanes $C_D$ & $C_D A$ increase with speed $C_D$
17	2-Axis Alum Vanes, no end plates. Pendulous on 2 ½ foot string	$3.5 \times 10^4$ to $1.1 \times 10^5$	1.12 to 1.25 Based on $A = .694 \text{ ft}^2$	1.20 based on $A = .694 \text{ ft}^2$ 1.69 based on $A = .491 \text{ ft}^2$	Ave. $C_D A = .831 \text{ ft}^2$
18	2-Axis Alum Vanes, with end plates. Pendulous on 2 ½ foot string	$3.5 \times 10^4$ to $1.7 \times 10^5$	1.02 to 1.66 Based on $A = .694 \text{ ft}^2$	1.3 based on $A = .694 \text{ ft}^2$ 1.83 based on $A = .491 \text{ ft}^2$	Ave. $C_D A = .902 \text{ ft}^2$ $C_D$ & $C_D A$ increase with speed
19	3-Axis Plastic Vanes, (10" x 10"), No ends. Pendulous on 2.3 foot string	$2.9 \times 10^4$ to $1.4 \times 10^5$	1.2 to 1.49	1.4 based on $A = .694 \text{ ft}^2$ 1.62 based on $A = .601 \text{ ft}^2$	Ave. $C_D A = .973 \text{ ft}^2$

FIGURE A-3 REYNOLDS SCALED DRAG COEFFICIENTS OF CROSSED VANES

Device No.	Drag Device Size and Shape	Reynolds or Froude Number Range	Range of Drag Coefficients, $C_D$	Average Drag Coefficient, $C_D$	Comments & Observations
20	3-Axis Plastic Vanes (10" x 10") No end plates, 20 gm. Ballast. Pendulous on 2.5' string	Re = $1.8 \times 10^3$ to $2.4 \times 10^4$	.56 to 1.34 (A = .694 ft <sup>2</sup> )	.9 based on A = .694ft <sup>2</sup>	Ave. $C_D A = .632 \text{ ft}^2$  $C_D A$ increases with speed. Froude Scaling Speeds
		Fr = .005 to .067		1.02 based on A = .61ft <sup>2</sup>	
21	2-Axis Plastic Vanes (10" x 10") No end Plates. Pendulous on 2.5' string	Re = $2.5 \times 10^3$ to $9.2 \times 10^3$	1.19 to 1.77 (A = .694 ft <sup>2</sup> )	1.51 based on A = .694 ft <sup>2</sup>	Ave. $C_D A = 1.05 \text{ ft}^2$ 26 gram ballast wt. on bottom of drogue.
				2.14 based on A = .49ft <sup>2</sup>	
22	2-Axis Alum (10" x 10") vanes, no end plates, no ballast. Pendulous on string	Re = $2.2 \times 10^3$ to $10^4$	.97 to 1.22 (A = .694ft <sup>2</sup> )	0.81 based on A = .694 ft <sup>2</sup>	Ave. $C_D A = .56 \text{ ft}^2$  Model speeds = .02 to .1 knots
		Fr = .0064 to .032		1.15 based on A=.49 ft <sup>2</sup>	
23	3-Axis Alum Vanes, no end plates or ballast, Pendulous on string	Re = $1.7 \times 10^3$ to $10^4$	1.09 to 1.46 (A = .694ft <sup>2</sup> )	1.3 based on A=.694ft <sup>2</sup>	Ave. $C_D A = .902 \text{ ft}^2$
		Fr=.0049 to .032		1.48 based on A=.601ft <sup>2</sup>	

FIGURE A-4 FROUDE SCALED DRAG COEFFICIENTS OF MODEL DROGUES

Device No.	Drag Device Size and Shape	Reynolds or Froude Number Range	Range of Drag Coefficients, $C_D$	Average Drag Coefficient, $C_D$	Comments & Observations
24	36" x 42" l. Buoyed Nylon Fish Net, 0.21" square mesh, .025" string dia.	$Re_1 = 10^4$ to $10^5$	0.14	0.25	Ave. $C_D A = 2.625 \text{ ft}^2$ Vel. = .02 to .2 knots $C_D$ based on full net area. 5-1/10 lb wts. along bottom edge.
		$Fr_1 = .032$ to .32	to 0.39		
25	36" x 42" l. Buoyed Nylon Fish Net, .125" w. Hex Mesh, .030" string dia.	$Re = 10^4$ to $10^5$	0.09	0.16	Ave. $C_D A = 1.68 \text{ ft}^2$ Vel. = .02 to .2 knots $C_D$ based on full net area. 2 - 1/4 lb wts at bottom corners
		$Fr_1 = .032$ to .32	to 0.39		
26	<u>Reynolds Test</u> 3" dia. Plastic Cylinder ( $L/D = 5$ ), 5.8-lb ballast wt.	$Re_D = 10^4$ to $5 \times 10^4$	0.99 to 1.45	1.31	Ave. $C_D A = 0.409 \text{ ft}^2$ Lateral oscillations at ~1 Hz (wt. acts as pendulum). Plastic flattened out into flow
27	<u>Froude Test</u> 3" dia. Plastic cylinder ( $L/D = 5$ ), 100-gram ballast wt.	$Re_D = 4 \times 10^3$ to $2 \times 10^4$ $Fr_D = .116$ to .58	0.44 to 1.13	0.82	Ave. $C_D A = 0.256 \text{ ft}^2$ Stiffness of plastic prohibited plastic from full deployment Vel. = .02 to .1 Knot

06



FIGURE A-5 REYNOLDS AND FROUDE SCALING TEST RESULTS OF MODEL DROGUES

Device No.	Drag Device Size and Shape	Reynolds or Froude Number Range	Range of Drag Coefficients, $C_D$	Drag Coefficient	Comments & Observations
28	Reynolds Test 8.5" dia. aluminum sphere (clamped)	$Re_D =$ $3 \times 10^4$ to $2 \times 10^5$	0.054 to 0.31	0.16	Ave. $C_D A = .063 \text{ ft}^2$ $C_D$ decreases with increasing speed. Vibration of sphere seems to reduce $C_D$
29	Window Shade Drogue No. 1 26"w/x26" h. triangle, Ballast wt.=.67 lb for Fr tests 	Fr = .008 to .04	1.22 1.53 1.73	$C_D$ (max.) = 1.73	W (ballast) = W (full scale) / $\lambda^2$ for Fr tests Froude Scaling Law $V_m = V_s$ Froude speeds: 0.02 to .2 knots
		Re = $10^5$ to $5.8 \times 10^5$	1.33 to 1.75	$C_D$ (max.) = 1.75.	
30	Window Shade Drogue No. 2 26" w.x 26" h. triangle (inverted) .69-lb ballast wt. 	Fr = .008 to .04	1.95 1.72 1.53	$C_D$ (max) = 1.95	W (ballast) = W (full scale) / $\lambda^2$ for Fr tests, $C_D$ decreases with increasing speed. Froude speeds = .04 to .2 knots
		Re = $10^5$ to $1.3 \times 10^5$	1.46 1.45	$C_D$ (max) = 1.46	
31	Window Shade Drogue No. 3 11.75"w. x 28" high Rectangle, .64-lb ballast 	Fr <sub>w</sub> = .012 to .06	1.54 2.13 1.77	$C_D$ (max) = 2.13	W (ballast) = W (full scale) / $\lambda^2$ for Fr tests Froude speeds = .02 to 0.2 knots
		Re <sub>w</sub> = $5 \times 10^4$ to $1.4 \times 10^5$	1.81 2.03 1.85	$C_D$ (max.) = 2.03	

FIGURE A-6 REYNOLDS AND FROUDE SCALING TEST RESULTS FOR MODEL SPHERE AND WINDOW SHADE DROGUE

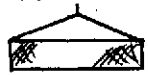
Device No.	Drag Device Size and Shape	Reynolds or Froude Number Range	Range of Drag Coefficients, $C_D$	Average Drag Coefficient, $C_D$	Comments & Observations
32	Window Shade Drogue No. 4 28.75" w. x 11.5" high rectangle, 0.65-lb ballast. 	Fr = .008 to .16	1.77 1.56	$C_D$ (max.) = 1.77	$W(\text{ballast}) = W(\text{full scale})/\lambda^2$ for Froude Tests Froude Speeds = .02 to 0.2 knots
		Re = $5 \times 10^4$ to $1.4 \times 10^5$	1.0 1.92 1.89	$C_D$ (max.) = 1.92	
33	Window Shade Drogue No. 5 18.37" x 18.37" square, .65-lb ballast wt. 	Fr = .005 to .05	1.97 1.83 1.63	$C_D$ (max.) = 1.97	$W(\text{ballast}) = W(\text{full scale})/\lambda^2$ for Froude Tests Froude Speeds = .02 to 0.2 knots
		Re = $4.7 \times 10^4$ to $1.5 \times 10^5$	1.51 to 1.89	$C_D$ (max) = 1.89	
34	Window Shade Drogue No. 6 9" w. x 39" high rectangle, 0.66-lb ballast 	Fr = .007 to .07	1.92 1.88 1.58	$C_D$ (max.) = 1.92	$W(\text{ballast}) = W(\text{full scale})/\lambda^2$ for Froude Tests $C_D$ decreases with increasing speed. Froude Speeds = .02 to .2 knots
		No Reynolds Tests	—	—	
35	Window Shade Drogue No. 7 38.5" w. x 9" high rectangle, 0.66-lb ballast 	Fr = .007 to .07	1.44 to 2.03	$C_D$ (max.) = 2.03	$W(\text{ballast}) = W(\text{full scale})/\lambda^2$ Froude Speeds only at 0.022 to 0.2 knots.
		No Reynolds Tests	—	—	

FIGURE A-7 REYNOLDS AND FROUDE SCALING TEST RESULTS FOR WINDOW SHADE DROGUES

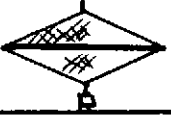
Device No.	Drag Device Size and Shape	Reynolds or Froude Number Range	Range of Drag Coefficients, $C_D$	Average Drag Coefficient, $C_D$	Comments & Observations
36	Window Shade Drogue No. 8 18.37" x 18.37" Sq. DIAMOND, .67-lb ballast wt. 	Fr=.005 to .05	2.24 1.58 1.53	$C_D$ (max.) = 2.24	W(ballast) = W(full scale)/ $\lambda^2$ for Froude Tests $C_D$ (Froude) decreases with increasing Speed. Froude Speeds=.02 to 0.2 knots
		Re=4.7 x10 <sup>4</sup> to 1.5x10 <sup>5</sup>	1.83 1.87 1.92 1.65	$C_D$ (max.) = 1.92	
37	Window Shade Drogue No. 9 19"w. x 35" long diamond, .65-lb ballast wt. 	Fr=.003 to .03	1.40 2.30 1.76	$C_D$ (max.) = 2.30	W(ballast) = W(full scale)/ $\lambda^2$ for Froude Tests Froude Speeds = .02 to .2 knots
		No Reynolds Tests	—	—	
38	Window Shade Drogue No. 10 35"w. x 19" long diamond, .71-lb ballast wt. 	Fr=.005 to .05	1.92 1.84 1.68	$C_D$ (max.) = 1.92	W(ballast) = W(full scale)/ $\lambda^2$ for Froude Tests $C_D$ (Froude) decreases with increasing speed. Froude speeds = .02 to 0.2 knots.
		No Reynolds Tests	—	—	
39	Window Shade Drogue No. 11 30" x 30" polyeth. (.006"), 26 gram ballast wt. (W) 	Re=1.5 x 10 <sup>4</sup> to 3.4x10 <sup>4</sup> Fr-.0066 to .015	1.55 to 1.97	$C_D$ (max.) = 1.97 ave. value = 1.70	Ave. $C_D A = 10.6 \text{ ft}^2$ Model Speeds = .035, .053, .08 knots W(ballast) = W(full scale)/ $\lambda^3$

FIGURE A-8 REYNOLDS AND FROUDE SCALING TEST RESULTS FOR WINDOW SHADE DROGUES

Device No.	Drag Device Size and Shape	Reynolds or Froude Number Range	Range of Drag Coefficients, $C_D$	Average Drag Coefficient, $C_D$	Comments & Observations
40	Window Shade Drogue No. 12 30" w. x 30" h. triangle, 26- gram ballast wt. (w) 	$Re = 9.3 \times 10^3$ to $3.4 \times 10^4$  $Fr = .004$ to $.015$	0.98  to 1.86	1.4	Ave. $C_D A = 4.37 \text{ ft}^2$ Model Speeds = .022, .035, .053, and .08 Knots $W(\text{ballast}) = W(\text{full scale})/\lambda^3$

94

FIGURE A-9 REYNOLDS AND FROUDE SCALING TEST RESULTS FOR WINDOW SHADE DROGUES

## APPENDIX B

### Full Scale Drogue Theoretical Performance Curves

Based on the data derived during scale model tests, numerous performance curves have been developed for use by ocean scientists. The overall goal of the theoretical data presented in Figures B-1 to B-9 is to derive a relative velocity (or slip velocity) at the drogue as a function of the drogue type, ballast weight, area, and horizontal component of drag force. This relative velocity is then employable in a vector velocity triangle like that shown in Figure 2 to enable one to correct for wind and current induced drag forces on the buoy and upper portion of the tether line.

The value of horizontal drag force arising from the above factors must be measured or estimated by the drogue user. A measurement could be made by instruments installed above the drogue or just below the buoy. Estimates of the horizontal drag force at the drogue can be made by calculating the wind forces on the surface buoy (direction and magnitude) and vectorically summing this with the forces arising due to water forces on the submerged portion of the buoy and tether line. In most cases buoys consist of various cylinders with a drag coefficient of approximately 1.0 to 1.2. Therefore by knowing the buoy size and the velocity of the air and water permits the calculation of buoy drag forces through an application of equation (9). This same vector drag force is assumed to act on the drogue.

In order to use Figures B-1 to B-9 one enters the nomographs with a calculated drag force and drogue area. In Figure B-1, the parachute performance curves, the relative velocity ( $V_{rel}$ ) is derived by a straight application of equation (9). In Figures B-2 to B-9, however, it is assumed that both crossed vanes and window shade drogues develop lift forces which ultimately destroy their performance as the drag force approaches the value of the ballast

weight. Figures B-2 and B-3 are performance curves for 2 and 3 axis crossed vanes respectively. The vanes are assumed to weigh 100 pounds (i.e., 100-pound ballast weight). In Figures B-4 to B-9, applicable to window shade drogues only, various values of ballast weight are assumed between 25 and 300 pounds. The effect of differing ballast weights at constant drogue area and drag force is evident at the higher drag forces.

Figure B-10 is a composite plot which includes information shown in Figures B-4 through B-9. It indicates the loci of the maximum relative velocities that a window shade drogue will permit before going unstable. This is seen to be a function of the drogue area and ballast weight.

Figure B-11 is a dimensionless summary of window shade drogue performance. An accompanying sketch summarizes the nomenclature employed for easy application of the data. It can be seen in this figure that if the drag force,  $F_D$ , is less than one-half of the ballast weight  $W$ , the curve is very nearly linear. In this case a simple application of equation (7) with a value of  $C_D = 1.93$  is in general very adequate for the determination of  $V_{rel}$  based on an estimate of  $F_D$ .

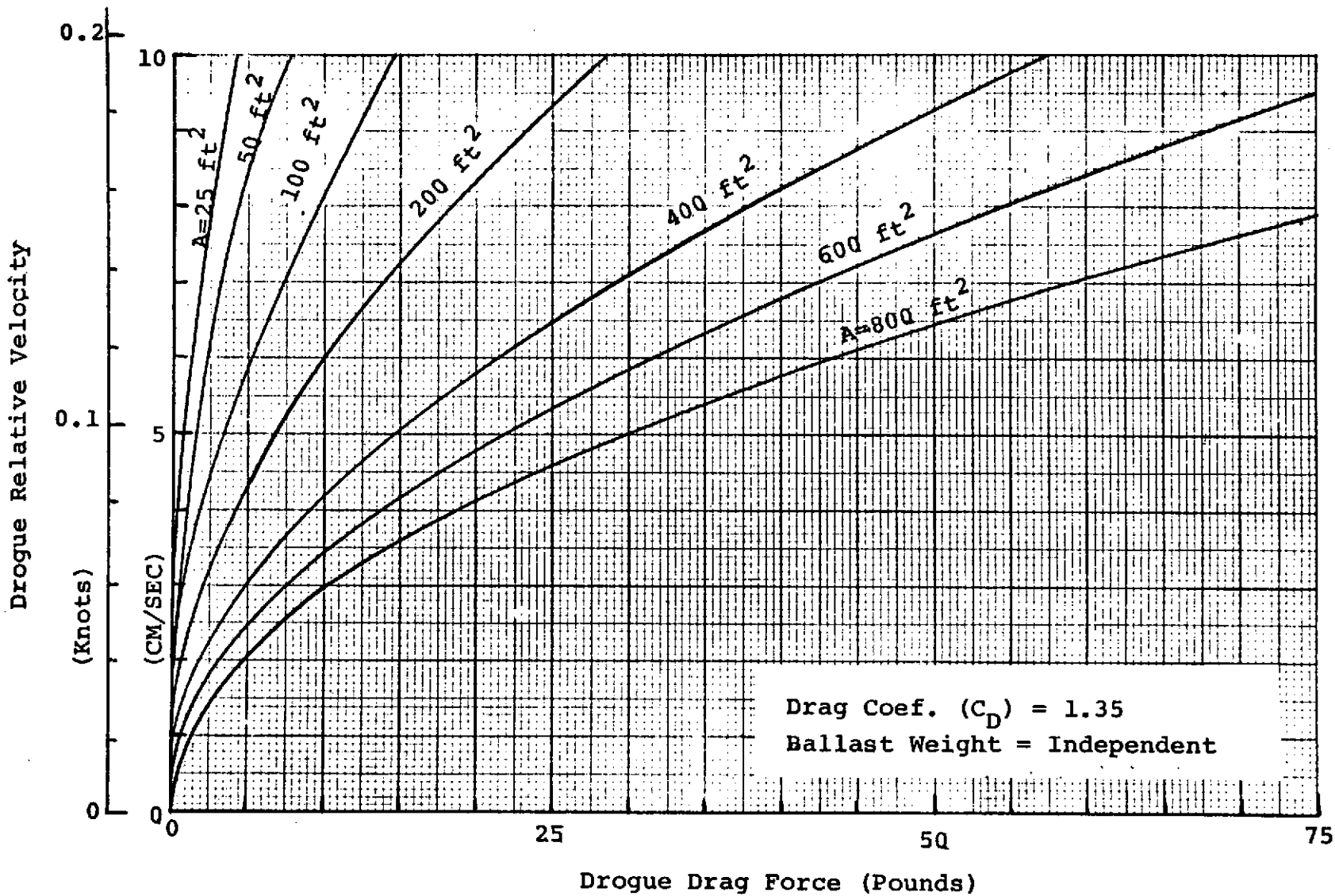


Figure B-1 Parachute Droque Performance Curves

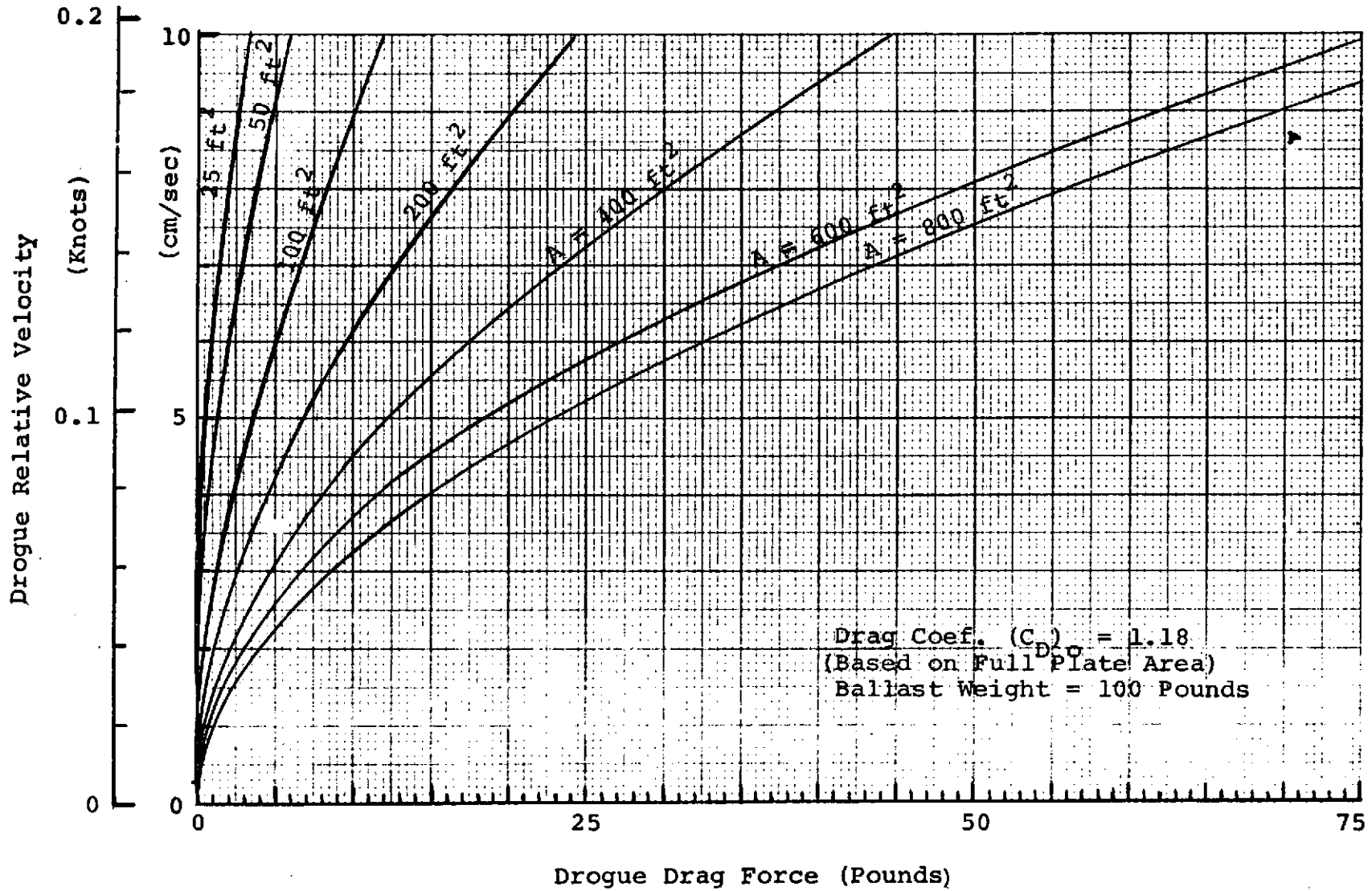


Figure B-2 Two Axis Crossed Vane Performance Curves

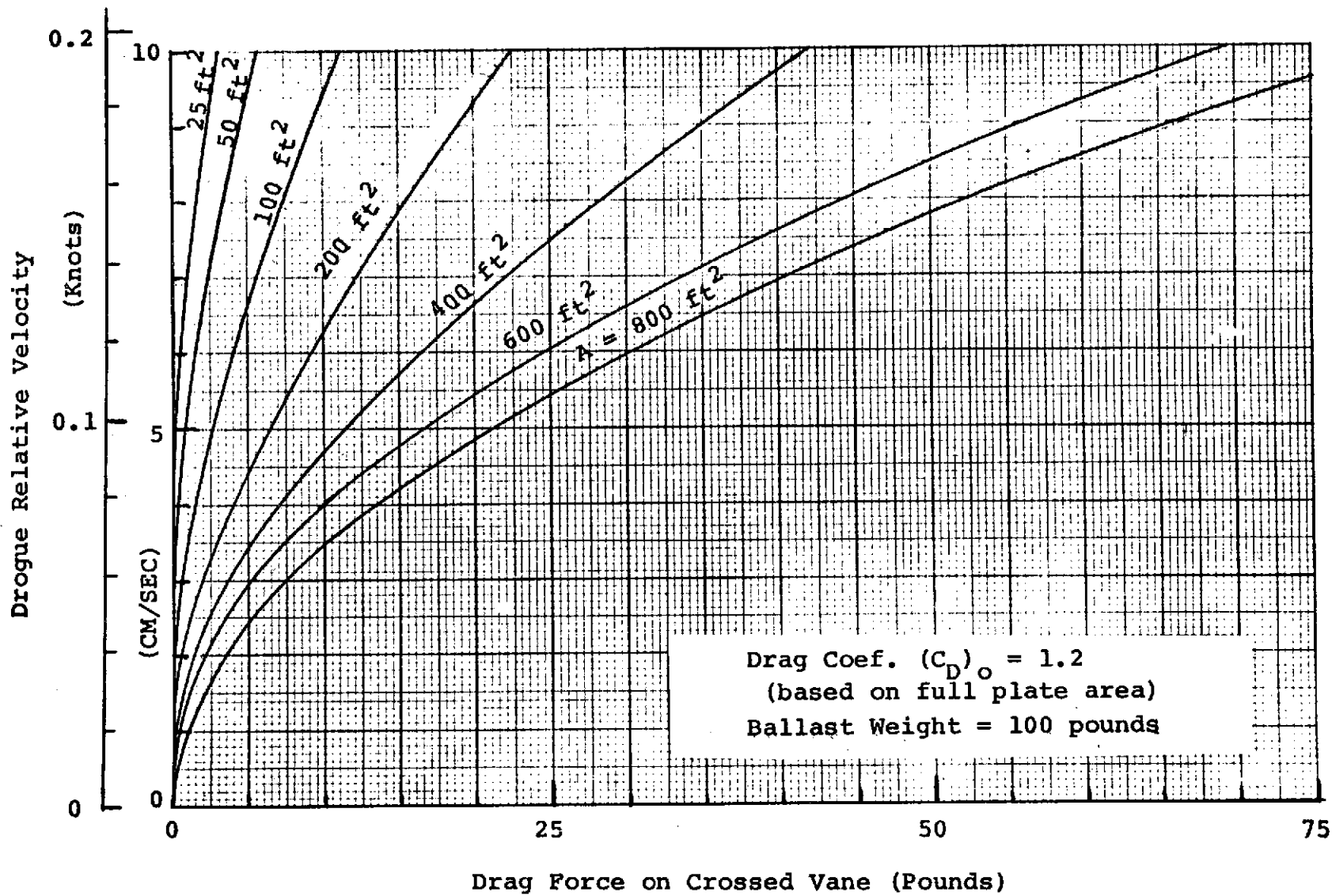


Figure B-3 Three Axis Crossed Vane Performance Curves

001

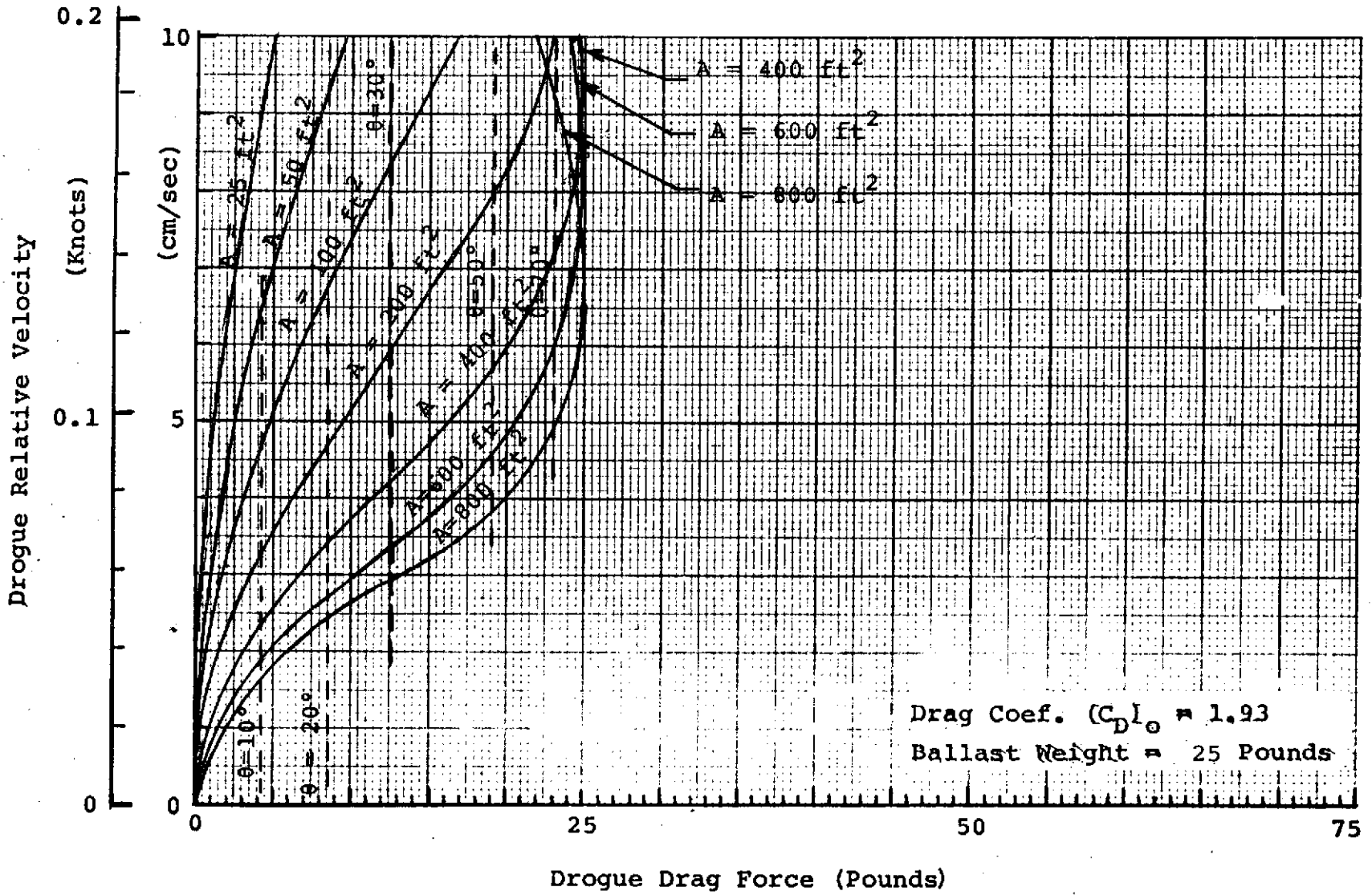


Figure B-4 Window Shade Drogue Performance Curves

## Drogue Relative Velocity

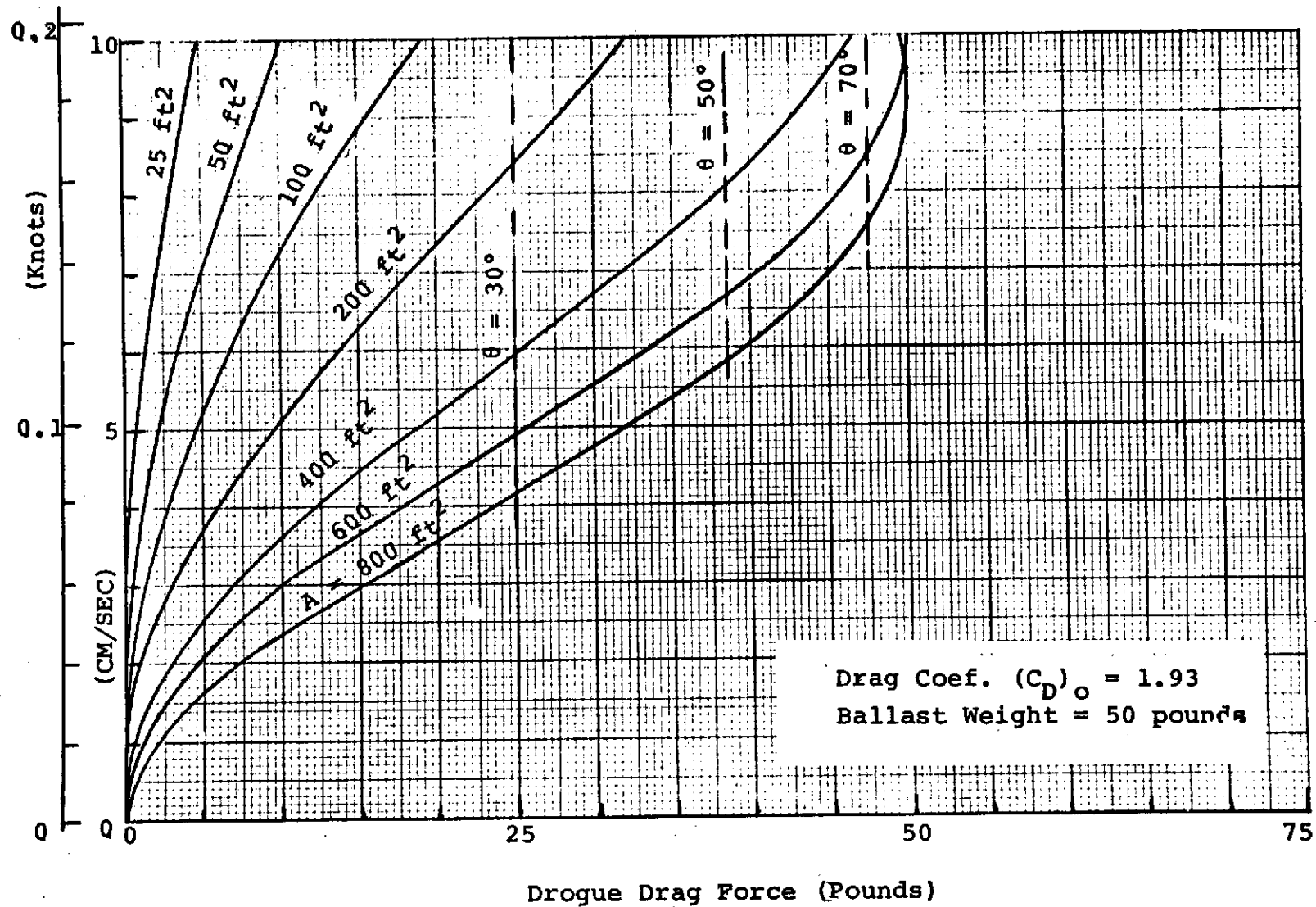
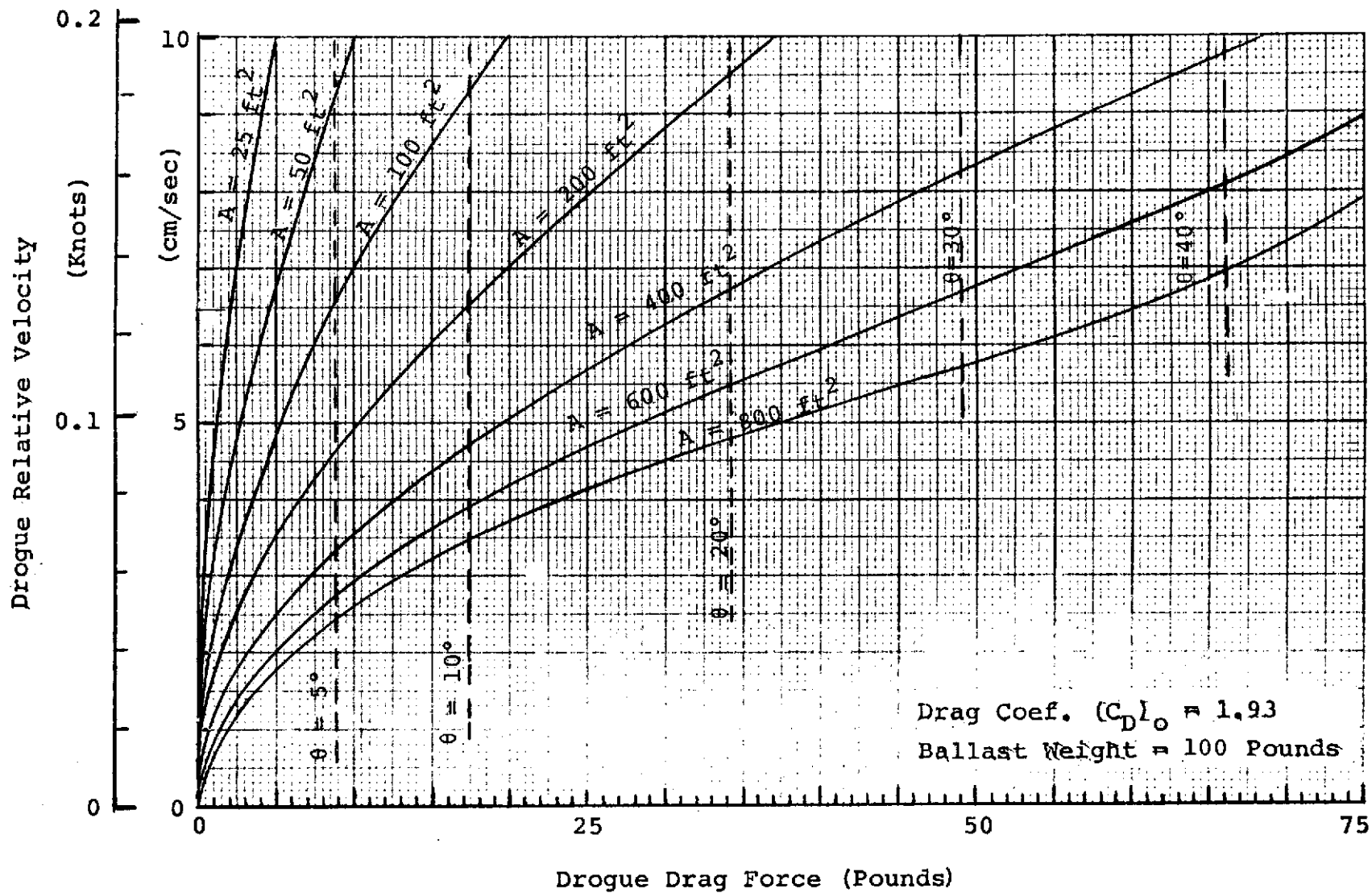


Figure B-5 Window Shade Drogue Performance Curves



801

Droge Relative Velocity

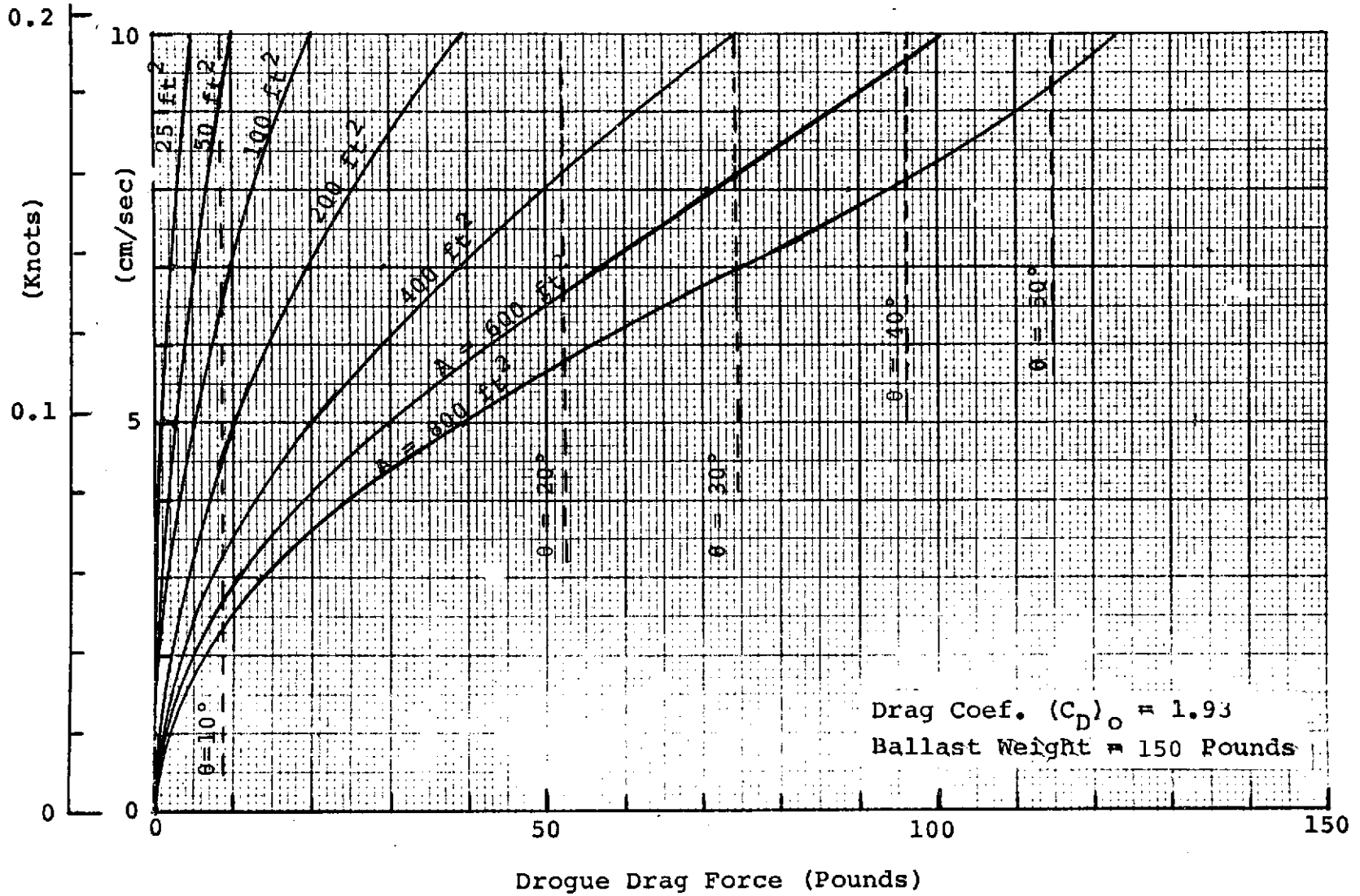


Figure B-7 Window Shade Droge Performance Curves

Drogue Relative Velocity

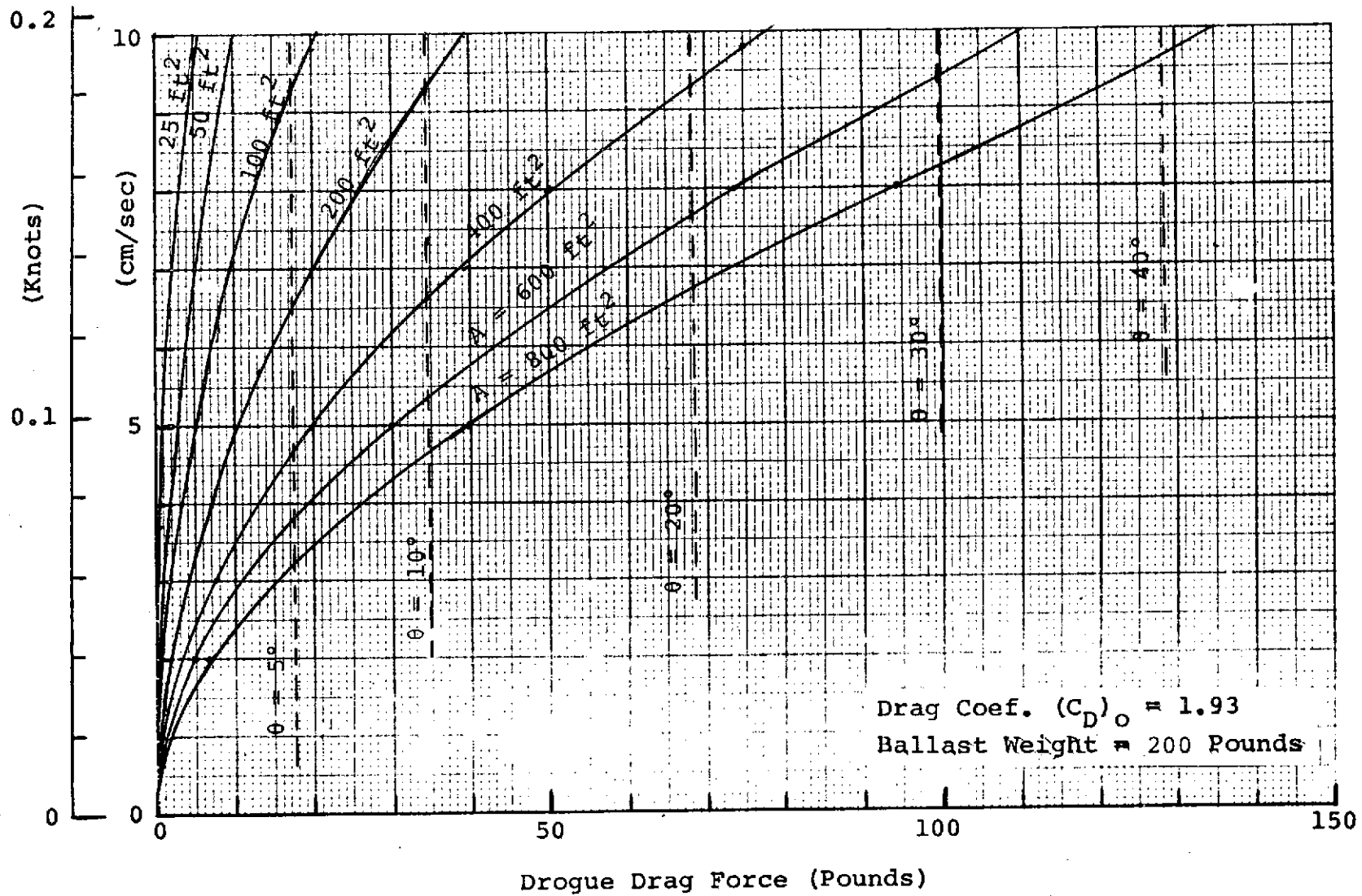


Figure B-8 Window Shade Drogue Performance Curves

## Drogue Relative Velocity

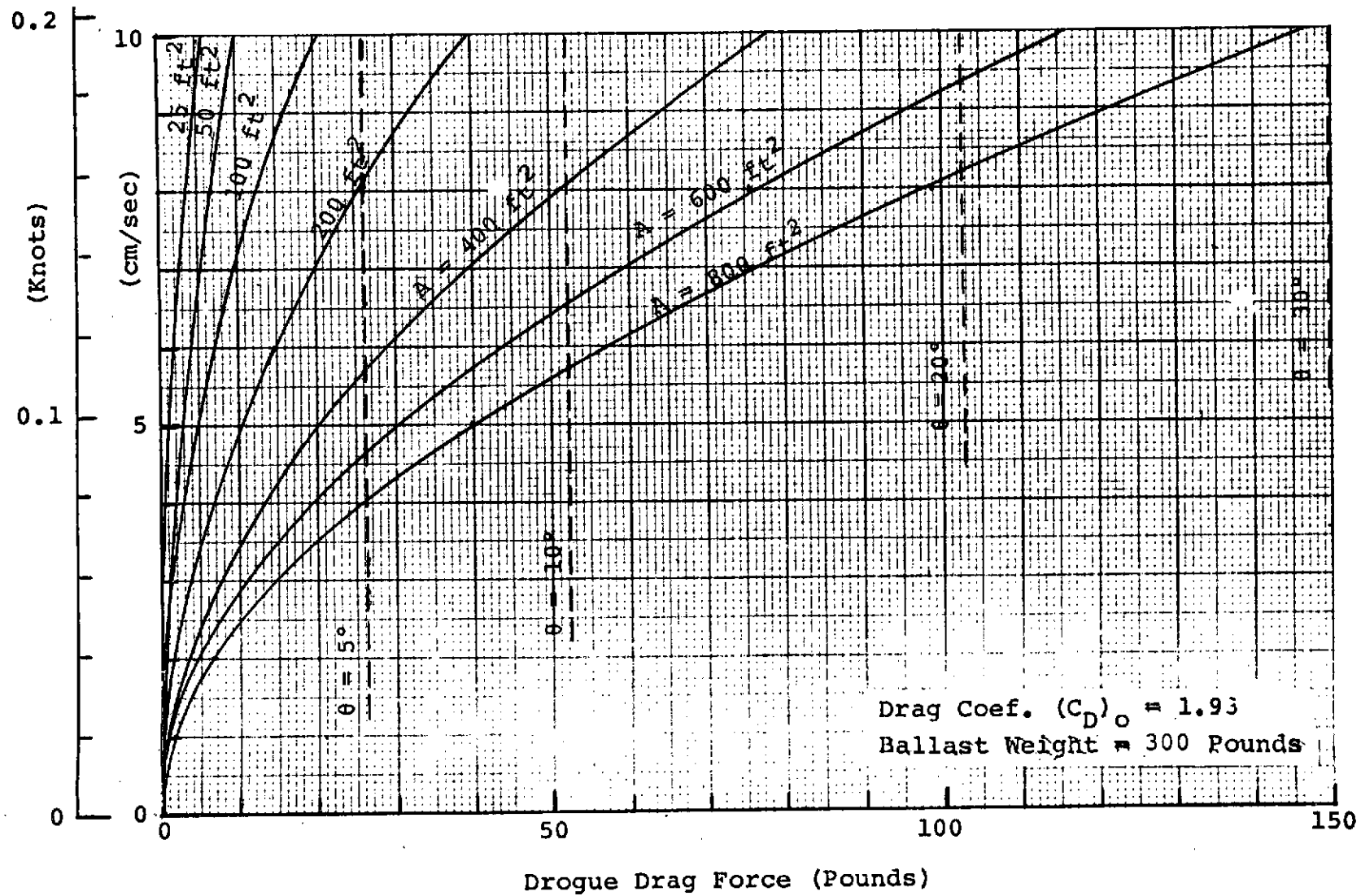
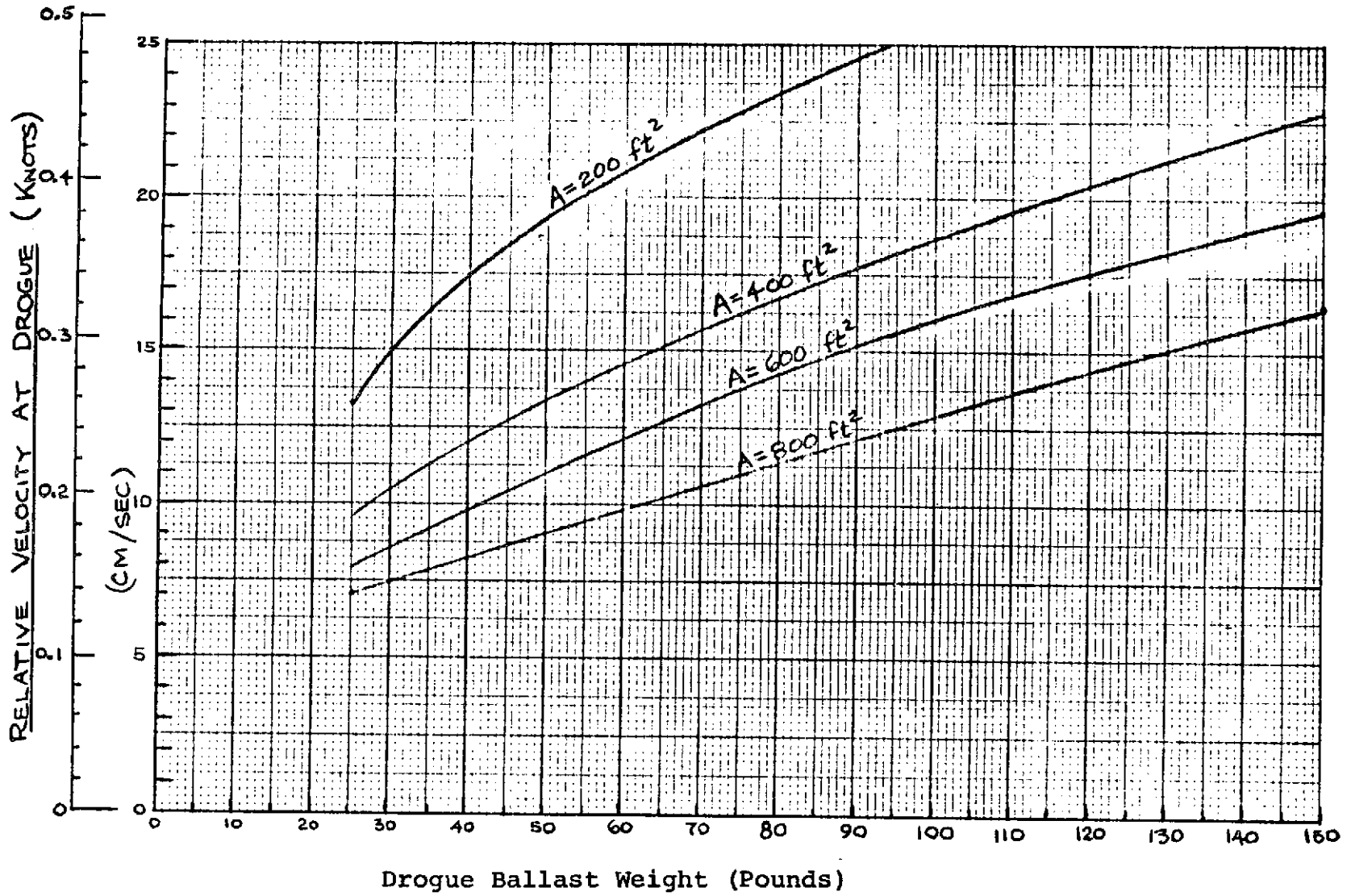


Figure B-9 Window Shade Drogue Performance Curves



Locus of Window Shade Drogue Instability Points When  $F_D = W$

Figure B-10

Dimensionless Relative Velocity

$$\frac{1}{2} \rho (C_D)_0 A_{\perp} V_{rel}^2 / W = \frac{\sin \theta}{\cos^3 (\theta/2)}$$

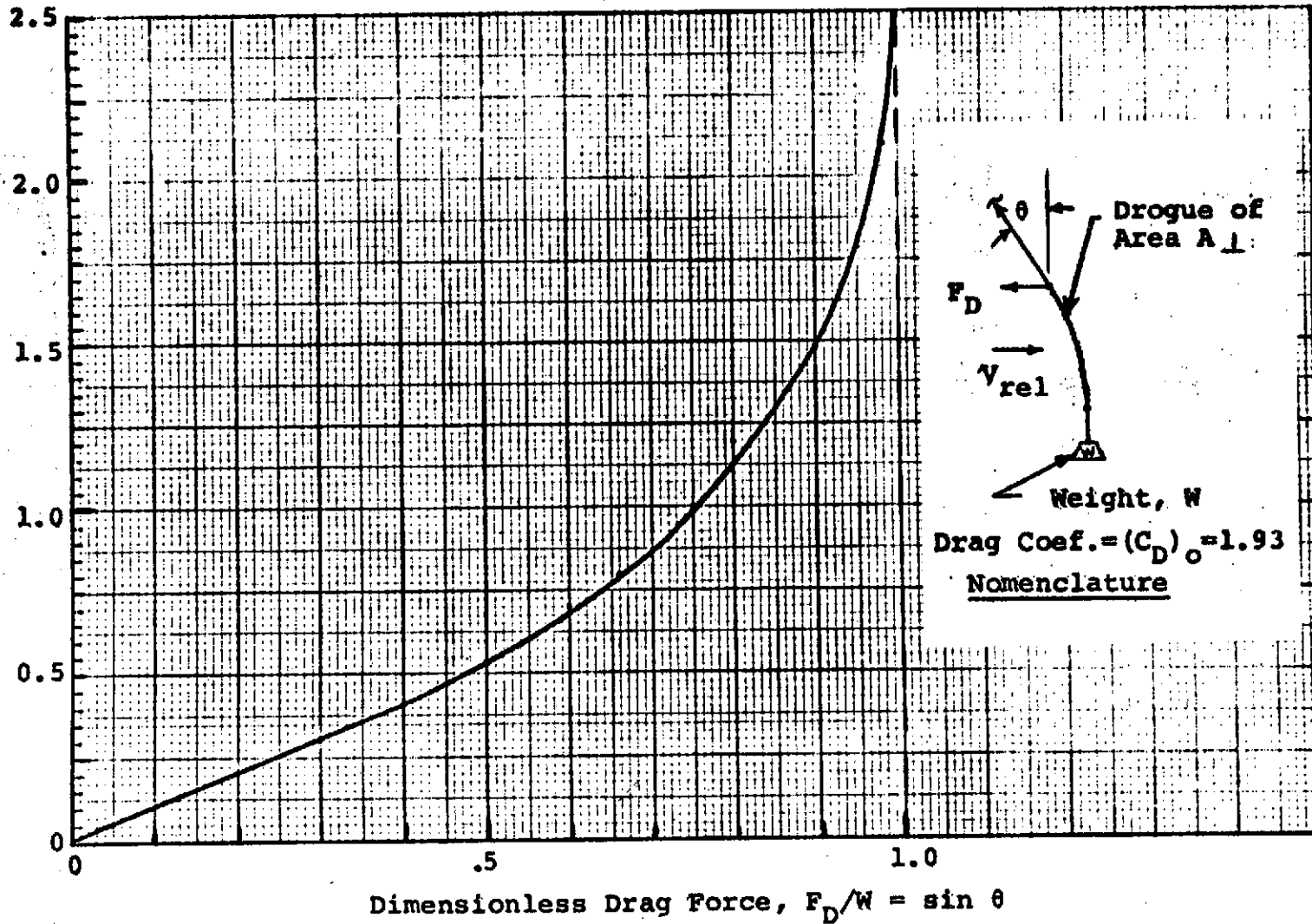


Figure B-11 Dimensionless Window Shade Drogue Performance (Theoretical)

## APPENDIX C

### Window Shade Drogue Depth Locking Accuracy

Inherent in specifying the water mass locking capability of a buoy/drogue combination is a knowledge of how well a given drogue maintains its specified depth in the presence of drag loads. If any of the drogues, whose performance is reported in this writing, are lightly ballasted, relatively small drag forces will cause the drogue to stream near the surface. In this way a drogue may be erroneously locked to currents at depths too shallow to be of value to an investigator. It is, therefore, important in most cases to properly weight all drogues in order to achieve the desired depth locking accuracy.

A simple study was done for the specific case of a window shade drogue with ballast weights of 50, 100, and 150 pounds. The tether line was assumed to be 200 meters of 0.160-inch diameter wire exhibiting a weight in water of 0.03 pounds per foot. The study made the simplifying assumptions that the currents are uniform over the whole tether line and drogue. The drag force imposed on the drogue ( $F_D$ ) is assumed to arise only from wind and current drag forces acting on the buoy; thus towing the drogue through the water.

The depth locking accuracy is found to be primarily a function of only the drag force on the drogue and the ballast weight. It is secondarily a function of the drag on the tether line. For the specific case outlined above the drag on the tether line is negligibly small. Therefore, it is possible as a first approximation to assume that the tether line is straight and streams at an angle off of vertical which is equal to the average of the angles at the drogue and at the buoy. Calculations of both angles differ by so little for the case outlined that for simplicity only the angle at the drogue is employed.

Figure C-1 depicts the results of an iterative calculation of the depth locking accuracy. An initial assumption of a drag force,  $F_{D1}$ , and a ballast weight,  $W$ , are made. An initial streaming angle with respect to vertical is calculated from the relation:

$$\theta_1 = \tan^{-1} \left( \frac{F_{D1}}{W} \right) \quad (C-1)$$

This angle, seen in Figure C-1, is used with equations (30) and (31) in the following manner in order to derive estimates of drag and lift forces ( $L$ ) created by the drogue:

$$F_{D2} = F_{D1} \cos^3 \left( \frac{\theta_1}{2} \right) \quad (C-2)$$

$$L_2 = F_{D2} \tan \left( \frac{\theta_1}{2} \right) \quad (C-3)$$

The updated streaming angle,  $\theta_2$ , is then calculated as follows:

$$\theta_2 = \tan^{-1} \left( \frac{W - L_2}{F_{D2}} \right) \quad (C-4)$$

This process can be continued until a satisfactory convergence is derived, using the general equations:

$$F_{Di} = F_{D,i-1} \cos^3 \left( \frac{\theta_{i-1}}{2} \right) \quad (C-5)$$

$$L_i = F_{Di} \tan \left( \frac{\theta_{i-1}}{2} \right) \quad (C-6)$$

where  $i$  is generalized subscript which is incremented with each iteration cycle. For the curves shown in Figure C-1, adequate convergence was found by only carrying the process as far as the calculation of  $F_{D3}$ .

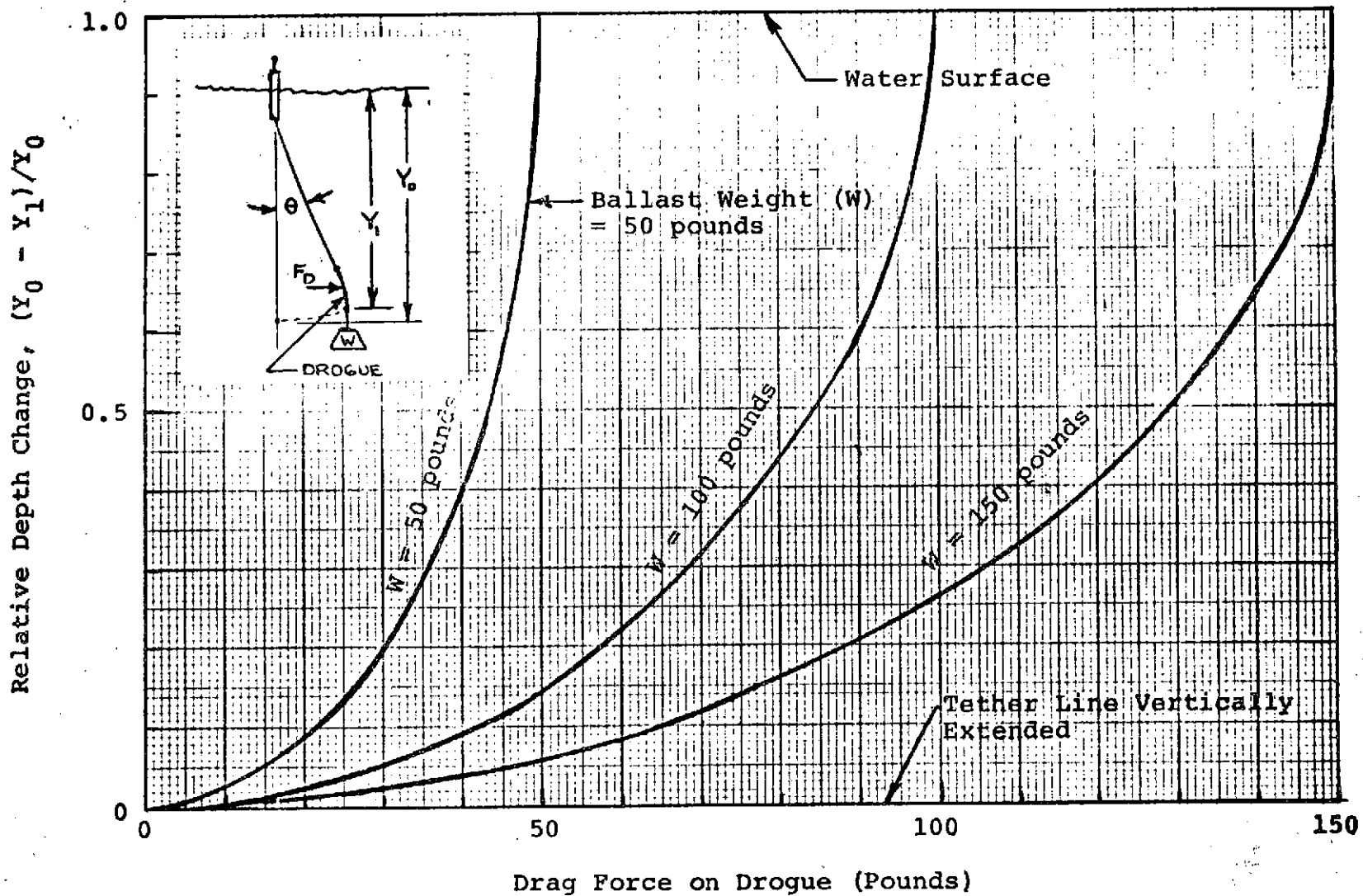


FIGURE C-1 DROGUE DEPTH ACCURACY

The ordinate in Figure C-1 is a dimensionless depth change or the drogue depth change as a fraction of the tether line length. An alternative expression for the ordinate is as follows:

$$Y_0 - Y_1 / Y_0 = 1 - \cos\theta \quad (C-7)$$

One uses the figure by entering with an estimate of the drag force on the drogue and proceeding vertically upward along a line of constant drag force until intersecting the line with the appropriate ballast weight. At this intersection the corresponding relative depth change on the ordinate is read.

A review of the literature pertinent to drogue depth locking accuracy reveals limited empirical data derived by Gerard and Salkind (1965). In their work the depth of a 28-foot diameter chute, ballasted with 200 pounds of iron, was measured for a number of days. The slow descent transient of a chute was revealed but the subsequent depth remained constant (within the depth measurement accuracy) for the remainder of the implantment.

## APPENDIX D

### Wave-Induced Drogue Dynamic Loads

If a drogue is used in an application wherein it may receive dynamic input from a pitching and heaving buoy, the dynamic loads thus created may cause severe stresses in the mooring line. In some cases stresses may cause the buoy to submerge or the mooring line to part. The situation in which this is most likely to be a problem is in near-surface drogue applications wherein the tether line exhibits very little catenary shape the change of which can act as an energy-absorbing spring. Furthermore, if a drogue exhibits a substantial drag area to motion in the vertical direction, it will resist buoy vertical motion and create substantial tether line tensions and/or submerge the buoy. This problem will be explored for assumed conditions by employing data derived by another investigator.

Independent tests have been conducted at the Water Management section of Environment Canada\* in order to measure the drag coefficient parallel to a surface of flexible canvas material. The tests were conducted by measuring the sinking rate of a weighted full size window shade drogue in water. In addition, the theoretical drag coefficient of plates and plastic sheets was predicted. The data which were derived are summarized in Table D-1 for which the drag coefficient is calculated based on equation (7) and the full frontal area of the drogue.

---

\* Data derived by personal communication with John Garrett, Head, Offshore Oceanography, Marine Sciences Directorate, Pacific Region 512 Federal Bldg, Victoria, B.C., CANADA, and presented with his permission.

TABLE D-1

## SLIP DRAG COEFFICIENTS OF PLATES AND SHEETS

<u>Drogue Description</u>	<u>Drag Coefficient (<math>C_D</math>)</u>
20'x20' Canvas with 2½" D. Pipes (Measured)	.061
20'x20' Canvas, No Pipes (Theoretical)	.045
387 ft <sup>2</sup> Rigid Smooth Plate, With Pipes (Theoretical)	.022
387 ft <sup>2</sup> Rigid Smooth Plate, No Pipes (Theoretical)	.005
10'x15' Plastic Sheet, No Pipes (Theoretical)	.058

The drag coefficients given in Table D-1 were based on measurements in which the tension in the fabric was very nearly zero. In addition, the sinking rates and drogue dimensions (i.e., approx. 1 meter/sec and  $l \approx 6$  meters) produce length Reynolds numbers which indicate turbulent flow on the trailing portion of the fabric. As a result it is felt that trailing regions of the fabric flutter violently in the flow, producing rather high drag coefficients in the direction of flow. Such a condition seems representative of the downward motion of a weighted drogue with zero tether line tension, one case that will be covered in this Appendix. During upward motion of a buoy and drogue, however, there can be considerable tension in the tether line and drogue fabric, minimizing the lateral flutter. It is felt that such conditions would give a lower value for the drag coefficient. Therefore, it is felt that calculated dynamic loads based on the data listed in Table D-1 which is applicable to fabrics may be conservative for upward motion of a drogue.

In order to examine the types of loads which a window shade drogue could impart to a heaving buoy, simplified analyses will be made based on certain assumptions. It will first be assumed that the buoy follows the wave motion perfectly and is not effected by loads produced by the drogue. Secondly, the drogue is assumed to be straight beneath the buoy (i.e., no catenary) attached by an inelastic tether line. The seas are

assumed to impart sinusoidal motion of varying amplitude to the buoy at a frequency which is a function of wave height according to the Pierson-Moskowitz sea spectra for fully developed wind driven seas (Pierson and Moskowitz, 1964). A summary of the pertinent parameters in the sea spectra are shown in Figure D-1 as a function of the wind velocity on a fully developed sea. The sea states listed are assumed to be a function only of wind velocity according to Marks (1956).

Two cases of dynamic loading on the buoy/drogue combination will be analyzed:

- (1) The maximum downward drag force imparted on a surface-following buoy by a window shade drogue as the buoy rises on the leading edge of a wave.
- (2) The wave height that can potentially cause shock loads in a drogue tether line as a function of drogue area and ballast weight.

For the first analysis the assumption is made that the vertical forces on the buoy are primarily composed of three elements as follows:

$$T_v = \frac{1}{2} \rho (C_D)_{||} A_{\perp} \dot{y} |\dot{y}| + (m_o + m_a) \ddot{y} + m_o g \quad (D-1)$$

where  $y$  is assumed positive upwards and

- $T_v$  = Vertical component of tether line tension.
- $(C_D)_{||}$  = Drag coefficient of drogue parallel to area,  $A$ .
- $y$  = Vertical position of drogue
- $m_o$  = Mass of cable, drogue, and ballast weight
- $m_a$  = Added mass of cable, drogue, and ballast weight for vertical motion
- =  $1/8 m_o$  (by assumption).

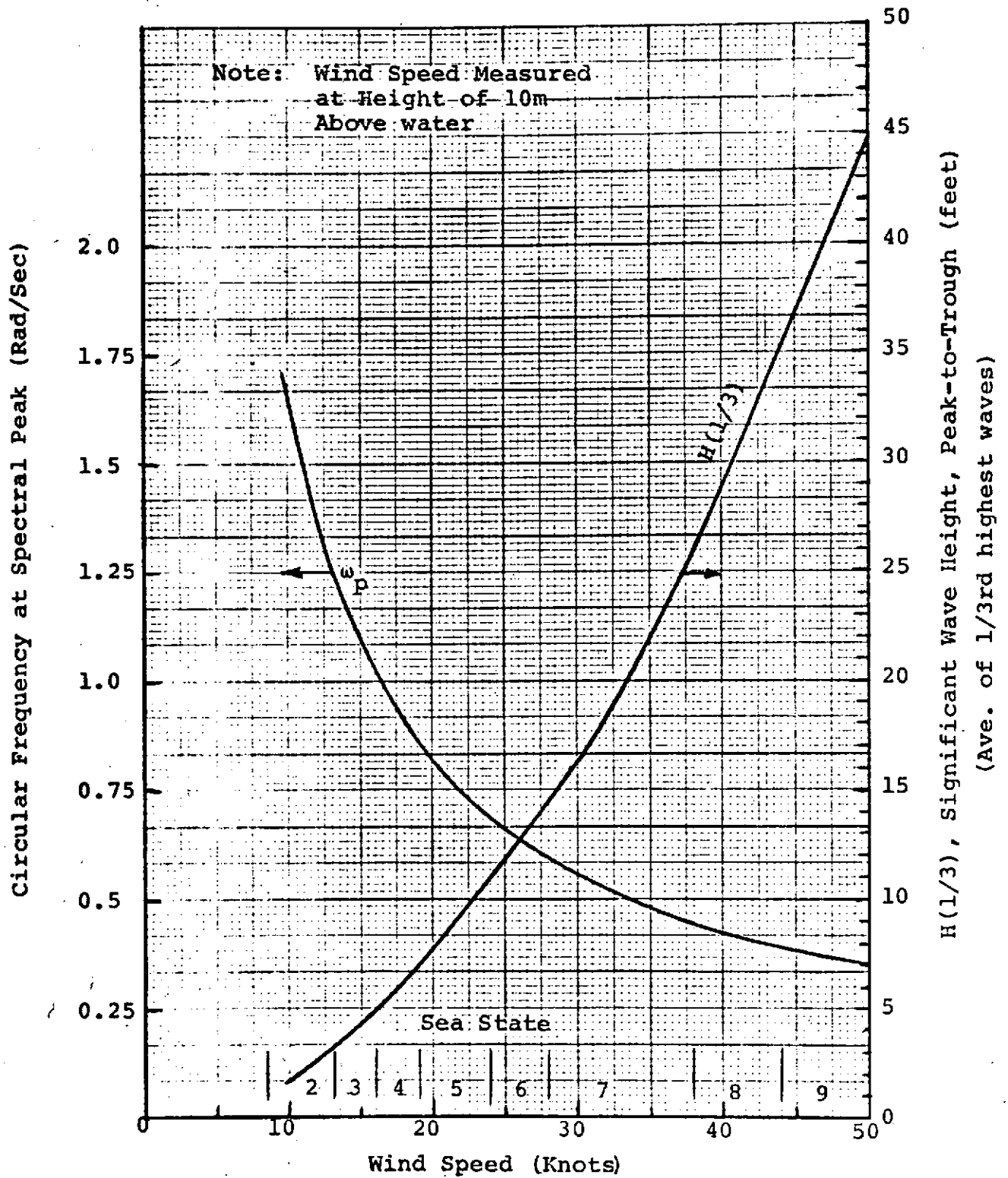


Figure D-1 Pierson-Moskowitz Sea Spectra For Fully Developed Seas

The dots over the  $y$  terms in equation (D-1) signify derivatives with respect to time; a single dot signifying a single derivative, etc. More rigorous calculations indicate that the added mass of a drogue to motion in the vertical direction depends on the angle of the drogue with respect to vertical. Other analyses conducted for this study suggest that the motion of least resistance for a drogue with a finite average angle with respect to vertical is for the drogue to move in the direction of the tether line. In other words, it slips through the water. Therefore a relatively small value of added mass is assumed.

The assumed sinusoidal motion permits the substitution of the following:

$$y = y_m \sin (\omega t) \quad (D-2)$$

where  $y_m$  is half the peak-to-trough height of the waves and  $\omega$  is the wave frequency ( $\omega = 2\pi f$ ). The substitution of (D-2) in (D-1) produces the following:

$$T_v = \frac{1}{2} \rho (C_D)_{||} A_{\perp} (y_m \omega \cos \omega t) |y_m \omega \cos \omega t| - (m_o + m_a) y_m \omega^2 \sin \omega t + m_o g \quad (D-3)$$

An independent evaluation of the first two terms in equation (D-3) is plotted in Figure D-2 assuming that  $(C_D)_{||} = .058$  (i.e., plastic material). The height of the seas listed are assumed to be the peak-to-trough height or equal to  $2y_m$ . The frequency of the seas as a function of wave height is given in Figure D-1. The combined mass of the cable, drogue, and ballast weight in units of pounds - mass is arbitrarily assumed to be equal to 1/2 of the drogue area in square feet. This ratio is chosen because it results in a ballast weight which is assumed to be heavy enough for minimizing drift errors and shock loading in the majority of sea states (to be explained later

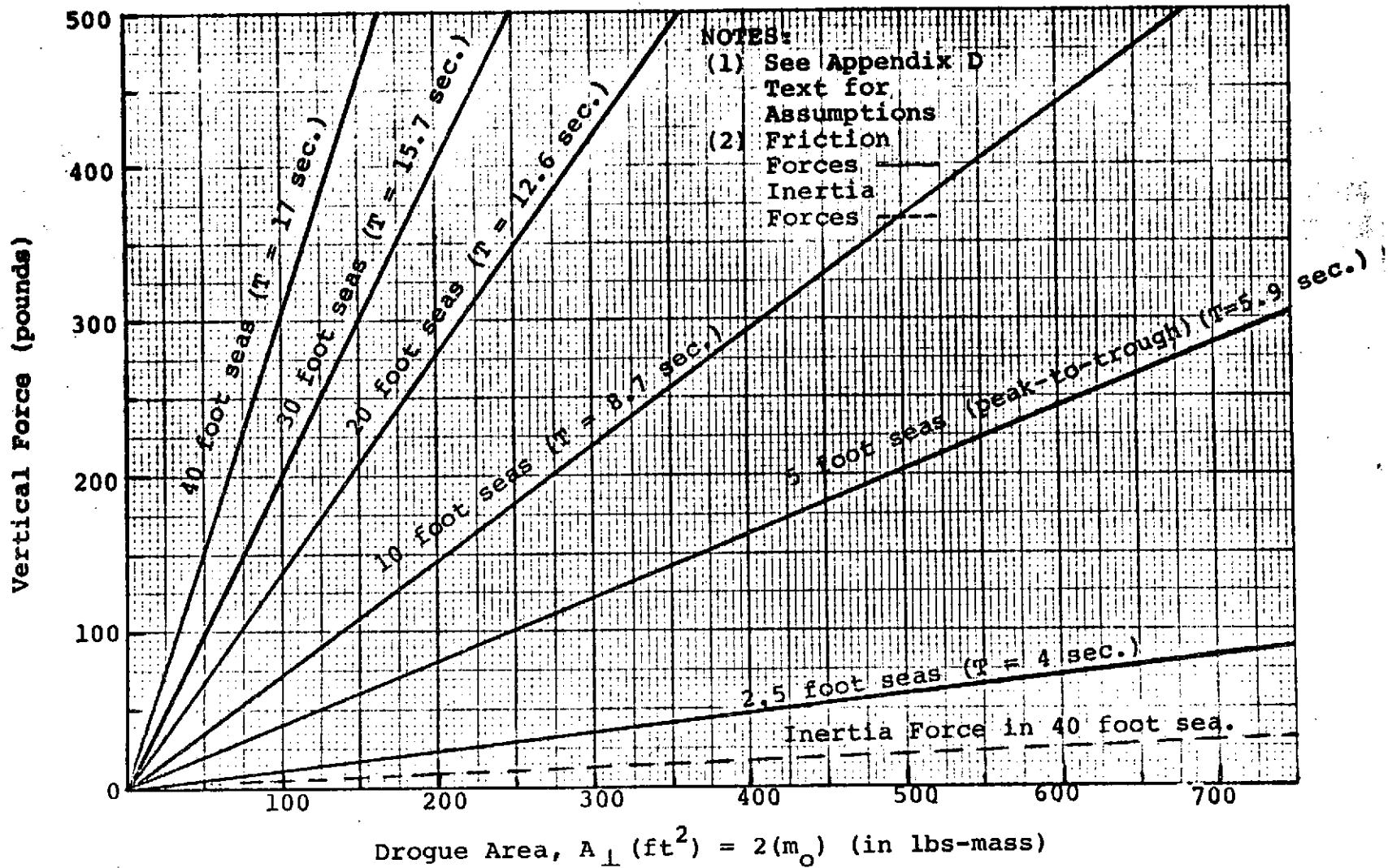


Figure D-2 Dynamic Forces from Near-Surface Window Shade Drogues on Non-Compliant Buoys (Theoretical Curves)

in this Appendix) and yet not submerging most surface buoys. Wherever possible the ballast weight should be as large as possible limited only by 2 design constraints:

- (1) the reserve buoyancy of the buoy and,
- (2) the inertia loading on the tether line and buoy.

The second design constraint will only become important when the ballast weight is larger compared to the drogue area than the case shown in Figure D-2.

It can be seen that the friction forces for plastic or canvas window shade drogues are dominant. The minus sign on the inertia term in equation (D-3) indicates that the maximum friction force occurs 90 degrees in phase after the maximum inertia force. If the ratio of ballast weight to drogue area is increased, the curve for inertia loading will shift vertically upward in direct proportion to the ballast weight. In order to find the maximum value of the sum of the drag and inertia loading at a given wave height and frequency a derivative is taken of equation (D-3) with respect to time and set equal to zero. The value of  $\omega t$  for maximum total loading is given by the relation:

$$\omega t = \sin^{-1} - \left\{ \frac{m_o + m_a}{\rho (C_D)_{||} A \downarrow y_m} \right\} \quad (D-4)$$

This value for the argument is then substituted into equation (D-3) for which the maximum value of tether line tension is calculated. It should be remembered, however, that the drag loading curves are potentially higher (i.e., more conservative) than in reality due to the manner in which the value of  $(C_D)_{||}$  was derived.

The types of loads shown in Figure D-2 are indicative of a potential limitation on the use of window shade drogues.

For deeper applications the cable elasticity and catenary will potentially absorb a greater portion of the peak loads due to buoy heave. In shallow applications four approaches can be followed to minimize the high dynamic loads on the buoy/drogue combination.

- (1) Install shock cord in the mooring line to build in compliance such that the buoy does not submerge and severe shock loads are minimized.
- (2) Employ rigid plates in a window shade or crossed vane drogue application. Table D-1 indicates the vertical drag loads may be considerably reduced.
- (3) Employ a window shade drogue with a non-submergible buoy (i.e., surface following) but employ rugged components throughout in order to prevent a tension or fatigue failure.
- (4) Employ a separate float or distributed buoyancy floats to support the drogue and its associated weights. This combination should have a sufficient reserve buoyancy such that it will not completely submerge in a heavy shear current situation in which near-surface currents, running counter to those at the drogue depth, impose a downward hydrodynamic force on the tether line. On the other hand it should not have so much buoyancy that it displays large windage. It should also pull under in the presence of large dynamic loads. That is, it should act like a "soft spring". A float with a total buoyancy of twice that of the cable, drogue, and ballast weight looks appealing. Installed it would then have a net reserve buoyancy equal to the weight of the drogue, cable, and ballast weight. It would,

however, be permitted to submerge when sea motion imparts dynamic forces from the drogue. It should have a generous leader line to the buoy with a length at least greater than the maximum expected wave height. The length could potentially be as long as the wave length of the surface waves in order to maximize isolation. Such a choice may impose unduly large horizontal drag loads on the buoy due to surface currents. The final choice will be a trade-off. The overall design goal is, however, to allow the buoy to follow the surface of the waves unimpeded by tether line and drogue vertical loads.

Because of the relatively high drag coefficients of canvas and plastic sheets in the presence of turbulent slip motion (Table D-1) a problem of shock loading can also arise when a buoy is descending to the trough of a wave. At this time the slip drag force of the drogue is opposing the ballast weight according to equation (D-1), where  $y$  is positive upwards. The inertia term in equation (D-1) can be neglected because it is generally small compared to other terms. This assumption is good for drogue areas, in square feet, larger than the combined weight of the drogue and ballast in pounds-mass. It can be seen that if the vertical velocity is sufficiently large the vertical drag will offset the weight force ( $m_0 g$ ) and the tether line will go slack. At this time it can be theorized that the drogue will be descending at its terminal velocity with zero tension in the tether line. Figure D-3 portrays an idealized case of a buoy undergoing vertical sinusoidal motion which is directly imparted to the attachment point of the drogue during upward motion. During downward motion, however, unless the drogue is adequately weighted it will descend at a constant terminal velocity. For illustrative purposes the  $\dot{y}|\dot{y}|$  function (proportional to drag load) is shown in the upper plot. In a

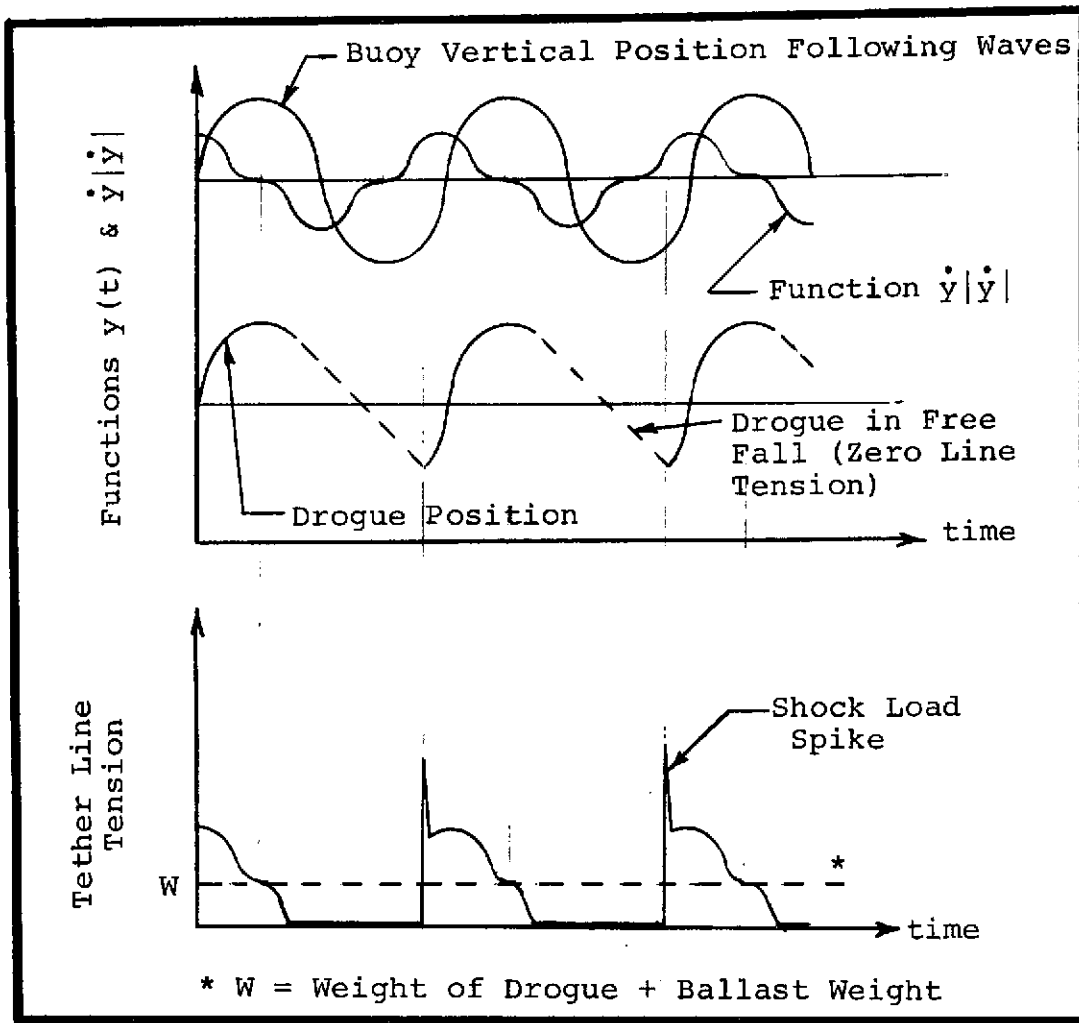


Figure D-3 Drogue Dynamic Loads

simulated tension record beneath the position curve of Figure D-3, it can be seen that the tension may go to zero during the drogue free fall until an upward motion of the buoy takes up the slack in the tether line. At this time the tether line should feel a shock load as it rapidly accelerates the drogue upward again.

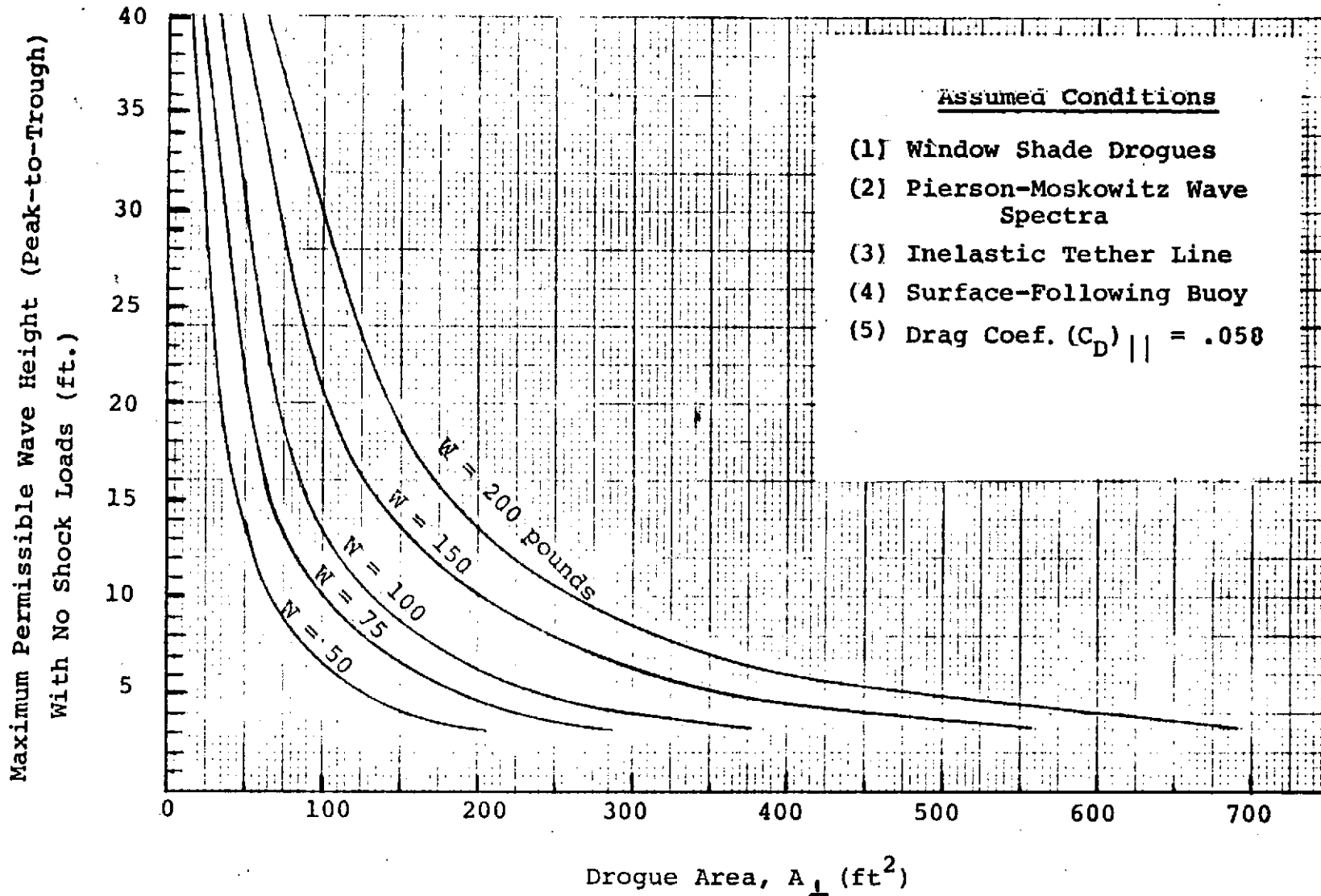


Figure D-4 Window Shade Drogue Dynamic Shock Load Conditions

The condition of zero tension in a drogue tether line should be avoided in order to prolong the life of the whole buoy. A series of nominal design curves are presented in Figure D-4 in order to adequately size the ballast weight for a given drogue area and expected sea state. The sea state is again assumed to be sinusoidal (equation D-2) at a frequency specified by the Pierson-Moskowitz sea spectra (Figure D-1). It can be seen that the larger the drogue area the larger is the ballast weight which must be employed in order to avoid shock loads in a given sea condition. This analysis points out that an overly large window shade drogue cannot be employed with impunity unless the surface buoy has sufficient reserve buoyancy to accommodate the required ballast weight.

## APPENDIX E

### Example - Specification of a Window Shade Drogue

As an example, the drogue performance and design data given in Appendices A through D will be applied in a systematic fashion to the specification of a window shade drogue for a given free drifting buoy. The input parameters inherent in the specification of the drogue are summarized in schematic form in Figure E-1. A missing combination of input parameters which is worthy of mention, but seems obvious, are available time and money. The output parameters of the drogue specification are the total drogue area, ballast weight, and tether line characteristics of material, diameter, and length. It should be recognized that not all of the input parameters are independent. That is, if some input parameters are fixed such as the buoy type it may force alterations in other input parameters. In addition, one requirement may encompass a totally different requirement. For example, the maximum sea state which the buoy must survive with no tether line shock loading dictates a certain ballast weight as a function of drogue area. The size of the ballast weight is also inherent in a specification of the current locking ability and depth stability. As will be pointed out, however, one may easily satisfy the chosen depth stability criterion with a given ballast weight but, that weight is insufficient to insure that the tether line will not undergo shock loading at the highest sea state which the whole buoy must survive. This particular problem arises because the buoy cannot support an adequate ballast weight to prevent shock loading for a given drogue area. One may always relax the desired performance of the buoy as a Lagrangian sensor (i.e., max.  $V_{rel}$ ) in which case a drogue of smaller area can be employed with

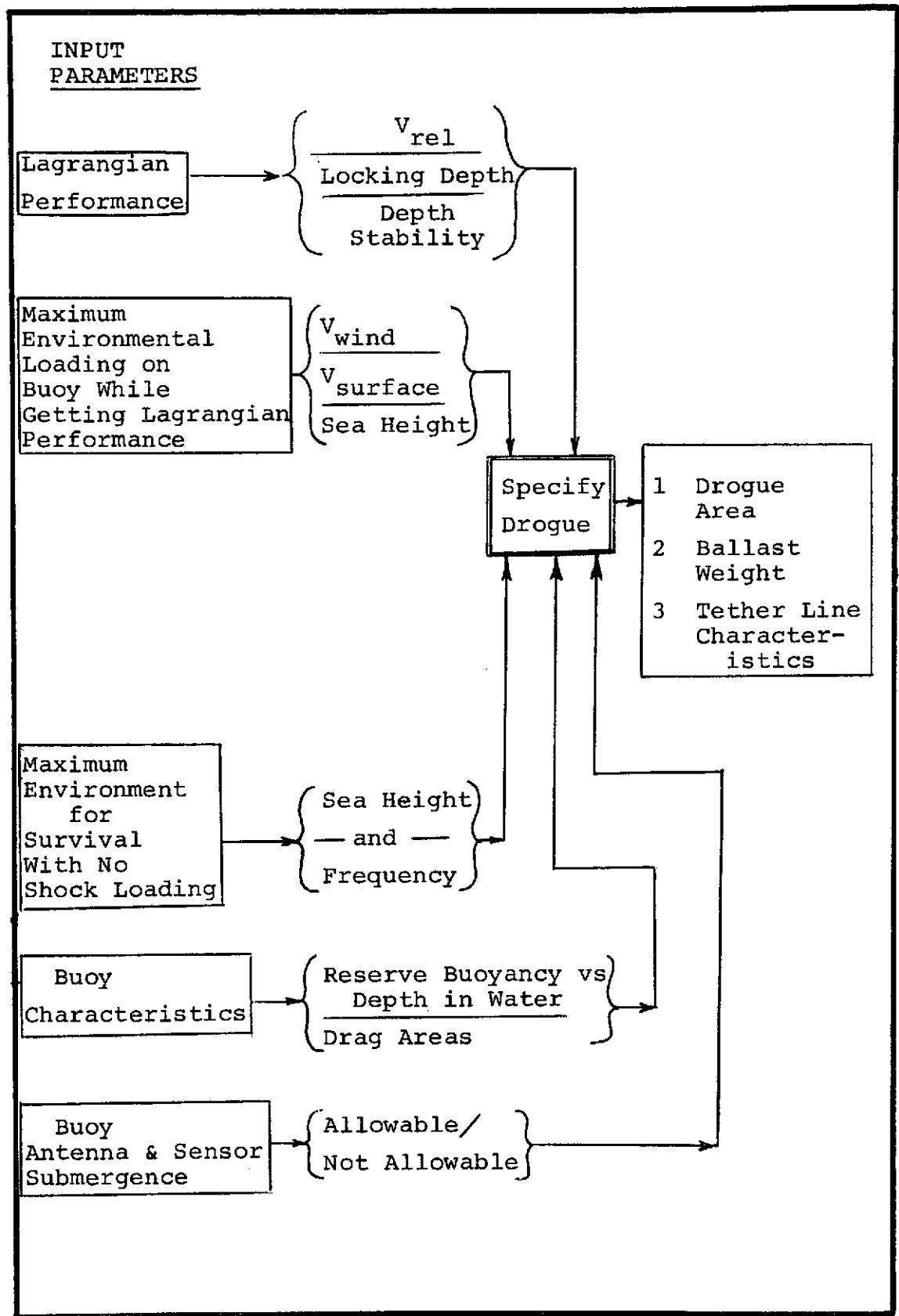


Figure E-1 Schematic of Pertinent Parameters in the Specification of a Drogue

less risk of tether line shock loading. Such an impass and others can be reached when certain input parameters are too rigidly specified. Ideally a buoy could be designed in response to the other input parameters.

The following example will illustrate a process of specifying a drogue for an available buoy. The buoy characteristics chosen are assumed to be approximately those of the mini-capability buoy built by Nova University for the National Data Buoy Office to be used in free drifting applications. It will be initially assumed that drogue performance as a Lagrangian sensor is the primary consideration.

The input parameters to the specification are assumed to be the following:

A. Lagrangian Performance:

1. Deep current locking velocity error  $\leq 5$  cm/sec  
~ .1 knots
2. Desired locking depth = 300 feet
3. Drogue depth stability  $\leq 5\%$  of locking depth.

B. Max. Environmental loading While Getting Lagrangian Performance:

1. Wind Velocity =  $V_w = 30$  knots
  2. Surface Current Velocity =  $V_c = .8$  knots
  3. Neglect wave drag effects on buoy
  4. Estimate of current profile = linear decrease to zero velocity at 300 feet.
- } same direction

C. Max. environment for survival with no shock loads on tether line = 15 foot seas.

D. Buoy characteristics:

1. Drag areas:

$$C_D A \text{ (above water)} = 4.8 \text{ ft}^2$$

$$C_D A \text{ (below water)} = 9.6 \text{ ft}^2$$

where it has been assumed that  $C_D$  for the cylindrical sections is 1.2.

2. Reserve Buoyancy (total = 225 pounds.)

E. Buoy antenna and sensor submergence:

allowable part of the time.

Analyses have not been carried out in which the buoy, tether line, and drogue dynamics are studied as a coupled dynamical system. Such analyses could potentially show that a buoy with modest reserve buoyancy will act like a spring, ameliorating the tether line tensions (Fig. D-2) and shock loading conditions (Fig. D-4) studied in Appendix D. For this example, however, the simpler, more stringent assumption of a perfect surface-following buoy will be made.

The point of initial departure in the design involves a computation of the maximum estimated horizontal drag load on the buoy and tether line which must be offset by the drag of the drogue. A small diameter tether line of 3/16-inch diameter jacketed wire rope with a rated breaking strength of approximately 4000 pounds is assumed. This is a realistic tether line, the choice of which includes a healthy steady load safety factor.

The total horizontal drag on the tether line is computed as follows:

$$(F_D)_{TOT} = (F_D)_{wind} + (F_D)_{current/buoy} + (F_D)_{current/line} \quad (E-1)$$

$$= \frac{1}{2} \rho_{air} (C_{DA})_{Above} V_W^2 + \frac{1}{2} \rho_W \left[ (C_{DA})_{Below} V_C^2 + (C_{DA})_{line} \overline{V_C^2} \right] \quad (E-2)$$

where:

$\rho_W$  = Water density

$\overline{V_C^2}$  = Average of the square of the current velocity by the tether line.

For this force analysis it will be assumed that the drogue is perfectly locked to the water at 300 feet. In reality it is pulled in the direction of the wind and current by a determinable amount, based on drogue area and ballast weight. This relative velocity at the drogue could be subtracted from the wind and current velocities in equation (E-2) for an improved estimate of  $(F_D)_{TOT}$ . Such an iteration would soon converge. Use of the simplifying assumption, however, produces a small error. Furthermore, any buoy settlement in the water due to the ballast and tether line weights is neglected. Inclusion of this effect would alter the value of the first 2 terms in equation (E-2).

A computation based on the design parameters results in the following:

$$(F_D)_{TOT} = 14.4 + 16.9 + 1.1 \text{ pounds} \quad (E-3)$$

$$(F_D)_{TOT} = 32.4 \text{ pounds.}$$

The next step is to determine the size of the ballast weight. A design goal is to maximize the ballast weight at the drogue bottom while being aware of buoy submergence. The weight is maximized for three reasons:

- (1) Keep the drogue from drifting upward and allowing a greater slip velocity for a given drag force.
- (2) Maintaining the desired depth locking accuracy.
- (3) Minimizing tether line shock loads in high seas.

Three hundred feet of 3/16" O.D. jacketed wire rope, weighing approximately .03 pounds/foot in water gives rise to 9 pounds of tether line tension at the buoy. The estimated current profile should give rise to negligible downward hydrodynamic forces because the maximum horizontal drag force on the tether line is approximately 1.1 pounds (See equation E-3). Downward force components would be approximately equal to the horizontal component times  $\cos^2\theta \sin\theta$ , where  $\theta$  is the tether line angle with respect to vertical, and thus always less than the horizontal component.

In order to actually specify the size of the ballast weight a value judgment must be made based on priorities. Given initially 225 pounds of reserve buoyancy at the buoy, 9 pounds is used up due to the weight of the tether line. This leaves 216 pounds as the maximum permissible ballast weight (neglecting drogue weight). If nearly all of this reserve is used for ballast, in order to enhance current locking and depth stability while minimizing shock loads, the buoy will most assuredly submerge a good portion of the time on the rising part of waves (Fig. D-2). It will be assumed here that buoy survival is more important than minimizing the chance of complete buoy submergence. Submergence may be less hazardous to buoy survival but, it may mean that meteorological sensors and a communications antenna on the buoy will be inoperable during much of the time in all but calm seas. This judgment must be made by an overall consideration of the system needs and capabilities.

By the above assumption on priorities, approximately 3/4ths of the remaining reserve buoyancy will be used for

ballast. It will be assumed that the drogue will be ballasted with a 150-pound weight in water. This combined with the tether line weight (9 pounds) leaves a total reserve buoyancy in the system of 66 pounds. A check on depth stability (Fig. C-1) indicates that the largest wind and current loads will produce a depth change of approximately 2.5% or 7.5 feet; better than desired. In order to achieve a maximum drift velocity error of less than 5 cm/sec, Figure B-7 indicates that a drogue with an area of 700 ft<sup>2</sup> must be chosen for the case of a 150-pound ballast weight and a total horizontal drag force of 32.4 pounds.

Dynamic loads caused by the vertical drag of a 700 ft<sup>2</sup> drogue will, however, pose problems. As already described, the remaining reserve buoyancy of the drogued buoy is only 66 pounds. According to the calculated curves in Figure D-2 the dynamic drag forces of a 700 ft<sup>2</sup> drogue in 2.5 foot seas will exert enough force to submerge the buoy. Furthermore, theoretical calculations shown in Figure D-4 indicate that a 700 ft<sup>2</sup> drogue with 150 pounds of ballast can incur shock loads in 3-foot seas if the buoy is a perfect surface follower. Because the buoy tends to submerge in seas of height greater than approximately 2.5 feet, the submergence will shift the design curves of Figure D-4 upward by an unknown amount. As already mentioned, more complex analyses involving the buoy dynamics as well as the sea input would be required to more precisely estimate a new shock loading condition.

It is, however, apparent that the input parameter C (max. environment with no shock loads) cannot be met in the specification, while endeavoring to meet the current locking requirement of  $V_{rel} \leq 5$  cm/sec.

The first cut at the design is complete at this point. Due to a low value of buoy reserve buoyancy, the maximum

environment in which no shock loading will occur may be less than originally desired. The components of the buoy and tether line should be ruggedized in order to survive the potential shock loading. The desired performance of the buoy has, however, been retained. Additional cuts at the design might back off on performance (i.e., reduce drogue area) while enhancing survivability.

A possible means of improving the design while attempting to keep the buoy from submerging would be to add surface distributed buoyancy adjacent to the surface buoy. This buoyancy could be in the form of faired, foam-filled packages attached to the tether line. The fairing would tend to minimize additional and unwanted surface drag due to the surface current (See Equation E-1). Sufficient flotation would be required to support the steady weight of the cable, drogue, and weight. Additional flotation would then act as a "soft spring" in the presence of dynamic loads; leaving the buoy relatively free of submerging loads. The actual detailed design would be rather involved and would result in a larger drogue in order to offset the additional surface drag, while retaining the same performance.

In looking at the suggested design more closely, the rather large deep current velocity locking error of 5 cm/sec is desired in the presence of a sustained 30 knot wind (i.e., 17-foot seas by Fig. D-1). Above these levels it might be assumed that either the data are uncorrectable or the process being studied is no longer valid. In general, it is felt that at even higher levels of drag, if the drag force can be adequately estimated and the buoy position adequately determined, drift velocity corrections can still be approximated by Figure B-7. At lower levels of loading, though, the current locking accuracy greatly improves. For example, a 10 knot surface wind inducing a .3 knot surface current results in a total drag force of 4.3 pounds and a drift velocity error of approx. 1.8 cm/s

DO NOT PHOTOGRAPH THIS PAGE

MANDATORY DISTRIBUTION LIST

FOR UNCLASSIFIED TECHNICAL REPORTS, REPRINTS, & FINAL REPORTS  
PUBLISHED BY OCEANOGRAPHIC CONTRACTORS  
OF THE OCEAN SCIENCE AND TECHNOLOGY DIVISION  
OF THE OFFICE OF NAVAL RESEARCH  
(REVISED SEPT 1973)

1	Director of Defense Research and Engineering Office of the Secretary of Defense Washington, DC 20301 ATTN: Office, Assistant Director (Research)	12**	Defense Documentation Center Cameron Station Alexandria, VA 22314
	Office of Naval Research Arlington, VA 22217		Commander Naval Oceanographic Office Washington, DC 20390
3	ATTN: (Code 480)*	1	ATTN: Code 1640
1	ATTN: (Code 460)	1	ATTN: Code 70
1	ATTN: (Code 102-0S)		
1	Cognizant ONR Branch Office	1	NODC/NOAA Rockville, MD 20822
1	ONR Res. Rep. (if any)		
	Director Naval Research Laboratory Washington, DC 20390		
6	ATTN: Library, Code 2029 (ONRL)		
6	ATTN: Library, Code 2620		

Total Required - 35 copies

\* Add one separate copy of  
Form DD-1473

\*\* Send 2 completed forms DDC-50  
one self addressed back to  
contractor, the other addressed  
to ONR, Code 480